Instituto de Neurociencias

Consejo Superior de Investigaciones Científicas

Universidad Miguel Hernández

MECHANOTRANSDUCTION IN MAMMALIAN TRIGEMINAL SENSORY NEURONS

DOCTORAL THESIS

ANNA LUCIA NICOLETTA CONTE

San Juan de Alicante, 2014

SUPERVISOR:

ANA GOMIS

UNIVERSITAS
Miguel
Hernández

Dr. Juan Lerma Gómez, Profesor de Investigación del Consejo Superior de Investigaciones Científicas, Director del Instituto de Neurociencias de Alicante, centro mixto UMH-CSIC,

CERTIFICA que la tesis doctoral titulada: "*Mechanotransduction in mammalian trigeminal sensory neurons*", ha sido realizada por Dña. Anna Lucia Nicoletta Conte, bajo la dirección de la Dra. Ana Gomis y da su conformidad para que sea presentada a la Comisión de Doctorado de la Universidad Miguel Hernandez.

Para que así conste a los efectos oportunos, firmo el presente certificado en San Juan de Alicante a 12 de mayo de 2014.

Fdo.: Prof. Juan Lerma Gómez

Director del Instituto de Neurociencias de Alicante

UNIVERSITAS
Miguel
Hernández

La **Dra. Ana Gomis**, Científico titular del Consejo Superior de Investigaciones Científicas, en el instituto de Neurociencias de Alicante, centro mixto CSIC-UMH

DA SU CONFORMIDAD a la lectura de la tesis doctoral titulada: "*Mechanotransduction in mammalian trigeminal sensory neurons*", realizada por Dña. Anna Lucia Nicoletta Conte, bajo mi inmediata dirección y supervisión en el Instituto de Neurociencias (CSIC-UMH) y que presenta para la obtención del grado de Doctor por la Universidad Miguel Hernández.

Para que así conste a los efectos oportunos, firmo el presente certificado en San Juan de Alicante a 12 de mayo de 2014.

Fdo.: Dra. Ana Gomis

UNIVERSITAS
Miguel
Hernández

El presente trabajo ha sido realizado en el Instituto de Neurociencias CSIC-UMH, en San Juan de Alacant.

Anna Lucia Nicoletta Conte ha sido beneficiaria de una beca predoctoral JAE-PreDoc-2009, perteneciente al Consejo Superior de Investigaciones Científicas.

Este trabajo se ha desarrollado gracias a la financiación procedente de Ministerio de Educación y Ciencia BFU2009-07853 y Consolider-Ingenio 2010 CSD2007-00023.

UNIVERSITAS
Miguel
Hernández

A mis padres Franca y Ugo,

UNIVERSITAS
Miguel
Hernández

Acknowledgment

Me gustaría que estas líneas sirvieran para expresar mi más profundo y sincero agradecimiento a todas aquellas personas que me han ayudado, apoyado, acompañado y compartido algo conmigo durante este largo camino.

En primer lugar, me gustaría agradecer a mi directora de tesis, la Dra. Ana Gomis, que me diera la oportunidad de haber hecho esta tesis. Su espíritu científico y criticas me han ayudado a crecer como científica.

A la Dra. Elvira De la Peña, el Dr. Felix Viana, el Dr. Roberto Gallego, y el Dr. Carlos Belmonte, que siempre que les he pedido algo me han ayudado sin problemas.

A los muchos compañeros del laboratorio, que han sido como una familia para mí.

A Imane, Bristol, Mariajo, Jan Albert, Rebecca, Carlitos, Hugo, Victor, Andrés, Joselito por lo momentos buenos y risas que me habéis dado en estos años y que han hecho que todo fuera más fácil.

A Enoch, por la mucha paciencia que ha tenido conmigo, los consejos y el apoyo que siempre me ha dado, por la disposición que siempre ha mostrado en ayudarme ante cualquier problema y los buenos ratos pasado dentro y fuera del laboratorio.

A Danny, por aguantar mis frecuentes quejas, apoyarme en los momentos difíciles e intentar contagiarme con su optimismo. Tenerte como compañero ha sido muy divertido, a pesar de nuestras pequeñas discusiones.

A la Dra. María Pertusa por haber contribuido a mi formación inicial y la Dra. Cruz Morenilla por los muchos consejos en biología molecular que me ha dado a lo largo de estos años.

A Eva, Ana M. y Mireille, por lo mucho que me habéis enseñado y ayudado en varias ocasiones.

A Rebeca y Clara, por los agradables momentos vividos en estos años de doctorado juntas, por compartir las penas y las alegrías, y por estar siempre allí.

A todos mis amigos físicamente lejanos pero siempre pendientes de mí, a Antonella, Maria, Anna, Rossella, Gianluca, Nicola, Alessia, Alessandra, Ana, Zafira, Mertxe y One,

por saber que puedo siempre contar con vosotros para charlar un rato, reírme, desconectar o compartir bailes “salseros” allí donde nos veamos.

A mis padres, por el gran apoyo que siempre me han dado, por lo mucho que creen en mí y por ser mi pilar y ejemplo a seguir. A mis hermanos, por el afecto y la energía que me transmiten. A mi sobrina Giulia y mi sobrino Daniele, por la alegría que me dan cada vez que los veo.

Y por supuesto a Miguel Angel, por el amor y la paciencia que me ha demostrado a lo largo de estos últimos años, por estar siempre a mi lado, tanto en los buenos como en los malos momentos, apoyándome y tranquilizándome cuando me parecía que todo era una “tragedia”.

TABLE OF CONTENTS

UNIVERSITAS
Miguel
Hernández

UNIVERSITAS
Miguel
Hernández

ABBREVIATIONS:

AP: action potential

ASIC: acid sensing ion channel

ATP: adenosine triphosphate

$[Ca^{2+}]_i$: intracellular calcium concentration

CA: cinnamaldehyde

Cap: capsaicin

CGRP: calcitonin-gene related peptide

CNS: central nervous system

DEG/ENaC: degenerin/epithelial Na channel

DMEM: Dulbecco's Modified Eagle Medium

DMSO: Dimethyl sulfoxide

dNTP: Deoxyribonucleotide triphosphate

DTT: dithiothreitol

ECM: extracellular matrix

FBS: fetal bovine serum

F_{340}: fluorescence emitted by Fura-2 excited at 340nm wavelength

F_{380}: fluorescence emitted by Fura-2 excited at 380nm wavelength

F-12: nutrient mixture F12

Fura 2-AM: acetoxymethyl ester Fura-2

Gd^{3+}: gadolinium

HC-030031: 2-(1,3-Dimethyl-2,6-dioxo-1,2,3,6-tetrahydro-7H-purin-7-yl)-N-(4 isopropylphenyl)acetamide, 1,2,3,6-Tetrahydro-1,3-dimethyl-N-[4-(1 methylethyl)phenyl]-2,6-dioxo- 7H-purine-7-acetamide

HBSS: Hank's Balanced Salt Solution

HEPES: 4-(2-hydroxyethyl)-1-piperazineethanesulfonic acid

IA: intermediately adapting

IB_4: isolectin 4

KCNK: two-pore-domain K^+ channel (K2p)

KO: knock out

MA: mechanically activated

MesV: trigeminal mesencephalic neurons

MS: mechanosensitive

NGF: nerve growth factor

Nomp C: no mechanoreceptor potential C

P1-4: postnatal mice of 1-4 days

PCR: polymerase chain reaction

PBS: phosphate-Buffered Saline

RA: rapidly adapting

RNase: Recombinant Ribonuclease Inhibitor

RR: ruthenium red

RT- PCR: reverse transcriptase polymerase chain reaction

SA: slowly adapting

SAC: stretch activated cation channel

siRNA: small interfering RNA

SLP3: stomatin-like protein 3

TG: trigeminal ganglia

TRP: transient receptor potential

TRPA1: transient receptor potential ankyrin 1

$Trpa1^{-/-}$: knock out for TRPA1

TRPC5: transient receptor potential canonical 5

TRPC3: transient receptor potential canonical 5

TRPV1: transient receptor potential vanilloid 1

TRPV2: transient receptor potential vanilloid 2

TTX: tetrodotoxin

Vm: membrane potential

VGSC: voltage-gated sodium channels

WT: wild type

UNIVERSITAS
Miguel
Hernández

UNIVERSITAS
Miguel
Hernández

Abstract

Many physiological processes depend critically on the proper sensing of mechanical forces, including hearing, proprioception and touch. Great efforts have been undertaken to unveil the mechanisms and discover the molecular entities responsible for mechanotransduction. Accordingly, recent studies have led to the description of the specific properties of mechanically activated (MA) currents in different subpopulations of mechanosensitive (MS) neurons from the dorsal root ganglia (DRG) of mice, although the channels that mediate these currents are largely unknown. Trigeminal (TG) neurons are primary sensory neurons that detect mechanical forces originating in the face and the head. However, unlike DRG neurons, the mechanosensitive conductances of TG neurons have not been described in detail.

The main aim of this study was to characterize mechanosensitive neurons in mice and to correlate their properties with neuronal type (non-nociceptive vs. nociceptive neurons) and mechanotransductor expression. I used Fura2-based fluorimetric calcium imaging and whole-cell patch-clamp recordings to characterize the responses of different populations of TG neurons from newborn and adult mice to a hypoosmotic solution (210 mOsml Kg^{-1}), a stimulus that causes membrane stretching, and to static indentation produced by a glass pipette driven by a micromanipulator system. I classified the neurons according to established criteria, like firing pattern and action potential shape, sensitivity to tetrodotoxin and IB4 labelling, for nociceptive and non-nociceptive neurons.

Using calcium imaging techniques I identified three mechanically sensitive populations of neurons that responded to hypoosmotic solution (18%), indentation (37%) or both stimuli (34%). The proportion of mechanosensitive neurons was comparable in newborn and adult animals. However, I observed a significant increase in the proportion of mechanical neurons with nociceptive properties in adult animals.

In patch clamp recordings, mechanical stimulation activated three types of currents that could be distinguished by their inactivation kinetics: rapidly (RA, 35%), intermediate (IA, 24%) and slowly (SA, 41%) adaptive currents. Both nociceptive and non-nociceptive neurons showed similar proportions of the three types of mechanically gated currents.

The correlation between the different subsets of mechanically activated neurons and the expression of specific ion channels proposed to be involved in mechanotransduction (*e.g.,* TRPA1, TRPC5, Piezo2, TRPC3 and ASIC3) was further investigated using single cell reverse transcription polymerase chain reaction (RT-PCR). While I observed considerable heterogeneity in the expression of mechanotransducer channels in the different neuronal subpopulations, the expression of the TRPA1, TRPC5 and Piezo2 genes predominated in the majority of the cells tested, regardless of the subpopulation.

Indeed, a series of candidate mechanotransduction genes have been proposed in mammalian cells, which includes TRPA1, encoding a channel predominantly expressed in mechanosensitive TG neurons. TRPA1 has been proposed to fulfil a fundamental role in mediating SA and IA currents in a subpopulation of adult DRG neurons. To investigate the role of TRPA1 in trigeminal neurons, I recorded mechanically-activated currents in newborn and adult mice lacking TRPA1. I found that genetic ablation of TRPA1 in adult mice produced a significant increase in the proportion of nociceptive neurons exhibiting RA currents and a significant decrease in the amplitude of IA currents.

In conclusion, I have identified distinct subsets of TG neurons that respond to different mechanical stimuli, suggesting that specific mechanical stimuli provoke distinct physiological responses. I also characterized mechanosensitive currents in nociceptive and non-nociceptive MS TG neurons. Heterogeneity in the expression of specific channels in distinct subpopulations of mechanosensitive neurons suggests that mechanotransduction is not dependent on a single molecule rather, it could depend on the activation of different mechanotransducers. Finally, my results indicate that TRPA1 may contribute to mechanically-activated currents in nociceptive neurons from adult mice.

Resumen

Muchos de los procesos fisiológicos más importantes, como por ejemplo la detección de los sonidos, el tacto y la propiocepción, ocurren a través de la detección y transmisión de los estímulos mecánicos. Durante los últimos años ha aumentado el número de grupos de investigación dedicados a caracterizar las células mecanosensibles en diferentes organismos e identificar las moléculas responsables de la detección y/o transducción de las fuerzas mecánicas. Los últimos trabajos científicos publicados en el campo, muestran las propiedades de las corrientes iónicas activadas por estímulos mecánicos en diferentes sub-poblaciones de neuronas de los ganglios raquídeos de ratones (DRG). Aunque no está completamente probado, se asume que la molécula mecanotransductora es un canal iónico, sin embargo, hasta ahora se desconoce en gran medida la identidad de los canales iónicos que median estas corrientes activadas por estímulos mecánicos. Las neuronas de los ganglios trigéminos (TG) son neuronas primarias aferentes que detectan y transmiten la información sensorial de la cara y de la cabeza y, a diferencia de las neuronas de DRG, sus conductancias mecanosensibles no han sido estudiadas.

El objetivo general de esta Tesis ha sido caracterizar las neuronas mecanosensibles de los ganglios trigéminos, relacionar sus propiedades con las neuronas nociceptivas y no nociceptivas y asociarlas con la expresión de canales iónicos considerados como posibles mecanotransductores. Para ello he usado la técnica de imágenes de calcio, mediante el indicador fluorescente Fura2, y registros electrofisiológicos de clampado de voltaje y de corriente (patch clamp) en la configuración de célula entera. Los experimentos se han realizado en neuronas trigeminales de animales neonatos y adultos en respuesta a una solución hipoosmótica (210 mOsml Kg^{-1}), que provoca un estiramiento de la membrana, y a una deformación de la membrana, producida por el desplazamiento de una punta de vidrio controlada por un sistema piezoeléctrico. Además, he clasificado las neuronas en nociceptivas y no nociceptivas en función de unos criterios establecidos, como el patrón de descarga, la forma del potencial de acción, la sensibilidad a tetrodotoxina y el marcaje con isolectina 4.

Usando la técnica de imagen de calcio, he identificado tres poblaciones de neuronas mecanosensibles que responden al estímulo hipoosmótico (18%), a la

deformación de la membrana mediante una punta de vidrio (37%) o a ambos estímulos (34%). La proporción de las neuronas mecanosensibles fue la misma en ratones neonatos y de adultos. Sin embargo, hubo un aumento significativo de las neuronas mecánicas nociceptivas en animales adultos.

Usando la técnica de "patch clamp", se han podido identificar diferentes poblaciones de neuronas en función de su respuesta a la deformación de la membrana. La estimulación mecánica activó tres tipos de corrientes iónicas en función de su cinética de inactivación, encontrando corrientes de adaptación rápida (RA, 35%), intermedia (IA, 24%) y lenta (SA, 41%). Los tres tipos de corrientes se registraron en las neuronas nociceptivas y no nociceptivas.

El siguiente paso fue estudiar la posible correlación entre los diferentes tipos de neuronas mecanosensibles y la expresión de canales iónicos que se han propuesto como posibles mecanosensores o mecanoreceptores, como por ejemplo los canales TRPA1, TRPC5, Piezo2, TRPC3 y ASIC3. La expresión de estas proteínas se detectó utilizando la técnica de "real time polymerase chain reaction (PCR)" en célula única. Los resultados indican que existe una heterogeneidad en la expresión de los canales mecanotransductores analizados en las diferentes poblaciones de neuronas, aunque TRPA1, TRPC5 y Piezo2 se detectaron en la mayoría de las células estudiadas.

Existen datos que sugieren que TRPA1 es uno de los canales implicados en la mecanotransduccion en los mamíferos. Se ha demostrado que participa en la activación de las corrientes SA e IA en neuronas de DRG en ratones adultos. Según mis datos, TRPA1 se expresa mayoritariamente en las neuronas trigeminales por lo que el siguiente objetivo de este trabajo fue estudiar la función del canal TRPA1 en dichas neuronas. Para ello he registrado las corrientes activadas por deformación de la membrana en ratones neonatales y adultos que no expresan el canal TRPA1 (TRPA1 knock-out). Los datos indican que en animales $TRPA1^{-/-}$ se produce un aumento significativo de la proporción de neuronas que expresan corrientes del tipo RA y una disminución significativa de la amplitud de las corrientes del tipo IA en la población de neuronas nocivas en ratones adultos.

Resumiendo, he identificado poblaciones de neuronas trigeminales que responden a diferentes estímulos mecánicos, lo que sugiere que diferentes estímulos

mecánicos podrían dar lugar a respuestas fisiológicas diferentes. También he caracterizado las corrientes mecanosensibles en las poblaciones de neuronas trigeminales nociceptivas y no nociceptivas. Sin embargo, la heterogeneidad en la expresión de canales iónicos específicos en las diferentes poblaciones de neuronas mecanosensibles sugiere que la mecanotransducción depende de la activación de diferentes mecanotransductores. Por otra parte, mis resultados sugieren que el canal iónico TRPA1 participa en la mecanotransducción de los estímulos nocivos.

UNIVERSITAS
Miguel
Hernández

1. Introduction

1. 1 Mechanotransduction

Mechanotransduction describes the cellular processes that translate mechanical stimuli into biochemical signals. The detection of force or pressure can affect a myriad of processes and this occurs ubiquitously in all living organisms from bacteria to humans, suggesting an early emergence of mechanotransducers molecules during evolution.

Mechanotransduction is not limited to a subset of specialized cells or tissues but rather, it is involved in a broad range of cellular functions. Mechanotransduction is necessary so that organisms can detect and integrate information of mechanical signals from the external world through touch and hearing, for the monitoring of internal states by sensing flow, osmotic pressure, blood pressure, balance and proprioception (the internal sensing of the relative position of our body parts). The detection and transmission of mechanical stimuli is also crucial for organ development and for the maintenance of many mechanically stressed tissues, including bone, muscle, cartilage and blood vessels. Signals generated by mechanotransduction influence the development of epithelial cells in the lungs, endothelial cells in the vasculature and osteoblasts in bone (Waters et al., 2002; Li et al., 2005; Mikuni-Takagaki, 1999). In the cardiovascular system, the physiology and morphology of the heart and vasculature is influenced by pressure and by the shear stress generated by the blood flow (Haga et al., 2007; Li et al., 2005). Mechanical forces can result in both constructive and detrimental cellular changes. For example, mechanical forces in the lung induced by the initiation of breathing in a newborn are essential for the correct differentiation of alveolar cell types (Joe et al., 1997). By contrast, turbulent blood flow at artery branch points causes shear stress which can lead to the development of atherosclerotic plaques at these sites (Birukov et al., 1995).

Defects in mechanotransduction, caused by mutation or the dysregulation of proteins involved in cellular and extracellular mechanosensitive mechanisms, are implicated in a broad range of diseases, including painful mechanical hypersensitivity, muscular dystrophies, hearing loss and cardiomyopathy, and in metastasis and cancer progression. Disrupting force transmission between the extracellular matrix (ECM), the cytoskeleton and the nucleus is a common cause of

many diseases related to mechanotransduction. In addition to defects that affect cell structure, mutations in proteins of the downstream signalling pathways involved in mechanotransduction can also have pathological effects. For example, mutations in proteins involved in intracellular calcium signalling of members of the Rho or mitogen activated protein kinase (MAPK) pathway, can promote a malignant phenotype in a model of breast cancer (Paszek et al., 2005).

In addition, mechanotransduction constitutes an important component of proprioceptive and extrasensory function and it is essential for auditory and somatosensory function. One of the best characterized mechanotransducer is the hair cell of the inner ear, which transduces mechanical forces (*e.g.* sound waves, pressure and gravity) into electrical signals. These mechanical forces cause small displacements in the stereocilia of the hair cells. Stereocilia are arranged in bundles with centrally increasing height and the deflection of the stereocilia causes tension in the tip links (small extracellular filaments that connect the stereocilia tip with adjacent stereocilia), thereby opening mechanically-gated ion channels (Pickles et al., 1984). Although the intricate structure of the hair bundle is well understood, many of the molecular components involved in this mechanotransduction machinery remain to be identified.

1.2 The mammalian somatosensory system

The somatosensory system is the most diverse of the classic sensory systems and it includes different subsystems with distinct sets of peripheral receptors (*e.g.* thermoreceptors, nociceptors, mechanoreceptors and chemoreceptors) as well as different central pathways.

The somatosensory system serves three major functions: proprioception, exteroception and interoception. *Proprioception* is the sense of oneself, *i.e.:* the sense of the position and movement of the body parts through the stimulation of muscle, tendons and joints. *Exteroception* is the processing of information relating to changes in the immediate external environment, including the sensation of fine touch, pressure, motion, vibration and thermal senses and it serves to identify objects. Finally, *interoception* is the sense of the physiological condition of the body and it mediates the sensations of pain, hunger and the movement of internal organs.

The transmission of afferent somatosensory information from the periphery to the brain begins with the activation of sensory fibres and the subsequent depolarization of the terminals of a sensory neuron. If depolarization reaches the threshold (receptor potential), the cell produces action potentials (APs) that are then transmitted to the central nervous system (CNS) via other neurons, known as first-, second- and third- order neurons, as described below:

- Primary afferent neurons are pseudo-unipolar neurons whose cell bodies are located in the trigeminal (TG) and dorsal root ganglia (DRG, to receive information from the head and body, respectively; Figure 1A). The sensory endings of the DRG and TG neurons can be activated by mechanical force, temperature and by different chemical agents, evoking sensations of touch, thermal sensations, itch, irritation and pain. The axons of the DRG and TG neurons project in two directions: inward into the dorsal horn of the spinal cord and outward to the periphery. The central processes of these neurons project to the spinal cord either ipsilaterally or contralaterally (Figure 1B).
- The cell bodies of second-order neurons are located in the brainstem nuclei, for mechanosensitive afferents, or in the outer part of the gray matter of the dorsal horn, for pain and temperature afferents. The fibres project to either the thalamus or the cerebellum.
- Third-order neurons are located in the ventral posterior lateral (VPL) and ventral posterior medial (VPM) nuclei of the thalamus and they project afferents to the cortical sensory areas where information is integrated and processed.

A B

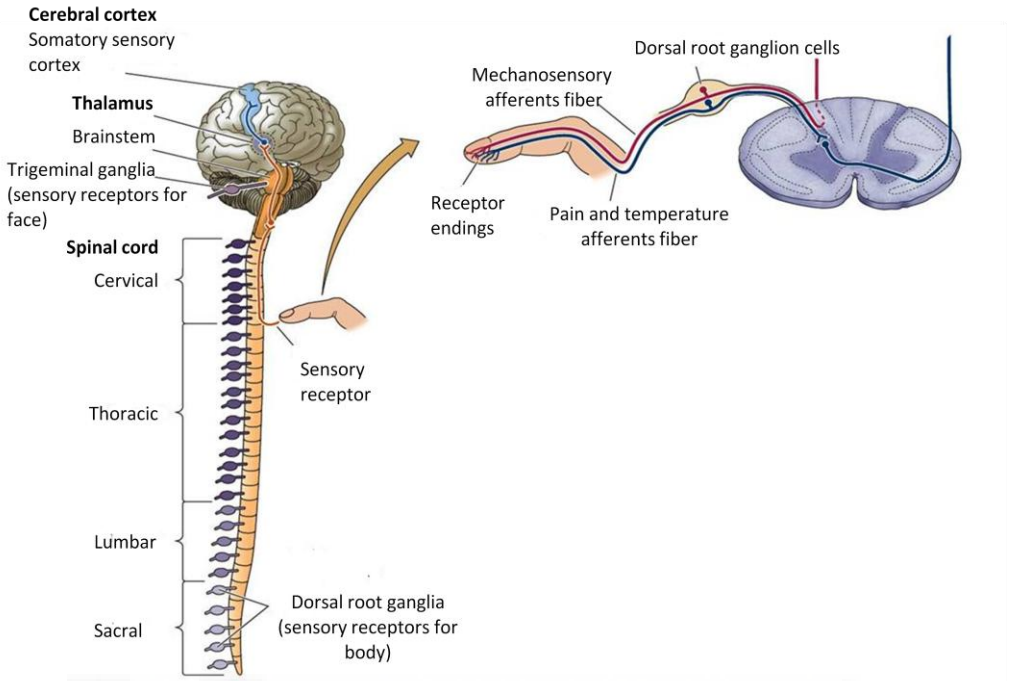

Figure 1. The somatosensory system conveys information from the peripheral endings to the central nervous system. (A) The cell bodies of the primary afferent neurons are located in the DRG, where they receive information from the body, and in the TG, where they receive information from the head. (B) Information on discriminative touch and proprioception (in red), and information on pain and temperature (in blue), are transmitted to the CNS via different pathways. Adapted from Purves D., Neuroscience, 4th edition (2008).

Sensory information processed by the somatosensory systems travels via different anatomical pathways depending on the nature of the information.

Thus, information pertaining to discriminative touch and proprioception is transmitted from DRG neurons to the thalamus via large diameter fibres that run through in the *dorsal columns* of the spinal cord and the *medial lemniscus* in the brain, which comprise the **dorsal column-medial lemniscus pathway** (Figure 2A). Fibres enter the dorsal horn and branch: one branch makes synapses deep in the dorsal horn with second-order sensory neurons, while the other branch of the axon ascends within the ipsilateral dorsal column of the spinal cord to the medulla. Once the information has been transmitted ipsilaterally, axons decussate to the contralateral ventral posterior nucleus of the thalamus. Thalamic neurons then project to specific regions of primary somatosensory cortex, in the posterior part of the central gyrus of the parietal lobe, an area known as the primary somatosensory cortex.

As occurs with the sensory information originating in the body, the somatosensory information from the face travels along distinct anatomical pathways depending on the nature of the information carried. Thus in the trigeminal pathway, neurons that conduct information pertaining to discriminative touch project to the principal nucleus of the TG complex after entering the pons of the midbrain. The second-order neurons cross and ascend to the ventral posteromedial nucleus of the thalamus and subsequently synapse with third-order neurons that project to the primary somatosensory cortex and the secondary somatosensory cortex, located in the upper bank of the lateral sulcus (Figure 2B).

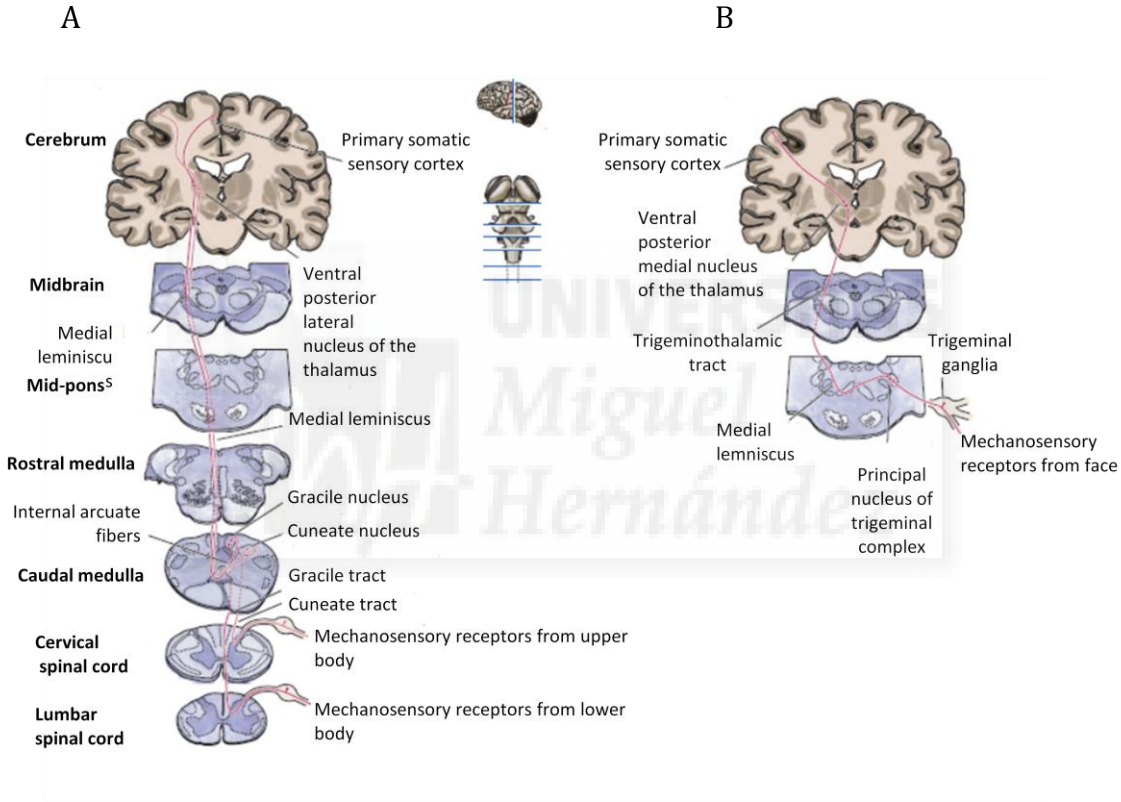

Figure 2. Representation of afferent touch information from the peripheral nerve endings to the cerebral cortex. (A) The dorsal column-medial lemniscus pathway transmits information from the neck down and it is supplied by input from sensory neurons located in the DRG. (B) The trigeminal pathway carries similar information from the face and is supplied by sensory neurons located in the trigeminal ganglia. Figure is adapted from Purves D., Neuroscience, 3th edition (2004).

Information relating to temperature, itch and pain are transmitted to the thalamus via small-diameter fibres that run through the *spinothalamic tracts* of the spinal cord and the *anterolateral* system in the brain (the **spinothalamic pathway**; Figure 3A). Axons of the nociceptive and thermosensitive neurons located in the DRG enter the spinal cord to connect with second-order sensory neurons. These neurons

are located in lamina I, II and V. Unlike the dorsal column-medial lemniscus pathway that mediates touch signalling, the axons of the second-order neurons immediately cross and ascend through the spinothalamic tract, running along the ventral surface of the spinal cord, until they reach the ventralaminar and ventral posterior controlateral nucleus of the thalamus. From here, the axons of these neurons project to the primary somatosensory cortex.

In the TG pathway, axons descend to the medulla in the spinal TG tract, and they make synapses in the pars caudalis and pars interpolaris of the spinal TG complex. Axons of second-order neurons immediately cross the midline and they synapse, via the trigeminothalamic tract, with third-order neurons located in the ventral posteromedial nucleus of the thalamus. Accordingly, information can be projected to the primary and secondary somatosensory cortex (Figure 3B).

The TG nerve also includes a motor root that travels with the mandibular nerve and innervates the muscles responsible for mastication. The cell bodies of the motor root fibres are centrally located in the pontine trigeminal motor nucleus.

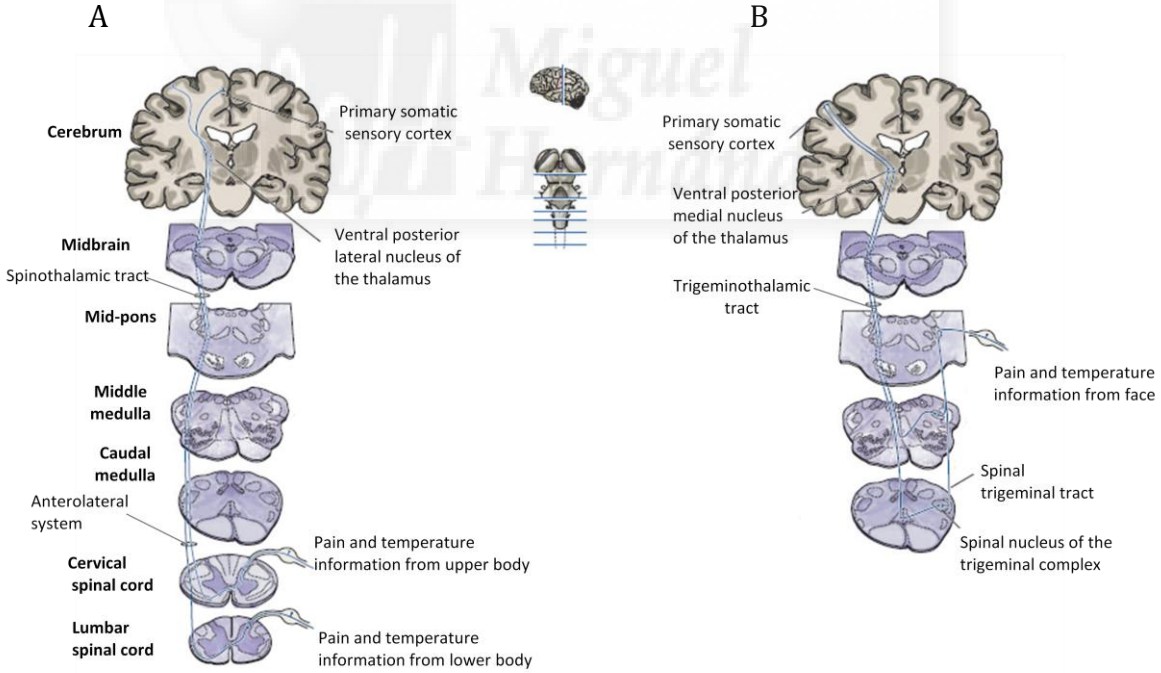

Figure 3. Representation of the transmission of afferent nociceptive and thermal information from the peripheral nerve endings to the cerebral cortex. (A) The spinothalamic pathway transmits information from below the neck and it is supplied by input from sensory neurons located in the DRG. (B) The TG pathway carries similar information from the face and it is supplied by input from sensory neurons located in the TG ganglia. *A*dapted from Purves D., Neuroscience, 3rd Edition (2004).

1.2.1 *The trigeminal system*

The TG or fifth cranial nerve is a general sensory nerve that transmits information regarding touch, temperature, nociception, and proprioception information from the face. Trigeminal literally means “three twins”, which refers to the three peripheral branches that make up the system: the ophthalmic (V1), maxillary (V2), and mandibular (V3) divisions (Figure4A). In humans, the ophthalmic (V1) branch passes through the superior orbital fissure and innervates the most superior structures of the head, including the orbit, conjunctiva and cornea, upper eyelid, nasal mucosa, forehead and meninges. The maxillary (V2) branch exits through the round foramen of the sphenoid bone and innervates more caudal structures, such as the lower eyelid, upper cheek, upper palate, upper lip and the maxillary teeth and gums. The mandibular (V3) branch projects through the oval foramen of the sphenoid bone and innervates the most anterior part of the tongue, the mandible, the lower lip and cheek, the mandibular teeth and gums, the anterior part of the external ear and part of the lateral scalp.

The cell bodies of the trigeminal ganglion are located in the middle cranial fossa, at the base of the skull (Figure4B). However the cell bodies of proprioceptive neurons are located in the mesencephalic nucleus (MesV) in the brainstem, rather than in the trigeminal ganglion (Cody et al., 1972; Alvarado-Mallart et al., 1975). These neurons lie at the outer border of the periaqueductal gray in the midbrain and the central gray of the pons and contain the cell bodies of primary afferent neurons receiving proprioceptive information of jaw position, of masticatory muscles and of periodontal receptors of both the maxillary and mandibula teeth (Jerge, 1963; Cody et al., 1972; Alvarado-Mallart et al., 1975). The neurons of the MesV, like other TG cells and DRG neurons, are pseudounipolar neurons with large, oval or round somata.

The peripheral and central components of TG afferent fibres are continuously attached to the cell body in the ganglia, via a single process, and the soma is enveloped by glial cells (Pannese, 1981). TG neurons are historically classified on the basis of their histological appearance (Gaik and Farbman, 1973), as large light (Type A) and small dark (Type B) cells. Neurons within the trigeminal ganglia are arranged somatotopically, whereby the cell bodies of the mandibular division are located in the lateral and posterior ganglion, whereas those of the maxillary and ophthalmic

divisions are interspersed in the medial and anterior ganglion, respectively (Figure 4B; Leiser and Moxon, 2006).

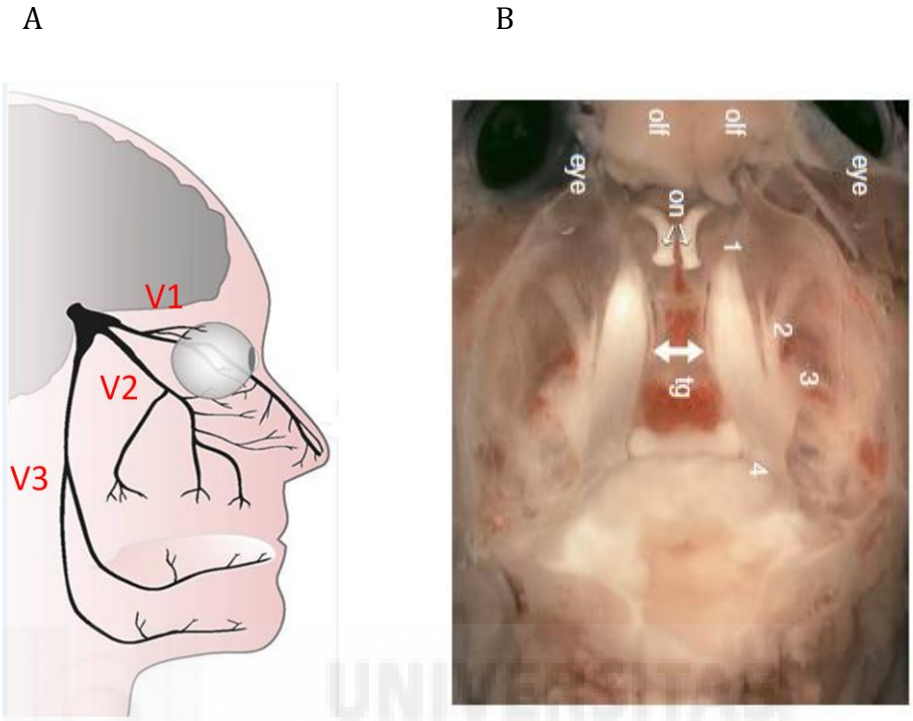

Figure 4. Localization and innervations of the trigeminal system. (A) Branches of the human trigeminal nerve innervating the face, eye, and the nasal and oral cavities. Adapted from Viana, 2011. (B) Location of the trigeminal ganglia in the mouse cranial cavity. The trigeminal ganglia are indicated with a double-headed arrow. On, optic nerves; olf, olfactory bulb; 1, ophthalmic; 2, maxillary; 3, mandibular; 4, fifth cranial nerve. Source: Malin et al., 2007.

1.3 Functional classification of somatic sensory afferents

The peripheral branches of sensory afferents are functionally and morphologically diverse. The following section describes the different types of sensory fibres and receptors found in the trigeminal nerve, based on their conduction velocity, mechanical threshold, adaptation properties, and modality (*i.e.,* the type of stimulus to which they best respond).

1.3.1 ***Conduction velocity***

The trigeminal nerve fibres present different conduction velocities that are mainly affected by axon diameter and the degree of myelination. Accordingly, the larger the diameter, the greater the speed of conduction and moreover, heavily

myelinated, large-diameter fibres conduct action potentials more rapidly due to the lower internal resistance to current flow along the axon. Indeed, Erlanger and Gasser (1938) studied and classified mammalian nerve fibres based on the electrical stimulation of whole nerves.

In terms of their conduction velocities, sensory afferents can be classified into four broad groups: Aα, Aβ, Aδ and C fibres. The A fibres are myelinated fibres, of which Aα fibres are sensory afferents that supply the sensory receptors in the muscle and they have the largest diameter and a conduction velocity of 80-120 m/s. Aβ fibres are heavily myelinated, large-diameter fibres with a conduction velocity of 30-70 m/s. These fibres innervate light-touch receptors that have low mechanical thresholds and that are associated with a variety of cell types in the periphery, including keratinocytes, Merkel cells, encapsulated terminals and hair follicles. They also carry sensory information from muscle spindles. Aδ fibres are moderately myelinated and have an intermediate conduction velocity of 5-30 m/s. These fibres function either as nociceptors, terminating as free-nerve endings in target tissues (AM fibres), or as light-touch receptors that associate with down hairs in the skin (D hair fibres). Finally, the C fibres are unmyelinated and have the lowest conduction velocity of the four types of sensory afferents (1-2 m/s). These small-diameter fibres terminate as free nerve endings in target tissues and respond to noxious mechanical, thermal and chemical stimuli (Brown and Iggo, 1967; Burgess et al., 1968; Perl, 1968; Knibestol, 1973).

Unmyelinated C fibres can be further categorized into two broad classes based on their expression of neuropeptide. The so-called peptidergic population produces neuropeptides like substance P and CGRP, and it expresses TrkA, the receptor for NGF (Snider and McMahon, 1998). The second population lacks peptides but it binds the plant lectin IB4 (Caterina and Julius, 2001; Dong et al., 2001; Molliver et al., 1997) as well as expressing $P2X_3$, $P2X_2$ and $P2X_7$ receptors, specific subtypes of ATP-gated ion channel (Silverman and Kruger, 1990; Staikopoulos et al., 2007; Dell'Antonio et al., 2002). These two populations differ anatomically (peptidergic neurons innervate basal regions of the epidermis, while non-peptidergic neurons innervate a more superficial epidermal region) and they terminate in distinct regions of the superficial dorsal horn of the spinal cord. The most superficial layer of this region, lamina I,

receives a direct input from CGRP+, IB4– nociceptors, while lamina II is innervated by CGRP–, IB4+ nociceptors (Stucky and Lewin, 1999). It appears that these two subpopulations of neurons also differ functionally. Indeed, pharmacological suppression of a population of non-peptidergic neurons results in the loss of sensitivity to noxious mechanical stimuli (Cavanaugh et al., 2009; Zylka et al., 2005). Similarly, pharmacological ablation of TRPV1-positive peptidergic neurons leads to deficits in heat nociception (Cavanaugh et al., 2009).

1.3.2 *Peripheral receptor type*

The restricted set of stimuli that can be detected by each somatosensory neuron is defined by the properties of the receptor expressed in its nerve terminal (Sherrington, 1906; Perl, 1996). Thus, peripheral receptor type is another functional parameter used to identify neuronal subpopulations.

Sensory receptors cells are specialized to transduce specific forms of energy, and each receptor contains a specialized anatomical region where transduction occurs. Depending on the nature of the stimulus that excites them, sensory receptors are classified as chemoreceptors, photoreceptors, mechanoreceptors, nociceptors, or thermoreceptors. Thus, by activating through specialized somatosensory receptors, organisms can detect different stimuli arising from both their external and internal environment. For example, the peripheral afferents of neurons that mediate touch and proprioception terminate in the non-neural capsule in the skin and muscle and they respond to mechanical deformation but not to changes in temperature or to mechanical forces that generate painful sensations. By contrast, the peripheral axons of neurons that sense noxious mechanical, thermal, or chemical stimuli terminate in the skin as free nerve endings often with multiple branches.

Sensory receptor cells are also classified according to their activation threshold and receptor adaptation. The activation threshold is the minimum stimulus intensity at which the receptor is activated, while receptor adaptation describes the decline in the electric response of the receptor in the persistent presence of a stimulus. By defining mechanotransduction according to these parameters, we can distinguish between **rapidly-adapting mechanoreceptors** (RA), which fire rapidly at the beginning and end of the stimulus (on-off responses), but fall silent in the

presence of continued stimulation and **slowly-adapting mechanoreceptors** (SA), which generate a sustained slowly adapting discharge in the presence of a persistent stimulus.

SA fibres detect the static qualities of a stimulus, such as size and shape, while RA fibres detect its dynamic qualities, such as the sensation of motion. Mechanoreceptors located in the glabrous skin are further subdivided into four subtypes (RA I, RA II, SA I and SAII), based on parameters such as firing pattern and receptive field. Thus, SA I and SA II responses are distinguished by the regularity of their static-phase firing rates; SA I fibres have a more irregular interspike interval than SA II fibres. Similarly, RA I responses are associated with small receptive fields and low-frequency vibrations (1-10Hz), while RA II innervate larger receptive fields and respond to high-frequency vibrations (80-300Hz; Talbot et al., 1968; Knibestol, 1973; Vallbo and Johansson, 1984).

1.3.3 ***Cutaneous mechanoreceptors***

As I mentioned before, the sense of touch involves discrimination of different aspects of a mechanical stimulus, including texture, vibration or direct pressure. Thus, for the sense of touch the somatosensory neurons include many distinct cell populations with specialized sensory endings to detect various features of touch and with specific threshold sensitivities and encoding capabilities (Lumpkin and Caterina, 2007).

The best characterized mechanoreceptors in mammals are located in the skin. Cutaneous afferents can be sub-classified on the basis of several properties, including receptor type, conduction velocity, activation threshold, receptor adaptation, skin stimulus and location (Figure 5). These afferents fall into two groups, found in both in glabrous and hairy skin: low threshold mechanoreceptors (LTMRs), that react to light pressure (innocuous touch) and high threshold mechanoreceptors (HTMRs) that respond to harmful mechanical stimuli (noxious touch).

The following section provides an overview of the properties of cutaneous mammalian mechanoreceptors based on the detection of innocuous and noxious stimuli in glabrous and hairy skin in mice.

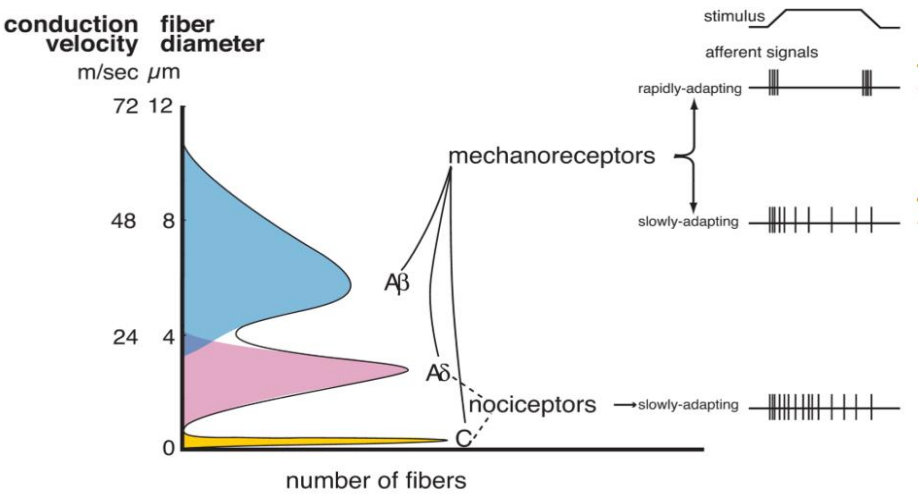

Figure 5. Classification of cutaneous mechanoreceptors in mammals. Mechanoreceptor nerve fibres can be classified in function of different properties, including conduction velocity, activation threshold and receptor adaptation. The Aβ, Aδ and C fibre subfamilies are defined by their conduction velocity; Aβ fibres have the highest conduction velocity and the unmyelinated C-fibres the lowest. Aβ fibres have low mechanical thresholds, they are thought to innervate mechanoreceptors in the skin and they can be slowly or rapidly adapting. By contrast, C-fibres innervate nociceptors in the skin, they exhibit slow adaptation rates and they often have high mechanical thresholds. Adapted from Geffeney and Goodman, 2012.

1.3.3.1 *Low-threshold mechanoreceptors*

The glabrous skin is innervated by four mechanoreceptive afferent neuron types. These are found at varying depths throughout the skin and in different body regions, and each is uniquely tuned to particular aspects of touch. RA I afferents terminate in Meissner's corpuscles, RA II afferents in Pacinian corpuscles, SAI afferents in Merkel cells, and SA II afferents in Ruffini corpuscles. While each of these neuronal types responds differently to cutaneous motion and deformation, all are connected to Aβ and Aα afferents. Some of the characteristics of these neuronal types are described below and summarized in Figure 6C.

Meissner's corpuscles are encapsulated nerve endings that consist of a flattened supportive cell surrounded by a capsule of connective tissue. They occupy dermal ridges and respond to dynamic skin deformation, detecting low-frequency vibration and the slippage of objects in the hand. They are connected to Aβ fibres, they form sparse connections with C fibres and they have a large receptor field (Figure 6C, 4).

Pacinian corpuscles are 1 mm long ovoid structures located in the subcutaneous tissue. The entire corpuscle is wrapped in a layer of connective tissue

and the inner core of the membrane lamellae is separated from an outer lamella by gelatinous material. One or more RA afferent axons lie at the centre of this structure. Thus, this capsule acts as a filter, enabling the specific detection of high-frequency vibration stimuli and changes in the strength of the stimulus (hence the term "acceleration detectors"). They have the largest receptive field of the four types of low-threshold mechanoreceptors (Figure 6C, 5: Gray and Sato, 1953).

Merkel complexes are found at the base of the epidermis and they consist of a nerve terminal and a flattened non-neural epithelial cell. They respond to skin indentation, and are particularly sensitive to edges and corners and they are responsible for texture discrimination and finger precision. Moreover they exhibit the greatest sensitivity to low-frequency vibrations and the highest spatial resolution (0.5 mm) of the cutaneous mechanoreceptors (Figure 6C, 1: Iggo and Muir, 1969).

Ruffini`s receptors lie in the dermis and they consist of strong connective tissue sheaths enclosing nerve fibres, with many branches that end in small knobs. These receptors detect skin stretching and they play a key role in detecting finger position and the direction of object motion (Chambers et al., 1972). They also produce sustained responses to static stimulation but have larger receptive fields than Merkel cells (Figure 6C, 3).

Hairy skin is innervated by hair follicles, which are low-threshold receptors that detect hair movement and pleasant touch. These are classified into three main types: guard, awl/auchenne and zigzag hairs.

Guard hairs are the longest and least abundant (1%), and they are innervated by Aβ RA fibres and Aβ SA fibres (Figure 6A, 3).

Awl/auchenne hairs are of medium size and they constitute 23% of hair follicles. They are triply innervated by Aβ RA, Aδ and C-LTMRs fibres (Figure 6A, 1).

Zigzag hairs are the finest and the most abundant type of hair follicle (76%) and they are innervated by Aδ and C-LTMRs fibres (Figure 6A, 2).

It has been proposed that hairy skin consists of repeated units containing one or two central guard hairs, ~20 surrounding awl/auchenne hairs and ~80 interspersed zigzag hairs (Li et al., 2011).

In rodents, Merkel cells are also associated with guard hairs in hairy skin (Figure 6 A7) and with whisker follicles. Merkel cells are also present in human hairy skin, although at a lower density (Fradette et al., 1995; Halata et al., 2003; Abraira and

Ginty, 2013). A specific subpopulation of free nerve endings of C-LTMRs, found exclusively in hairy skin, is maximally activated by stimuli that move slowly across their receptive field and that are therefore proposed to act as “caress detectors” that mediate the perception of pleasant touch (Figure 6A, 8: McGlone et al., 2007; Vallbo et al., 1993; Vallbo et al., 1999; Douglas and Ritchie, 1957; Iggo, 1960).

The central projections of all of these fibres terminate in distinct, but partially overlapping laminae of the dorsal horn of the spinal cord. Thus C-LTMRs terminate in lamina II, Aδ-LTMRs in lamina III and Aβ-LTMRs in lamina IV and V (Figure 6B, 8). The large myelinated Aβ axons enter the dorsal horn and divide into two branches. One branch forms synapses in the deep part of the dorsal horn (laminae II, IV and V) and interferes with pain transmission (Figure 6B, 4), while the principal central branch ascends in the spinal cord through the ipsilateral dorsal column and forms synapse with second-order neurons in the medulla, the *gracile nucleus* (receiving information from the lower half of the body) and the *cuneate nucleus* (receiving information from the upper half of the body; Figure 6B, 5-6). Second-order neurons cross the midline immediately to form a tract on the controlateral side of the brainstem, called the *medial lemniscus*, which ascends through the brainstem to the thalamus (Figure 6 B7). Here, in the ventral posterior nucleus complex of the thalamus, these neurons synapse with third-order neurons that send their axons to the somatosensory cortex.

The scheme in Figure 6 outlines all the cutaneous mechanoreceptors expressed in mammalian glabrous and hairy skin, as well as their projections.

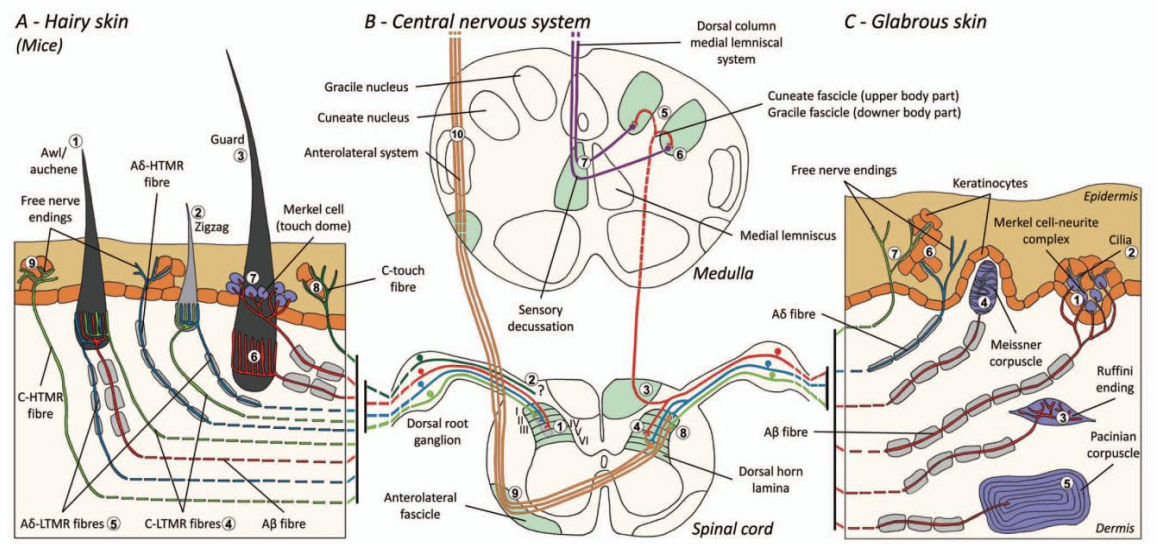

Figure 6. Organization and projections of cutaneous somatosensory receptors in mammals. (A) In hairy skin touch is detected by awl/auchenne (A1), zigzag (A2) and guard (A3) hairs. Pleasant touch is detected by a subpopulation of C-fibres (A8), whose central projections are shown in B2 and B1. (C) In glabrous skin innocuous touch is detected by four types of mechanoreceptors: Merkel cell-neurite complexes (C1), Ruffini endings (C3), Meissner corpuscles (C4) and Pacinian corpuscles (C5). Noxious touch is detected by the free nerve ending in the epidermis of both hairy (A9) and glabrous skin (C7). The central projections of these fibres, the anterolateral system (noxious touch) and the dorsal column-medial lemniscus pathway (innocuous touch) are shown in B8-10 and B3-7, respectively. Source: Roudaut et al., 2012.

1.3.3.2 *High-threshold mechanoreceptors*

Nociceptors are primary sensory neurons that are capable of transducing and encoding stimulus intensities within the noxious range and thus they represent the first line of defense against potentially harmful stimuli. HTMRs are mechano-nociceptors that are only excited by injurious mechanical stimuli, and poly-modal nociceptors that respond to different injurious stimuli, including noxious heat and irritative chemical compounds (Perl, 1996; Bessou and Perl, 1969). HTMRs include Aδ and C free nerve-endings. They are not associated with specialized structures and are present in both hairy and glabrous skin.

Due to the presence of both fibres types, pain is sensed in two distinct phases: an initial sharp pain followed by a more prolonged and slightly less intense pain, known as second pain. The first pain is the earliest sensation of injury, which is transient and it is accompanied by reflexes that cause rapid withdrawal from the noxious stimulus (Lewis and Pochin, 1937; Fields 1987). The sensation of sharp pain is mediated by the fast-conducting Aδ fibres that carry information from damaged

thermal and mechanical nociceptors. The second pain develops slowly, over a period of several seconds and it persists well after the disappearance of the noxious stimulus. It is transmitted by C-fibres that convey signals from polymodal nociceptors and that respond to mechanical but not thermal stimuli (Bessou and Perl, 1969; Cain et al., 2001).

Aδ-HTMRs contact second-order neurons that are predominantly found in the lamina I and V of the spinal cord, whereas C-HTMRs terminate in laminae I and II. Second-order neurons in the dorsal horn send their axons across the midline to ascend within the white matter on the contralateral side of the spinal cord, forming the anterolateral system, and they terminate in the thalamus and brainstem. Here they synapse with third-order neurons that send their axons to the somatosensory cortex.

HTMRs are normally only activated by stimuli that are strong enough to cause tissue damage. However, inflammatory responses evoked by tissue injury or diseases may also sensitize nociceptors, decreasing their threshold for activation. Thus, the sensitization process can give rise to alterations in the pain pathway, resulting in hypersensitivity. Consequently, some innocuous stimuli can provoke a painful reaction (a phenomenon known as allodynia), or mild painful stimuli may provoke an exacerbated feeling of pain (hyperalgesia).

1.3.4 ***Proprioceptors***

Proprioceptors, which include muscle spindles, Golgi tendon organs and joint receptors, provide information concerning three-dimensional movement and the position of the body in space. This is information that is required to maintain effective balance, posture and general locomotive movement under ever-changing internal and external conditions (Lam and Pearson, 2002).

The most detailed knowledge of proprioception has been derived from studies of *muscle spindles,* which detect changes in muscle length. A diagram of their structure is shown in Figure 7. These spindles consists of several collagen encapsulated bundles of specialized muscle fibres, called intrafusal fibres, and they are distributed among and parallel to the extrafusal fibres. Sensory afferents are coiled around the central part of the intrafusal spindle and, when the muscle is stretched, the tension

placed on the intrafusal fibres stimulates mechanically activated ion channels in the nerve endings, triggering action potentials. Two classes of fibres innervate the muscle spindle: primary and secondary endings. Primary endings (Group Ia afferents) produce RA responses and transmit information about the velocity and direction of movement, whereas secondary endings (Group II afferents) produce SA responses to constant muscle length and they transmit information about the static position of limbs. Moreover, the intrafusal fibres are controlled by a separate set of motor neurons, the Aδ motor neurons which terminate and form motor end plates towards the lateral edges of the fibres (Brown, 1981; Matthews, 1964).

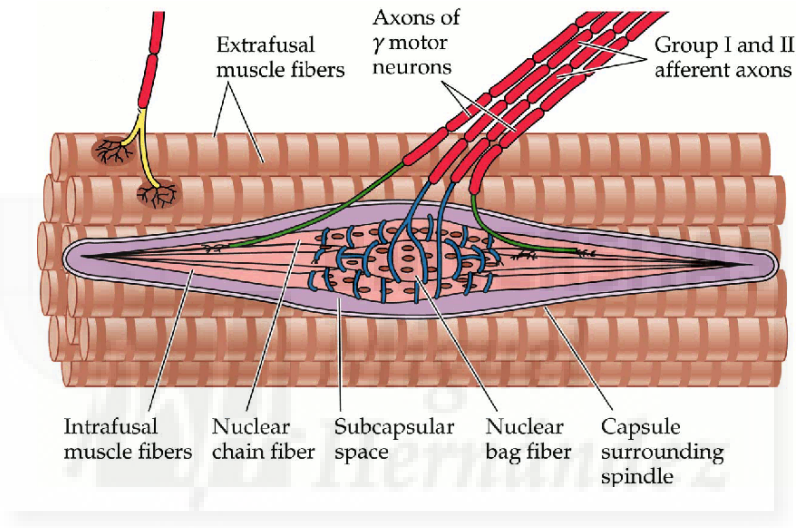

Figure 7. Diagram of a muscle spindle, the sensory receptor that detect changes in muscle length. Muscle spindles are sensory receptors embedded within most muscles. The spindles comprise eight to ten intrafusal fibres arranged in parallel with the extrafusal fibres that make up the bulk of the muscle. Two classes of sensory fibres innervate the muscle spindle: group Ia and group II afferents, that are coiled around the central part of the intrafusal fibres and mediate very rapid reflex adjustments when the muscle is stretched. Aδ motor neurons also terminate in muscle spindles, regulating the sensitivity of the sensory afferents. Source: Purves D., Neuroscience, 3rd Edition (2004).

Whereas muscle spindles have specialized to detect changes in muscle length, *Golgi tendon organs* provide information about changes in muscle tension, particularly the forces on the tendon generated by the contraction of skeletal muscle fibre. Golgi tendon organs consist of collagenous strands connected at one end to a muscle fibre, while the opposite end is inserted into the tendon itself. Thus, while muscle spindles are aligned parallel to skeletal muscle fibres, Golgi tendon organs are arranged in series with extrafusal fibres. This anatomical arrangement, coupled with sensory innervations, is what distinguishes the types of information provided to the

spinal cord by these specialized sensory receptors. These mechanoreceptors are innervated by Group Ib afferents that are distributed among the collagen fibres that form the tendons (Houk and Henneman, 1967; Moore, 1984).

1.4 Gating models of mechanotransduction channels

As explained above, the richness of the mechanosensory experience is mediated by the wide variety of highly specific mechanoreceptor cells. Each receptor responds to a specific kind of mechanical energy and in some cases only to energy with a particular temporal or spatial pattern. Thus, cells detect forces ranging from tiny touch signals, like the brush of a feather on the skin, to large pressure changes, such as those affecting blood vessels. However how these mechanical stimuli are transduced by ion channels remains a matter of debate It is unclear whether mechanotransducer channels are gated by directly sensing mechanical forces, such as membrane stretching or pressure, or via a downstream signalling pathway.

Several criteria have been established to consider whether a candidate protein is directly activated by the mechanical stimulus. Firstly, mechanotransduction needs to be fast and hence, ion channels are gated directly by mechanical forces and they open very rapidly with a latency of less than 5 milliseconds (Gillespie and Walker, 2001). This process was first observed in the movement of bullfrog hair cells, which produce an electrical response within 40 μs (Corey and Hudspeth, 1979). This interval is shorter than that measured in light-stimulated channels in the vertebra retina, which involves a chemical intermediate, suggesting that transduction is too fast to involve a chemical intermediate and that the fast electrical response is a consequence of the direct gating of a transduction channel.

Secondly, mechanotransduction requires a high degree of sensitivity to discriminate between different grades of mechanical force; increases in mechanical stimuli are associated with a corresponding increase in the kinetics of channel activation, which in turn result in a graded receptor potential.

Thirdly, mechanotransduction should involve a mechanical correlate of channel gating, such as an observable movement or change in mechanical force, in the sensory cell or organ over the same range of stimuli that induce channel opening. Channel opening causes an increase in the area of the membrane and subsequent relaxation of

the lipid bilayer. The relaxation of lipid surface tension thereby constitutes the mechanical correlate of channel gating.

Fourthly, the channel must be necessary for the electrical response of the sensory cell to the mechanical stimulus. Thus, the candidate channel should be localized to the correct cells and at the site of mechanotransduction within the cell, and it must be expressed in the cells by the time during development that the mechanically sensitive current is detected. Therefore, blocking channel expression by knockdown or knockout should block the mechanically activated conductance.

Fifthly, mechanical forces must gate the channel expressed in other cells, *i.e.* in an heterologous system or in a lipid bilayer, and the gating should recapitulate the mechanically activated current observed in its native environment. This criterion is quite difficult to demonstrate, especially if force is conveyed to the channel by structural proteins that are present only in the sensory cells.

Sixthly, if the candidate protein is a pore-forming subunit, the pharmacology and permeation properties of the MA conductance, observed in the heterologously expressed candidate, should be similar to those observed in the sensory cells.

Finally, to demonstrate that the candidate protein is a force-sensing subunit, the native conductance should be altered when the candidate protein is mutated or overexpressed in the sensory cells (Ernstrom and Chalfie, 2002; Christensen and Corey, 2007).

Different models have been proposed to explain the activation mechanisms of mechanosensitive channels. They are shown schematically in Figure 8. The first model proposes direct activation of mechanosensitive channel in response to changes in lipid bilayer tension (Figure 8A). These channels are found throughout a broad range of bacterial and eukaryotic cell types and they belong to structurally distinct ion-channel families (Kung, 2005). The second model proposes activation through the tethering of the channel to the extracellular matrix or the intracellular cytoskeleton, whereby the tension generated by this tether controls channel gating (Figure 8B; Gillespie and Walker, 2001; Christensen and Corey, 2007; Hu et al., 2010). The tether model emerged from studies of mammalian hair cells of the inner ear (Jiang et al., 2002), where stereocilia, specialized microvilli arranged in a height-dependent manner, are the site of mechanotransduction. Thus, each level of stereocilia is

connected to the one above it by a sprig protein strand called the tip link, which is proposed to be in series with the gating spring that opens mechanotransuction channels when hair bundles move. A third possibility is that mechanotransduction channels sense force indirectly as part of a signalling pathway lying, downstream of the mechanotransduction complex (Figure 8C). In this scenario, the force sensor in the receptor's cell membrane must be distinct from the ion channel and, accordingly, the ion channels are mechanically sensitive but not mechanically gated (Christensen and Corey, 2007). For example, in polymodal sensory neurons of *C. elegans*, activation of the transduction channel may require the production of lipid metabolites (Kahn-Kirby et al., 2004). One characteristic of such indirect mechanisms is that they are intrinsically slower than direct mechanical gating, which has led to some controversy as to the validity of the indirect gating model (Lumpkin and Caterina, 2007). Moreover, these gating mechanisms are not mutually exclusive and they may coexist in a given cell.

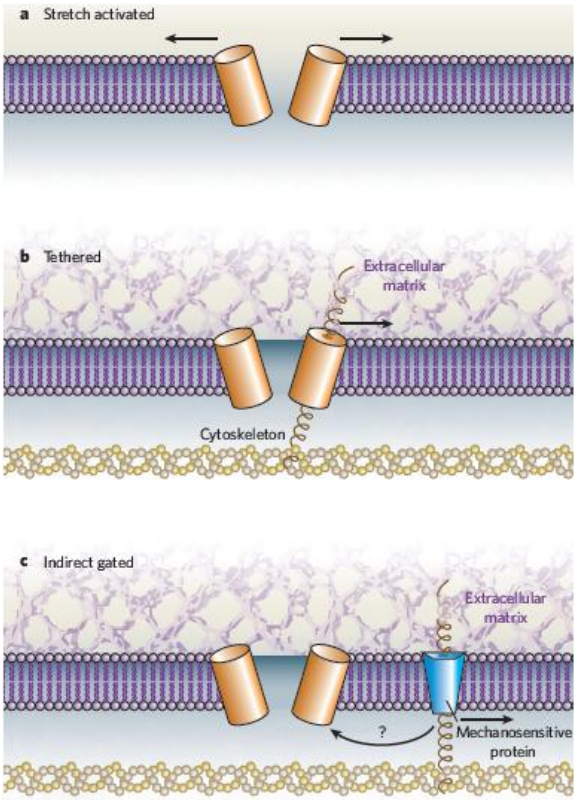

Figure 8. Proposed models by which a mechanotransduction channel may be gated by mechanical stimuli. (A) *Stretch-activated channel model*. Mechanical force creates tension in the lipid bilayer inducing a conformational change of the channel complex and direct activation of the channel. (B) *Tethered model.* Accessory proteins, such as extracellular matrix or cytoskeletal elements, are bound to the channel itself. Mechanical force is transferred by these proteins directly opening the channel. (C) *Indirect gating model.* The putative channel is not directly gated by mechanical force but it is regulated by mechanosensitive proteins that control channel opening through a signalling intermediate. These transduction proteins may require tethers or may respond to changes in the lipid bilayer. Source: Lumpkin and Caterina, 2007.

1.5 Experimental strategies to study mechanotransduction

As mentioned above, the local depolarization caused by mechanical forces can trigger action potential firing in the primary sensory neuron that is propagated towards the CNS. It is thought that local receptor potentials are generated by the activation of excitatory ion channels that depolarize the terminal. Complete characterization and identification of mechanosensitive channels has been hampered by several obstacles. Firstly, due to the small size and inaccessibility of sensory nerve endings, direct recording of transduction channel activity *in situ* has not been achieved. Secondly, mechanosensitive channels are typically expressed weakly, making them difficult to identify using biochemical approaches (Arnadottir and Chalfie, 2010). Thirdly, it is difficult to functionally express mechanosensitive

channels in heterologous systems as some mechanosensitive channels need to be tethered to the cytoskeleton and/or extracellular matrix to function correctly, and they may also depend on auxiliary subunits, conditions that are difficult to reproduce in a heterologous system especially when these components are unknown (Gillespie and Walker, 2001). Lastly, the biophysical properties of mechanosensitive channels recorded from different cell types reveal large variations, suggesting that the molecular nature of mechanosensitive channels is highly heterogeneous (Arnadottir and Chalfie, 2010).

The skin-nerve preparation is a useful technique to characterize mechanotransduction events in a more native setting. This technique involves the removal of a section of skin from the hind limb of a mouse or rat with a portion of the nerve still attached (Kress et al., 1992; Reeh, 1986). Recordings from several axons of individual neurons allow neuronal types to be characterized based on conduction velocity and adaptation processes. The advantage of this technique is that the intact terminal structure is maintained. However, recordings are limited to firing rates and ionic currents in nerve endings are not characterized. Sensory endings in the skin are too small to be accessed by electrophysiology and most types of endings terminate in the dermis rather than the epidermis, complicating access.

The extracellular recording of nerve terminal activity in the cornea is another useful technique to study mechanotransduction and to investigate the mechanical role of several channels. This technique was first developed by Brock and Belmonte in 1998 (Brock et al., 1998) and it was used to identify and characterize somatosensory receptors in the guinea pig cornea (Brock et al., 1998;Brock et al., 2001;Carr et al., 2002;Carr et al., 2003). Later on, the same technique was translated to the mouse to record the activity of single sensory nerve endings of the cornea, supplying functional properties of cold thermoreceptors (Parra et al., 2010).

Measuring the activity of mechanosensitive currents in acutely isolated sensory neurons offers an alternative means to study the properties and identities of mechanotransducer channels in mammalian sensory neurons. The soma of cultured sensory neurons has been used extensively as a model of transduction owing to the close similarities between the properties of the cell bodies in culture and those of the central and peripheral terminals, which cannot be accessed by patch-clamping (Julius

and Basbaum, 2001). In vivo, the channels are synthesized in the soma and are transported along the axon to the terminals. Thus, using the soma as a surrogate of the terminal is fully accepted as a valid tool to record tranduction channels in a native condition.

As I mentioned before, as mechanosensory channels are activated by multiple mechanisms therefore, recorded channels can be activated by different stimuli. Several types of mechanical stimuli have been used to study mechanosensory channels, including cell stretch, fluid shear stress, crenators and cup formers, osmotic challenge, magnetic particles and electrical driven mechanical probes. A schematic of these different strategies is shown in Figure 9. While all of these stimuli induce membrane deformation, each has the potential to activate different populations of MS channels.

Cell stretch can be induced using two different methods: surface elongation of the substrate (radial stretch) on which cells have been seeded (Bhattacharya et al., 2008) or application of positive or negative pressure to the patch membrane through a patch pipette (Bryan-Sisneros et al., 2003; Honore, 2007; Sharif-Naeini et al., 2009; Gomis et al., 2008).

Fluid shear stress can be induced by altering the perfusion flow, positioning a pressurized stream of bath solution close to the cell, or changing the viscosity of the perfusion solution (McCarter et al., 1999).

Osmotic challenges include challenge with hypotonic solutions that causes cell swelling, or hypertonic solutions that induce cell shrinkage. Osmotic stress causes cytosolic alterations, such as increases in intracellular calcium concentration, when using hypo and hypertonic solutions, and osmolyte exchange. The disadvantage of these approaches is that they alter the ionic strength and electrochemical equilibrium. This can be avoided by keeping the ionic concentrations constant during challenge and by adding (for hypertonicity) or omitting (for hypotonicity) the appropriate concentration of a neutral osmolyte such as D-mannitol or sucrose (Raoux et al., 2007). While the scientific community considers the membrane stress caused by osmotic variations a type of mechanical stimulus (Martinac, 2004), there is some debate as to whether cell swelling is an appropriate representation of the mechanical stimuli experienced by somatosensory neurons *in vivo.* In fact, osmotic stress does not create uniform tension in the cell membrane and it is associated with

cytosolic alterations, complicating data interpretation (Sachs, 2010). However, osmotic stress can be used to deliver stimuli to large cohorts of cells, and the responses monitored allowing direct comparisons to be made between sensory neuron subtypes under identical conditions, thereby facilitating quantitative population studies. Moreover, in this experimental setting, cells are readily accessible for pharmacologic manipulation and mechanical stimuli can be delivered over a wide and graded range of intensities, allowing for relatively detailed dose-response analysis.

Crenators and cup formers are amphipathic compounds that cause changes in cell shape, as explained by the 'bilayer couple theory' (Sheetz and Singer, 1974). This theory assumes that, in a cell at resting potential, charged amphipathic compounds accumulate preferentially in one half of the lipid bilayer (negatively charged compounds in the outer layer, positively charged compounds in the inner layer) and induce membrane curvature in opposite directions (crenation or cup formation). Arachidonic acid, general anaesthetics and lysophospholipids act as amphipathic compounds and can modify the gating of ion channels (Patel et al., 1999; Patel et al., 2001; Perozo et al., 2002).

Magnetic particles can be coated with specific ligands, allowing them to bind to receptors on the cell membrane. Like the magnetic twisting and magnetic tweezers techniques, application of a magnetic field pulls on the particles, delivering nanoscale forces at the ligand-receptor bond (Sniadecki, 2010).

An electrically driven mechanical probe is used to apply focal force to the plasma membrane. The probe used is a heat-polished glass pipette with a tip diameter of 3-5 μm and driven by a micromanipulator system. The mechanical probe is typically positioned at a 45-65º angle from the horizontal plane and it is driven by software that allows several parameters to be controlled, such as the velocity, intensity and duration of the mechanical stimulus (Figure 9B). Several research groups have used this strategy to study MA currents while simultaneously performing electrophysiological recordings ("mechano-clamp"), stimulating the soma of sensory neurons (Drew et al., 2002; Di et al., 2006; McCarter et al., 1999; McCarter and Levine, 2006; Lechner et al., 2009; Rugiero and Wood, 2009; Rugiero et al., 2010; Vilceanu and Stucky, 2010; Coste et al., 2010) or the neurites (Hu and Lewin, 2006; Wetzel et al., 2007; Lechner and Lewin, 2009; Hu et al., 2010; Brierley et

al., 2011). This form of mechanical stimulation can also be used in conjunction with calcium imaging and provides a high level of control of the parameters of mechanical stimulation. By contrast, piezo-driven mechanical stimulation is limited to single-cell assays and the applied force is quantified by indirect measurement.

A B

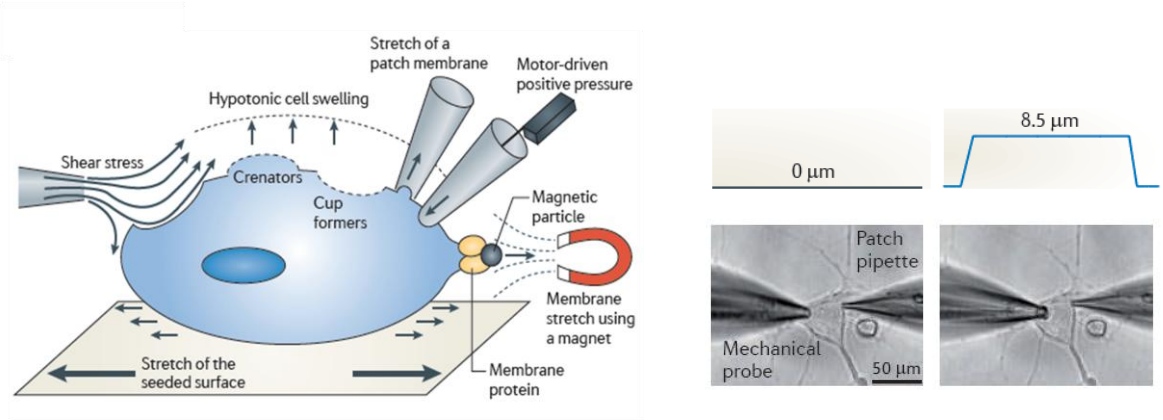

Figure 9. Strategies to induce mechanical stimulation at cellular level. Several techniques have been developed to activate mechanosensitive channels. All induce membrane deformation but each technique can recruit different populations of mechanosensitive channels. (A) Cell stretch, fluid shear stress, crenators and cup formers, osmotic stretch and magnetic particles. (B) The mechano-clamp technique permits the recording of ion channel currents during stimulation with an electrically-driven mechanical probe. Adapted from Delmas et al., 2011.

1.6 The molecular basis of mechanotransduction

Research in genetics, genomics and electrophysiology has converged to further our understanding of mechanosensitive channels in vertebrates and invertebrates. The first mechanosensitive ion channel identified, MscL, was cloned from the bacteria *Escherichia coli.* Activity assays in reconstituted liposomes revealed that the channel opens at a pressure of ~ 100mmHg and has a conductance of 3 pS (Sukharev et al., 1994). Thus, this channel opens in response to high membrane tension and mediates the response to osmotic shock in bacteria. Since the discovery of MscL, several bacterial and fungal mechanosensitive channels have been identified, all of which are gated by bilayer tension (Anishkin and Kung, 2005).

Mechanotransduction in multicellular organisms appears to be more complex than in bacteria. Three main classes of ion channels have been implicated in mammalian somatosensory mechanotransduction: DEG/ENaCs, KCNK subunits and TRP channels (Figure 10A).

Degenerin/epithelial sodium channels (DEG/ENaCs) form a group of voltage-insensitive Na^+ channels that can be blocked by amiloride (Kellenberger and Schild, 2002) and they are composed of two transmembrane domains, two short intracellular domains and a large extracellular loop (Figure 10B). The first **DEG** identified as a mechanosensitive channel was uncovered in studies on the nematode *C. elegans*, when a mechanosensitive channel complex formed by MEC-4, MEC-10, MEC-2 and MEC-6 was identified that senses gentle touch (Chalfie and Au, 1989). In this complex, MEC-4 and MEC-10 form the channel pore, while MEC-2 and MEC-6 are accessory subunits that link the channel to the cytoskeleton and extracellular matrix and that are required for channel function (Arnadottir and Chalfie, 2010; O'Hagan et al., 2005; Goodman, 2006).

Acid-sensing ion channels (ASICs) belong to a proton-gated subgroup of the DEG/ENaC family in mammals that is comprised of four members: ASIC1, 2, 3 and 4. Several studies suggest that the ASIC1, 2 and 3 channels participate in mechanotransduction, as explained below.

Interestingly, **ASIC1** knock-out mice show increased mechanical sensitivity of visceral sensory afferents but no changes in cutaneous mechanosensation (Page et al., 2004).

ASIC2 deletion affects the firing rate of a subset of low-threshold, rapidly adapting mechanosensors (Price et al., 2000) and it alters the baroreceptor sensitivity, decreasing baroreflex gain (Lu et al., 2009). By contrast, **ASIC3** deletion decreases the responses of cutaneous HTMRs to noxious stimuli and reduces the mechanosensitivity of visceral afferents (Price et al., 2001). Moreover, it has been shown that a stomatin-like protein 3 (SLP3), which is essential for the function of a subset of cutaneous mechanoreceptors in mice, associates *in vitro* with ASIC2 and ASIC3 (Wetzel et al., 2007) and inhibits the endogenous proton-gated currents in heterologous systems as well as in sensory neurons. Taken together these data strongly suggest a role of ASICs in mechanotransduction, possibly as important modulators, although the lack of evidence for mechanical gating of these channels suggests that ASICs do not themselves act as mechanotransducing channels (Lingueglia, 2007).

Two-pore-domain potassium (KCNK) channels form the family of two-pore domain K^+ channels. Since these channels can be opened independent of the membrane potential, they are central in setting the resting membrane potential. They

contain four transmembrane segments, two pore-forming domains and intracellular amino (N) and carboxyl (C) termini (Figure 10B; Dedman et al., 2009). Several KCNK channels are expressed in somatosensory neurons (Medhurst et al., 2001). **TREK1**, also known as KCNK2, is expressed in a subset of C-fibre nociceptors and it is activated by pressure and heat (Alloui et al., 2006). Mice lacking TREK1 show decreased mechanical and thermal hyperalgesia, indicating that this channel participates in sensitizing nociceptors (Alloui et al., 2006).

Two related K^+ channels, **TREK2** (also known KCNK10) and **TRAAK** (also known as KCNK4), are also activated by membrane stretch and membrane crenation (Maingret et al., 1999; Bang et al., 2000; Kang and Kim, 2006).
Because the opening of these K^+ channels results in neuronal hyperpolarization rather than depolarization, it is unclear whether these channels function as transducers of mechanical stimuli or as regulators of neuronal excitability.

Transient Receptor Potential (TRP) channels constitute a large superfamily of cation selective channels that are activated by several chemical and physical stimuli, and some of them have been suggested as mechanotransducer channels. TRP channels were discovered in 1969, when a *Drosophila* mutant showed a transient instead of a sustained response to bright light when photoreceptors were exposed to continuous intense light (Cosens and Manning, 1969). The mutant was later named *trp* (for transient receptor potential) after this phenotype (Minke et al., 1975). Two decades later the *trp* gene was cloned (Montell and Rubin, 1989) and TRP proteins were proposed as ionic channels based on sequence homology with voltage-gated potassium channels (Hardie and Minke, 1992), leading to speculation that TRP was a Ca^{2+}-permeable cation channel. In the last decades it has been widely demonstrated that these proteins play an important role in numerous somatosensorial transduction processes including thermosensation, mechanosensation, pheromone reception, taste, phototransduction and nociception (Clapham, 2003; Voets et al., 2005; Gees et al., 2012; Foster, 2005).

The basic architecture of a TRP channel has been demonstrated by Julius's group through an electron cry-microscopy technique and revealed a tetrameric structure for TRPV1 (Figure 10B), with four-fold symmetry around a central ion

pathway formed by transmembrane segments 5-6 (S5-S6) and the intervening pore loop, which is flanked by S1-S4 voltage-sensor-like domains (Liao et al. 2013).

Based on amino acid homology, the TRP superfamily can be divided into seven subfamilies (Venkatachalam and Montell, 2007): TRPC, TRPV, TRPM, TRPA, TRPN, TRPP and TRPML. The C, V, M and A families are structurally much more similar to one other than to the P and ML families, which stand alone as separate subfamilies (Birnbaumer et al., 2003). The TRPC subfamily contains proteins with the greatest homology to the *Drosophila* TRP protein (´C` stands for canonical or classical) and consists of seven different channels (TRPC1-7). The other subfamilies are named after their first identified members. Thus the TRPV subfamily, consisting of six members (TRPV1-TRPV6), was named after the identification of vanilloid receptor 1 (VR-1, known as TRPV1). The TRPM subfamily, containing eight different channels, was named after the identification of tumor suppressor melastatin 1 receptor (TRPM1), which was first identified in melanoma metastasis (Duncan et al., 1998). The TRPA subfamily, which contains only one member in mammals, is named after a protein denoted ankyrin-like with transmembrane domain 1 (TRPA1 formerly ANKTM1), due to the presence of a large ankyrin repeat domain in the amino-(N) terminus. The TRPN subfamily, named after identification of *no mechanoreceptor potential C* (*nompC*) gene, is not expressed in mammals, but it is found in *C.Elegans*, *Drosophila* and *zebra fish*. The TRPP family contains 3 members and it was named after the identification of polycystic kidney disease-related protein 2 (PKD2 or TRPP2). Finally, the TRPML superfamily contains three members and it was named after the identification of mucolipin 1 receptor (TRPML1), which is implicated in the inherited disorder Mucolipidosis type IV.

TRP channels are found in almost all eukaryotes (Xiao and Xu, 2009) and nearly all subfamilies of these channels contain members that are involved in mechanosensation in a variety of cell systems (Christensen and Corey, 2007; Eijkelkamp et al., 2013), as discussed in the following paragraphs.

TRP channels in mechanotransduction

In *Drosophila melanogaster*, mutations in the *nompC* gene, which encodes the **TRPN1** channel, and it is involved in touch, hearing and proprioception, result in deficiencies in bristle mechanotransduction (Kernan et al., 1994; Walker et al., 2000).

While TRPN1 is an excellent candidate for a mechanotransduction channel in flies and fish, *nomp-C* homologues have not been found in the mammalian genome (Sidi et al., 2003; Shin et al., 2005; Li et al., 2006).

In *C. Elegans* two members of the TRPV subfamily, **OSM-9** and **OCR-2,** are required for avoidance of nose touch, high osmolarity and chemical stimuli and they are co-expressed in ciliated mechanosensory endings (Colbert et al., 1997; Tobin et al., 2002; Kahn-Kirby and Bargmann, 2006; Kim et al., 2003).

The OSM-9 mammalian orthologue **TRPV4** is indirectly activated by cell swelling (Vriens et al., 2004) and it is involved in touch responsiveness. In fact, TRPV4 knock-out mice do not regulate their osmotic equilibrium as well as wild-type counterparts do (Liedtke and Friedman, 2003) and they show a reduced sensitivity to noxious mechanical stimuli (Brierley et al., 2008). TRPV4 is therefore important in regulating the response of nociceptive neurons to osmotic stimuli and to mechanical hyperalgesia during inflammation (Liedtke et al., 2000; Alessandri-Haber et al., 2004).

Some evidence has implicated other vertebrate TRPV channels in mechanosensation. For example, **TRPV1** is expressed in the bladder epithelia and TRPV1 knock-out mice show defects in bladder voiding (Birder et al., 2002), a process mediated by TRPV1 located in urothelial cells (Birder et al., 2001).

TRPV2 is expressed in aortic myocytes and it can be activated by membrane stretch and hypotonic stimulation (Muraki et al., 2003; Beech et al., 2004).

Several TRPC members are implicated in mechanosensation and in sensing the local cellular environment. **TRPC1** channels also contribute in mechanotransduction and stretch-activation (Hillyard et al., 2010; Maroto et al., 2005; Staaf et al., 2009). Recently it has been shown that TRPC1 contributes to mechanosensation mediated by D-hair Aδ and SA-Aβ fibres that innervate Merkel cells and are limited to afferents that are typically involved in the response to innocuous touch (Garrison et al., 2012). However, pressure-induced constriction of cerebral arteries in smooth muscle cells is unaffected in TRPC1 knock-out mice, indicating that TRPC1 is not an obligatory component of stretch-activated ion channel complexes in vascular smooth muscle (Dietrich et al., 2007).

TRPC6 is also activated by mechanically and osmotically induced membrane stretch (Spassova et al., 2006). TRPC6 knock-out mice show increases in vascular smooth muscle contractility and blood pressure. The loss of TRPC6 expression

appears to induce a compensatory upregulation of TRPC3 and TRPC7, which exhibit higher basal activity (Dietrich et al., 2005). Moreover, recent findings support a role of TRPC6 and **TRPC3** in low-threshold mechanical responses in DRG neurons (Quick et al., 2012).

TRPC5 is directly activated by lysophospholipids (Flemming et al., 2006), suggesting that this channel is sensitive to the structure of the lipid bilayer. TRPC5 is also present in baroreceptors (Glazebrook et al., 2005), which sense arterial pressure and it is thus a good candidate to mediate mechanosensation. A recent study found that TRPC5 is activated by hypo-osmotic and pressure-induced membrane stretch and that this activation is associated with PLC-independent increases in cytosolic Ca^{2+} concentration (Gomis et al., 2008). The stretch activation of TRPC5 involved a delay of several seconds after application of pressure, leading the authors to propose possible coupling between the channel and a force-sensing mechanism. Furthermore, TRPC5 hypo-osmotic activation is prevented by the spider toxin GsMTx-4 (Gomis et al., 2008), a blocker of stretch-activated channels (Suchyna et al., 2000; Park et al., 2008).

TRPM3 channel, on the other hand, is activated by cell swelling when transfected into HEK cells (Grimm et al., 2003).

Finally the **TRPA1** channel has also been implicated in mechanosensation. Given the focus of this thesis on the role of this channel, a more extensive review of the properties of this polymodal ion channel is presented in the following section.

1.6.1. *TRPA1 as a mechanosensitive channel*

TRPA1 was initially identified as a noxious cold sensor activated by cold temperatures below 18ºC (Story et al., 2003), although the cold sensitivity of TRPA1 has been questioned by some authors (Nagata et al., 2005; Bautista et al., 2006). TRPA1 is also considered one of the most important chemosensors as it can be activated by several natural compounds such as allyl isothiocyanate, the pungent compound found in mustard oil and wasabi (Jordt et al., 2004), allicin from garlic (Bautista et al., 2005), cinnamaldehyde from cinnamon (Bandell et al., 2004), menthol (Karashima et al., 2007), tetrahydrocannabinoid from the cannabis plant (Jordt et al., 2004) and nicotine (Talavera et al., 2009). TRPA1 is also activated by endogenous substances that are released after inflammation (Macpherson et al., 2007), oxidative stress (Trevisani et al., 2007) and tissue damage (Macpherson et al., 2007). Co-

expression studies in sensory neurons have linked TRPA1 expression with that of nociceptive markers. In fact, TRPA1 is expressed in small-diameter to medium-diameter neurons and almost all TRPA1-positive neurons express calcitonin gene-related peptide (CGRP), substance P, and the TRPV1 channel (Nagata et al., 2005; Story et al., 2003; Kobayashi et al., 2005).

Moreover, it seems that TRPA1 is involved in mechanotransduction. *Drosophila* larvae that lack *painless*, the invertebrate orthologue of TRPA1, show reduced mechanical nociception (Tracey et al., 2003). Moreover, the *C. elegans* orthologue of mammalian TRPA1 is expressed in some mechanosensory neurons and it is involved in the touch responses of these cells (Kindt et al., 2007).

In vertebrates, TRPA1 was initially proposed as a strong candidate for the hair cell transduction channel (Corey et al., 2004). This proposition was based on three main observations: TRPA1 is expressed in the hair cells of both the cochlea and vestibular system; TRPA1 messenger RNA transcripts appear on embryonic day 17, matching the onset of mechanotransduction, and, most importantly, disruption of TRPA1 expression in zebrafish with morpholino oligonucleotides and in mice with small-interference RNA strongly inhibits hair cells mechanotransduction.

However two different TRPA1$^{-/-}$ mouse lines have normal hearing or vestibular function (Kwan et al., 2006; Bautista et al., 2006), ruling out the fundamental role of TRPA1 as the long sought hair cell mechanotransducer. Still, other findings suggested a possible role of TRPA1 in mechanotransduction. Indeed, only one of the two lines of TRPA1 knock-out mice exhibit pain hyposensitivity, as indicated by their higher mechanosensory pain thresholds with respect to TRPA1$^{+/+}$ mice and reduced responses to supra-threshold stimuli (Kwan et al., 2006). Recordings from skin-nerve preparations from TRPA1 $^{-/-}$ mice have also shown that the firing rate of C fibre nociceptors to mechanical stimuli is decreased by 50% compared to wild type controls (Kwan et al., 2009).

TRPA1 is required for visceral mechanotransduction in normal as well as inflamed afferents (Brierley et al., 2009). In dissociated DRG neurons genetic ablation of TRPA1 reduces specific mechanosensitive currents, suggesting that TRPA1 may constitute the molecular counterpart of these currents (Vilceanu and Stucky, 2010; Brierley et al., 2011).

The large ankyrin repeat domain in the N-terminal region seems to constitute the mechanosensitive component of this channel. It has been hypothesized that this domain can interact with the intracellular cytoskeleton, to which it confers elasticity, and that it act as a spring to open TRPA1 when under mechanical stress (Corey et al., 2004; Sotomayor et al., 2005).

Altogether, these findings suggest that the TRPA1 channel plays a role in mechanosensation although it remains to be determined whether TRPA1 channel acts as a mechanotransducer channel or if it indirectly participates in mechanosensation by amplifying or modulating the signal from the transduction channel.

1.6.2 *Other mechanosensory proteins*

Piezo proteins, a recently identified novel protein family, are required for evoking mechanically activated currents in a mammalian cell line (Coste et al., 2010). These are large integral membrane proteins with 24-36 predicted transmembrane domains, three large extracellular loops and cytoplasmic amino (N) and carboxyl (C) termini and they display little structure homology to other ion channels (Figure 10B). Two Piezo proteins are expressed in vertebrates, **Piezo1** and **Piezo2** (also called FAM38A and FAM38B), where they are found in several tissues including the bladder, colon and lung. While Piezo2 is abundant in the DRG, Piezo1 is barely expressed in this structure. Overexpression of Piezo1 or Piezo2 in heterologous systems produces mechanosensitive cation currents that are inhibited by gadolinium, ruthenium red and GsMTx4, three known inhibitors of many stretch activated channels (Bae et al., 2011). It was recently demonstrated that *Drosophila melanogaster* Piezo (DmPiezo) and mouse Piezo1 (MmPiezo1) proteins are pore-forming ion channel that induce mechanically activated currents in cells lines. The MmPiezo1 protein weigh ~1.2 million Daltons with 120-160 transmembrane segments which seems to be the largest plasma membrane ion channel complex identified, (Coste et al., 2012). Even more recently, it has been demonstrated that Piezo2 is required for mechanotransduction in Merkel cells, being the first line of evidence that Piezo channels have a physiological role in mechanosensation in mammals (Woo et al., 2014; Ikeda et al., 2014).

Several different **voltage-gated sodium channels (VGSC)** are also involved in mechanotransduction. At resting membrane potentials, VGSCs are closed, requiring depolarization to be activated. Upon activation, they play a critical role in the initiation and propagation of action potentials in neurons and other excitable cell types. They consist of a large α subunit that contains four repeat domains, each with six membrane-spanning segments. One α subunit alone is sufficient to form a functional channel. However α subunits associate with other proteins, such as the β subunit, which modulates the channels biophysical properties and trafficking. The VGSC family can be divided into nine subfamilies, NaV1.1 to NaV1.9, two of which are involved in mechanotransduction.

NaV1.7 knock-out mice exhibit a loss of acute noxious mechanosensation and inflammatory pain. Conversely, gain-of-function mutations in the gene codifying NaV1.7 lead to pain hypersensitivity (Nassar et al., 2004; Cox et al., 2006). Moreover, behavioral studies in mice in which **NaV1.8** expressing sensory neurons were ablated show loss of the response to noxious cold and noxious mechanical stimuli (Abrahamsen et al., 2008).

Apart from the specific proteins described above, accessory proteins linked to the transduction channel are also implicated in touch sensitivity. In fact genetic deletion of shared auxiliary subunits may reveal more severe deficits in the response to touch as these proteins can affect the function of multiple channel-forming subunits. This is the case with the stomatin-like protein **(SLP3)**, a mammalian MEC-2 homologue expressed in mammalian DRG neurons. As mentioned above, SLP3 binds to both ASIC2 and ASIC3, altering their activity. Moreover, SLP3 knock-out mice show a decrease in the proportion of mechanically sensitive Aβ and Aδ fibres that innervate the skin and in the proportion of dissociated DRG neurons with mechanosensitive currents (Wetzel et al., 2007; Martinez-Salgado et al., 2007). Although the role of SPL3 remains unknown, this protein may constitute a link between transduction channels and the intracellular cytoskeleton, as proposed for its homologue MEC2 (Huang et al., 1995).

Despite the breakthroughs made in identifying sensory mechanotransduction channels, many outstanding questions and controversies regarding the molecular basis and mechanisms of mechanotransduction remain to be resolved.

Table 1 gives an overview of the main ion channels involved in mechanosensation, indicating their sites of expression and the types of mechanical stimuli by which they are activated.

A B

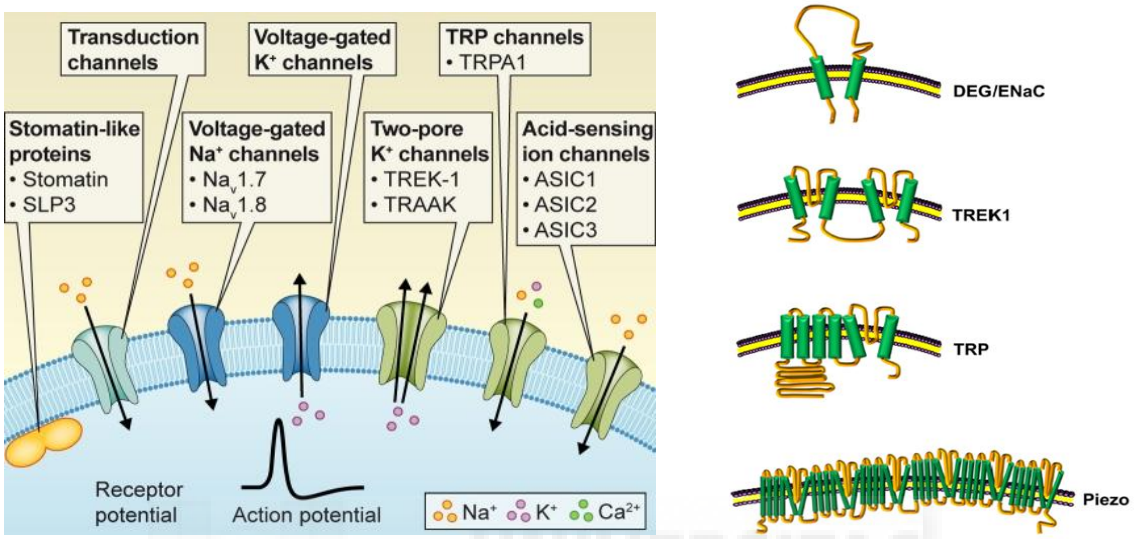

Figure 10. Ion channels implicated in mammalian somatosensory mechanotransduction. (A) Transduction channels (cyan) convert the stimulus into receptor currents through the opening of voltage-activated sodium and potassium channels (blue), and in the generation of action potentials. Other channels (green), such as ASICs, and KCNK and TRP channels, are sensitive to mechanical stimuli that can modify the signal or set membrane excitability. Stomatin-like proteins (yellow) are accessory subunits that link the channel to the cytoskeleton and extracellular matrix, altering touch sensitivity. Source: Lumpkin et al., 2010. (B) Scheme of mechanosensitive channels in eukaryotes. Only one subunit is shown for each channel. The membrane topology shown for Piezo is one of several possible topologies. Source: Xiao and Xu, 2010.

Table 1. Mechanosensitive channels in different organisms

Name	Family	Organism	Mechanosensitivity
MscL	MscL	Bacteria	Osmolarity
MEC4-MEC10	DEG/ENaC	Nematode	Gentle touch
ASIC1	DEG/ENaC	Mammals	Visceral mechanoperception
ASIC2	DEG/ENaC	Mammals	Cutaneous and visceral mechanoperception
ASIC3	DEG/ENaC	Mammals	Cutaneous and visceral mechanoperception
TRPN1	TRPN	*Drosophila*/fish and amphibian	Touch and audition
OSM-9/OCR-2	TRPV	Nematode	Osmolarity, audition and touch
TRPV1	TRPV	Mammals	Stretch and osmolarity?
TRPV2	TRPV	Mammals	Stretch and osmolarity?
TRPV4	TRPV	Mammals	Noxious pressure, shear stress, osmolarity and stretch
TRPA1	TRPA	Mammals	Pressure, stretch, osmolarity and touch
TRPC1	TRPC	Mammals/*Xenopus*	Touch, stretch, osmolarity and shear stress
TRPC3	TRPC	Mammals	Gentle touch and audition
TRPC5	TRPC	Mammals	Osmolarity and pressure
TRPC6	TRPC	Mammals	Osmolarity, pressure, touch and audition
TRPM3	TRPM	Mammals	Osmolarity
TREK1	KCNK	Mammals	Touch
TREK2	KCNK	Mammals	Osmolarity
TRAAK	KCNK	Mammals	Osmolarity
Piezo 1-2	Piezos	Mammals	Static indentation
NaV1.7	VGSC	Mammals	Noxious touch
NaV1.8	VGSC	Mammals	Noxious touch

Adapted from Gees et al., 2012; Eijkelkamp et al., 2013.

1.7 Mechanosensitive currents in sensory neurons

As mentioned above, the development of techniques to study mechanotransduction has facilitated the investigation of the molecular and cellular bases of this process. Using the mechano-clamp technique, mechanically induced currents have been characterized in dissociated neurons.

Recording mechanosensitive currents in DRG neurons was first performed in the laboratory of Jon Levine in 1999, revealing that some sensory neurons exhibit mechanosensitive inward currents upon mechanical stimulation of the cell soma (McCarter et al., 1999). Subsequent studies corroborated these findings by stimulating both the cell soma and the neurites of sensory neurons (McCarter et al., 1999; Drew et al., 2002; McCarter and Levine, 2006; Lechner et al., 2009; Rugiero et al., 2010; Vilceanu and Stucky, 2010; Hu and Lewin, 2006; Coste et al., 2010).

These studies showed that neurons responded to the mechanical stimulus with currents with variable kinetics. Based on the kinetics of current decay, mechanically activated currents have been classified into 3 groups, illustrated in Figure 11: rapidly adapting (RA; $\tau < 10$ ms), intermediately adapting (IA; 10 ms $< \tau < 30$ ms) and slowly adapting currents (SA; $\tau > 30$ ms) (Hao and Delmas, 2010; Hu and Lewin, 2006; Roudaut et al., 2012).

Many authors have described correlations between different mechanosensitive currents and specific subsets of sensory neurons. Thus neurons with non-nociceptive phenotypes activated by low stimulus amplitude respond mainly with RA currents, whereas nociceptive neurons activated by high stimulus amplitude respond mainly with IA or SA currents. However, this correlation is not very stringent as RA currents are also observed in a subpopulation of nociceptive neurons and some non-nociceptive neurons display SA currents (Hu and Lewin, 2006; Hao and Delmas, 2010; Drew et al., 2002; Drew et al., 2004; Coste et al., 2007). It is possible that the RA and SA mechanosensitive currents activated *in vitro* constitute low and high-threshold mechanotransducers *in vivo,* respectively.

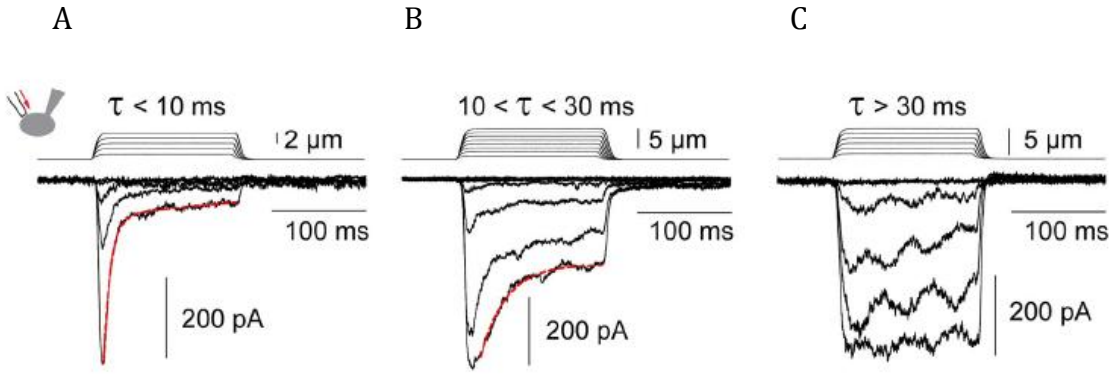

Figure 11. Classification of three distinct types of mechanosensitive currents in DRG sensory neurons. Representative traces of mechanosensitive rapidly-adapting (A), intermediate-adapting (B) and slowly-adapting (C) currents, recorded using the mechano-clamp technique from a holding potential of -60 mV. Time constants of current decay are indicated in each panel. Source: Coste et al., 2010.

Biophysical characterization of mechanosensitive currents has been carried out to determine whether the different kinetics of mechanosensitive currents are due to the activation of distinct populations of ion channels. Measurement of the reversal potential of RA, IA and SA currents revealed that this value ranges from -4 to 15 mV (Delmas et al., 2011), indicating that these are non-selective cation currents. Another study reported a very positive reversal potential of RA currents, +80 mV, indicating very high sodium permeability of this specific channel (Hu and Lewin, 2006).

Pharmacological tools have also been used to determine the pharmacological sensitivity of mechanically gated currents.

Lanthanide gadolinium (Gd^{3+}), a blocker of stretch-activated channels, blocks all MS currents in sensory neurons (McCarter et al., 1999; Drew et al., 2002; Hu and Lewin, 2006).

Ruthenium red, a pore blocker of some TRP (e.g. TRPV1, TRPV3, TRPV4 and TRPA1) and other cationic channels (Caterina et al., 1997), has inhibitory effects on MS currents (Drew et al., 2002; Drew et al., 2004). However, while some authors reported no significant effect on the amplitude of RA currents they did observe a clear reduction in the amplitude of SA currents (Hu and Lewin, 2006).

Amiloride and its analogue, benzamil, blockers of the Deg/ENaC family (Drew et al., 2004), partially block cationic MS currents at high (≥1mM) but not at low concentrations (McCarter et al., 1999; Drew et al., 2002; Coste et al., 2007). FM1-43, a dye commonly used to fluorescently label cell membranes, acts as a long-lasting

blocker of cationic MS channels (Drew and Wood, 2007), while HC-030031, a selective antagonist of TRPA1 channels, preferentially blocks SA (Vilceanu and Stucky, 2010) or IA currents (Brierley et al., 2011) rather than RA mechanosensitive currents.

The toxin GsMTx-4, which isolated from the tarantula and that block stretch-activated cation channels in cardiomyocytes, astrocytes and smooth and skeletal muscles (Suchyna et al., 2000; Bode et al., 2001), has no effect on either RA or SA mechanosensitive currents in DRG neurons (Drew and Wood, 2007), although it inhibits Piezo1 mechanosensitive currents (Bae et al., 2011).

Taken together, the distinct pharmacological profiles of cationic MS currents in sensory neurons indicate that there is considerable heterogeneity in the composition of channels that mediate different mechanically-activated currents.

In conclusion, the studies outlined above provide important insights into the mechanosensitivity of DRG neurons and the properties of mechanically-activated currents. However, similar studies of TG neurons have not yet been conducted. Here, I have used a multidisciplinary approach to characterize the mechanosensitivity of trigeminal neurons in order to elucidate the functional differences between subpopulations of nociceptive and non-nociceptive neurons. Moreover, this work shed light about the identity of the mechanotransducer channels that mediate the different mechanically-activated currents in specific populations of trigeminal neurons.

2. Aim of the study

The general aim of this thesis was to investigate the molecular mechanisms underlying the mechanical sensitivity of primary sensory neurons of trigeminal ganglia.

The specific goals were:

- To characterize the mechanical properties of individual trigeminal sensory neurons, classified according to their discharge pattern and action potential shape, sensitivity to tetrodotoxin and IB4 labelling, trying to establish functional differences between neurons that respond to innocuous (low threshold neurons) and to noxious (high threshold neurons) mechanical stimuli.
- To analyze the expression of candidate mechanotransducer channels in the different populations of neurons characterized in the first specific objective.
- To correlate the properties of the different subsets of mechanically activated trigeminal sensory neurons with the expression of the ion channels identified in the second specific objective.
- To study the potential role of the TRPA1 channel in mechanotransduction in trigeminal sensory neurons.

3. Materials and Methods

3.1 Trigeminal primary sensory neurons culture

All the experiments performed in the present study were carried out in compliance with rules of the Animal Experiment Committee at the University Miguel Hernández according to the Spanish (RD 53/2013) and European Union (2010/63/EU) regulations.

Newborn mice C57BL/6 (from P1 to P4) were sacrificed by decapitation and their trigeminal ganglia were excised. The ganglia were collected in ice-cold PBS solution (Sigma-Aldrich, St Louis, MO, USA), cut into small pieces and digested for 45 min at 37ºC in DMEM containing 0.25% collagenase (380 units/mg, type IA, Sigma-Aldrich, St Louis, MO, USA) with an atmosphere of 5% CO_2. The enzymatic digestion was stopped by diluting the solution to 5 ml with HBSS medium (Sigma-Aldrich, St Louis, MO, USA), containing 10% FBS (Life Technologies, Carlsbad, CA, USA) and ganglia were gently triturated 5-10 times through a fire-polished glass pipette. The cells were then recovered by centrifugation for 5 min at 201G and they were resuspended in 120 µl of culture medium, containing 45% DMEM (Sigma-Aldrich, St Louis, MO, USA), 45% F-12 (Sigma-Aldrich, St Louis, MO, USA), 10% FBS (Life Technologies, Carlsbad, CA, USA), 4 mM L-Glutamine (Life Technologies, Carlsbad, CA, USA), 200 µg/ml streptomycin, 125 µg/ml penicillin and 17 mM glucose. The neurons were then plated on round glass coverslips (6 mm) in a 35 mm Petri dish and they were maintained in a humidified incubator at 37 °C with an atmosphere of 5% CO_2. The coverslips had previously been coated with 0.01% poly L-lysine (Sigma-Aldrich, St Louis, MO, USA) for 20 minutes, washed three times with distilled water and dried. After a 2 hour incubation, 2 ml of fresh culture medium containing 100ng/ml NGF (Sigma-Aldrich, St Louis, MO, USA) was added to each Petri dish. TG neurons were used in experiments 18-24 h after plating.

The protocol used to culture trigeminal ganglion neurons from adult mice (P28–P35) was similar to that used for newborn mice, except for the following details. Mice were sacrificed by inhalation of CO_2, and they were then rapidly decapitated. The trigeminal ganglia were removed, collected in an ice-cold PBS solution and then incubated for 45-50 minutes in a mixture of collagenase type XI (0.66 mg/ml) and dispase (3 mg/ml), dissolved in a medium containing 155mM NaCl, 1.5mM K_2HPO_4, 5.6 mM HEPES, 4.8 mM NaHEPES and 5mM glucose. After mechanical

dissociation, the cells were cultured in medium containing 89% MEM, 10% FBS, 1% MEM vitamins (GIBCO,Life Technologies, Carlsbad, CA, USA) and 100µg/ml penicillin/streptomycin. After maintaining the cells for 2 hours, 2 ml of the same medium supplemented with 100ng/ml NGF was added in each plate. Coverslips were first coated with 0.01% poly L-lysine and they were then incubated for 50 min at 37 ºC with 1%/cm^2 laminin (Sigma-Aldrich, St Louis, MO, USA), subsequently drying them without washing. TG neurons were used 18-24 h after plating.

Trigeminal neurons cultures from null mutant mice for TRPA1 (on a C57BL/6 genetic background) were established in the same way as for wild type mice.

3.2 Bath solutions

The extracellular solutions used in the different experiments are detailed in table 2. For electrophysiological recordings I used the solution A. For calcium measurements, solutions of different osmolarities were employed: a control (solution A), an isotonic (solution B) and a 210 mOsml kg^{-1} solution (30% hypoosmotic; solution C). The osmolarity of each solution was measured using a cryoscopic osmometer (Gonotec, Berlin, Germany). In the solution B to maintain a constant ionic composition D-mannitol was added. A 30mM KCl solution (D) was used at the end of the recordings to check the healthiness of neurons.

Cells were continuously perfused in a low recording chamber with a complete solution exchange of 1 min. The perfusion could be switched to one of several test solutions via a multibarelled stopcock. All electrophysiological and calcium recordings were performed at a temperature between 32 and 34º C, controlled by a watercooled CL-100 Peltier device (Warner Instruments) placed directly on the cell field.

Table 2 List of solutions used in this study

	Solution A	Solution B	Solution C	Solution D
Components	Concentration (mM)	Concentration (mM)	Concentration (mM)	Concentration (mM)
NaCl	140	90	90	113
KCl	3	3	3	30
$CaCl_2$	2.4	2.4	2.4	2.4
$MgCl_2$	1.3	1.3	1.3	1.3
Glucose	10	10	10	10
Hepes	10	10	10	10
Mannitol	/	100	/	/
Osmolarities (mOsm)	317	317	217	317
PH= 7.4				

3.3 Fluorimetric calcium measurements

Intracellular calcium levels were measured through the fluorimetric analysis of fura-2AM (Williams et al., 1985; Moore et al., 1990; Viana et al., 2001). Accordingly, neurons were incubated for 45 min at 37ºC in darkness with the acetoxymethylester form of fura-2 AM (Life Technologies, Carlsbad, CA, USA) at a final concentration of 5 μM, and with 0.02% pluronic acid in the extracellular solution A (a non-ionic surfactant polyol that facilitate the solubilisation of the dye in physiological solutions).

Fluorescence measurements were obtained under a Leica inverted microscope (DMI3000B). Fura-2AM was excited at 340 nm and 380 nm with a computer controlled filter wheel (LAMBDA-LS, Sutter Instrument Company; USA) and the fluorescence emitted was long-pass filtered at 510 nm and detected with an Orca ER CCD camera (Hamamatsu Photonics, Japan). The ratio between fluorescence at the 2 different wavelengths ($F340/F380$) is directly related to the intracellular calcium concentration (Williams et al., 1985; Moore et al., 1990). Images were acquired at intervals of 1-3 seconds.

3.4 Electrophysiological recordings

Whole-cell patch clamp recordings, in voltage or current clamp mode were performed using a Multiclamp 700B amplifier (Molecular Devices Corp, USA), and currents and voltages were digitized with a Digidata 1322A (Molecular Devices Corp, USA). Data acquisition was performed using Clampex 9.0 software (Molecular Devices Corp, USA).

Patch pipettes were pulled from borosilicate glass capillaries (1.5 mm O.D. and 0.86 mm I.D.; Harvard Apparatus Ltd.) with a P-97 puller (Sutter Instrument Company, USA) to obtain a final resistance of 5–8 MΩ. A silver chloride wire (Ag/AgCl) was used as the reference electrode. Current was sampled at a frequency of 50 kHz and filtered at 6 kHz and, to minimize the voltage error, 70% of the series resistance was compensated.

After establishing whole-cell configuration with the voltage clamp circuit at −60 mV, neurons were studied in current clamp mode. Current injection was used to evoke action potentials (-80 to +200 pA in 20 or 50 pA increment for 200 ms).

The recording mode was switched back to voltage clamp to record mechanically activated inward currents at a holding potential of −60 mV. A positive response was considered when the amplitude of the current change was 2 times that of the baseline, which on average was 35 pA. The external solution corresponded to solution A (Table 2), while the pipette solution contained (in mM): 140 KCl, 9.6 NaCl, 4 MgATP, 0.4 NaGTP and 10 HEPES (pH 7.4).

3.5 Mechanical stimulation

Mechanical stimuli were applied using a heat-polished glass pipette with a tip diameter of 3-5 µm, measured with an ocular micrometer fitted to the microscope eyepiece and driven by MM3A Micromanipulator system (Kleindiek Nanotechnik, Germany). The pipette is positioned at an angle of 45 degrees to the surface of the coverslip. The micromanipulator system allows parameters such as intensity, velocity and duration of the mechanical stimulus to be controlled (Figure12A).

The micromanipulator is driven by a piezoelectric motor, a nanomotor that works in two modes: the “fine mode” and the “coarse mode”. The fine mode is used to

control the manipulator in extremely small steps for very fine movements and, thus, the maximum movement in fine mode corresponds approximately to 1000 nm (Hu and Lewin, 2006). In the coarse mode, the motor moves a slider very rapidly larger single step than the fine mode. All the experiments were performed in the coarse mode. The nanocontrol unit is controlled by NC9.04 software (Kleindiek Nanotechnik, Germany) and the single-step size was calibrated by instructing the motor to move a larger number of steps and measuring the total distance moved through the ocular micrometer fitted to the microscope eyepiece.

In all the experiments, the probe was initially positioned ~ 2μm from the cell body and the final approach, bringing it as close as possible to the membrane without touching it, was made immediately after membrane clamping. All subsequent movements were applied from this starting position, moving the probe forward in a step of 0.5 μm and then in steps of 1 μm, for 250 ms and then withdrawing it to the original starting position. If there was no response, the probe was moved forward again with an increase in amplitude and this procedure was repeated until a mechanically activated current was recorded. The largest stimulus applied was 15 μm. The stimuli were applied every 10 sec, to allow full recovery of the MA currents. The mechanical protocol used is represented in Figure 12B.

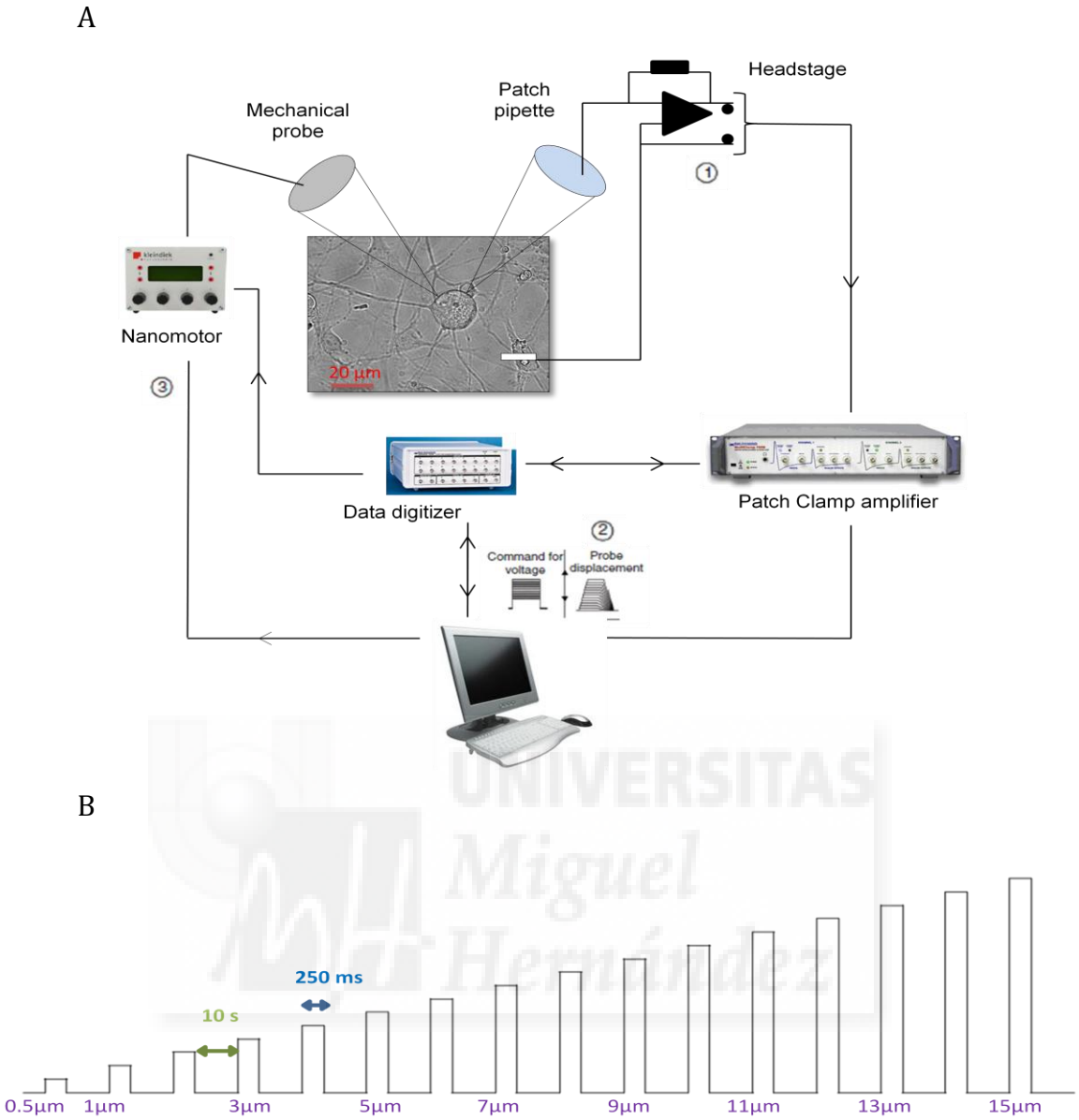

Figure 12. Schematic representation of the mechanical stimulation protocol used in this work (A) Schematic representation of the mechano-clamp circuit. (1) Dissociated sensory neurons are recorded using the patch-clamp technique. The patch pipette is connected to the patch-clamp headstage, a current to voltage converter. The patch-clamp amplifier is connected to a computer through a Digidata digitizer, that is responsible for data generation, acquisition and analysis. (3) The mechanical probe is connected to a nanomotor controller, through which the parameters for micro- and nano- movements are adjusted. The nanomotor controller is connected to a computer, and the parameters like stimulus duration and speed of stimulation can be configured through specialized software. The voltage signal from the nanomotor is recorded by the P-clamp software. (B) Protocol of the static indentation stimulus. The probe was moved forward in steps of 1 μm, after an initial stimulus of 0.5 µm for 250 ms, and then withdrawn. The stimulus was applied every 10 seconds.

Larger steps were applied to some neurons, even if they responded to the mechanical stimulus. For example, if a neuron responded to a 3 µm stimulus, the probe was moved back to the starting position and after 10 sec, a 4 µm stimulus was applied in the same area of the membrane. Figure 13 A-D illustrates how mechanical stimulation was applied to a patch-clamped adult TG neuron. In figure 13 A the starting position of the mechanical probe is shown, while in B and C the neurons are subjected to mechanical steps of 4 and 6 µm, respectively. Finally, in D the mechanical probe has been retracted to its original position and it is possible to appreciate a deformation of the cell membrane caused by applying a very large stimulus (>10 µm).

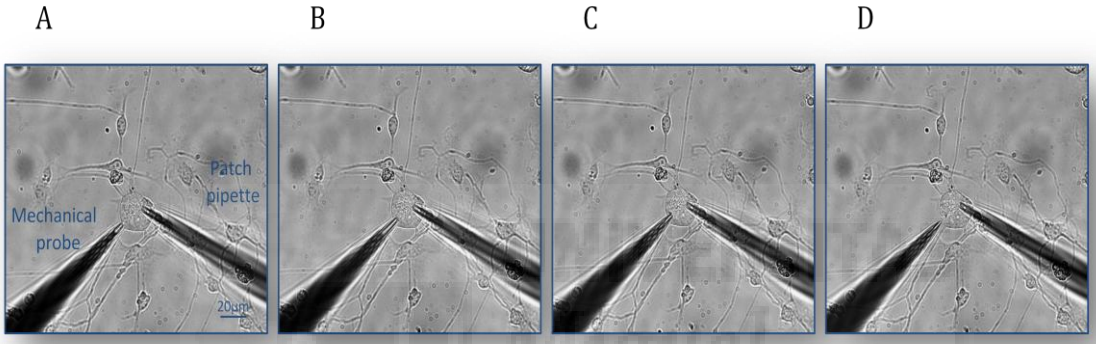

Figure 13. The mechano-clamp technique in TG neurons. Photographs showing the mechanical stimulation of a patch-clamped TG neuron. The neuron was subjected to mechanical steps of 0 (A), 4 (B) and 6 (C) µm. Application of a larger stimulus (>10 µm) caused deformation of cell membrane (D).

The velocity of the motor can be set by changing frequency, which affects the speed of the manipulator and the size of steps. The probe had a velocity of 0.5 μm ms^{-1}. The voltage signal, sent to the nanomotor by the control unit, was simultaneously fed into a second channel of the Multiclamp 700B amplifier so that the timing of the nanomotor movement in relation to the mechanically activated current could be accurately determined.

3.6 Data Analysis

Calcium measurements were acquired with Metafluor software (Version 6.1; Molecular Devices Corp., USA), while Origin 7.0 software (Origin Lab Corporation) was used for the graphics and analysis. A positive calcium response was considered when the fluorescence signal (F_{340}/F_{380}) differed at least four times the standard deviation of the baseline which on average was 0.2 ratio units.

Electrophysiological recordings were analyzed using the pClamp9 software (Molecular devices Corp, USA), measuring several electrophysiological parameters: the cell capacitance, the input resistance, the membrane potential, the rheobase current, the action potential shape and the firing pattern.

Two separate populations of neurons can be distinguished, based on the shape of the AP: S-type neurons that exhibit a long duration AP with a strong inflexion or hump in the repolarizing phase of the AP, and F-type neurons that have a short duration AP with no inflexion in the repolarizing phase of the AP (Cabanes et al., 2002). The shape of AP was assessed by calculating the first derivative with the software Origin 7.0. Neurons without inflexion present narrow APs and have only one negative peak in its first derivative, whereas neurons with a hump in their APs have two negative peaks in the first derivative (Figure 14A).

In voltage clamp mode the kinetic properties of the MA currents were also examined with the Origin 7.0 software. The decay phases of the currents were fitted to exponentials using the Chebyshev non-linear least-squares regression analysis (Hao & Delmas, 2010), thereby allowing the time constant for current inactivation (τ) to be calculated. Traces were fitted using the following equation: $I\ (t) = A\mathrm{f}\cdot\exp(-t/\tau\mathrm{f}) + A\mathrm{s}\cdot\exp(-t/\tau\mathrm{s}) + A\mathrm{o}$. MA current relaxations fitted by single exponential functions indicate a single type of MA current, whereas those fitted by multiple exponential functions indicate the presence of a mixture of MA currents, due to the inactivation of ion channels that have different inactivation kinetics, some faster and others slower.

The latency between the onset of probe movement and current activation as well as the amplitude of MA currents were measured (Figure 14B).

The current density, the electrical current per unit area of cross section, was also measured. Current density is defined by the amplitude of the current in pA divided by the capacitance of the neuron in pF. This parameter allows the current amplitude of

cells having different soma size to be compared, as occurs with newborn and adult TG neurons.

The size of the neuron's soma was measured with an ocular micrometer fitted in the microscope eyepiece. Most sensory neurons are generally oval so the two diameters were measured and the elliptical area was derived from the equation: $A=pi*r_1*r_2$.

All data in the histograms are presented as the means ± SEM, whereas the data in pie charts are proportions. Statistical comparisons were made using Sigmastat 3.0 software (Jandel Scientific Software, Erkrath, Germany). A Student's t-test was used to compare means values when the distribution was normal, while a Mann-Whitney Rank Sum test (MWR) was used when the distribution was not normal. A Z-test or a F- test were used to compare proportions.

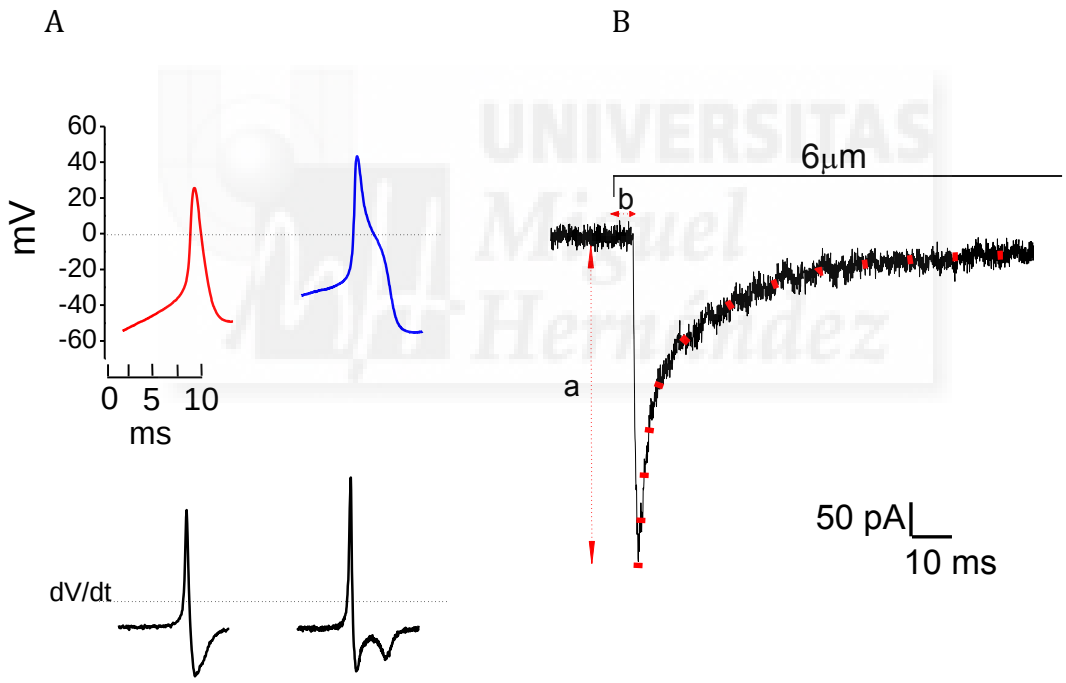

Figure 14. Analysis of the shape of action potentials and of the MA current parameters. (A) Example traces of APs (upper traces) and time derivatives (lower traces) evoked in TG neurons by a depolarizing current pulse. The red trace represents a narrow uninflected AP whose first negative dV/dt has only one negative peak. The blue trace represents a wider AP with a hump in the falling phase, which is represented as two negative peaks in the first derivative dV/dt. (B) The parameters of the mechanically activated current measured in TG neurons: *a,* current amplitude; *b*, latency between probe onset and current activation; *c* time constant for current inactivation (τ).

3.7 Criteria for the identification of nociceptive neurons

To distinguish between populations of nociceptive and non-nociceptive neurons, different strategies were used: lectin IB_4 staining, resistance to tetrodotoxin (TTX), and responses to capsaicin and cinnamaldehyde.

Lectin IB_4

Lectin IB_4 labelling was achieved by incubating the neurons with 3µg/ml IB_4-Alexa 488 (Molecular Probes; Life Technologies, Carlsbad, CA, USA) in solution A for 10 minutes at RT prior to recordings. The cells were then washed in solution A three times and IB4 positive neurons, characterized by intense green fluorescence, were classified as subpopulations of non-peptidergic nociceptive neurons (Figure15) (Caterina and Julius, 2001; Silverman and Kruger, 1990; Molliver et al., 1997; Dong et al., 2001). These neurons correspond to unmyelinated fibres, small size neurons that have long-duration AP and a higher density of TTX-resistant Na^+ currents and that contribute to inflammatory pain. Conversely, the IB4 negative neurons correspond to a distinct population of peptidergic neurons that have different characteristic to IB4+ neurons: shorter AP duration, denser TTX-sensitive Na^+ currents, and a stronger response to noxious heat (Stucky and Lewin, 1999; Wu and Pan, 2004). Moreover, in contrast to IB4+ neurons that are all nociceptive neurons, the IB4 – neurons include nociceptive as well as non-nociceptive neurons.

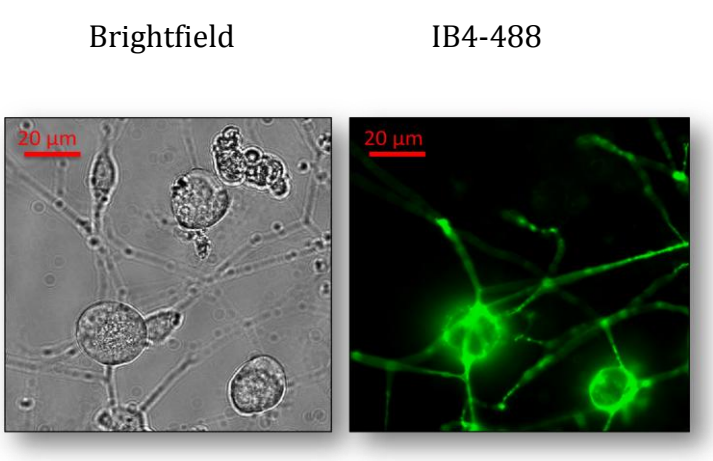

Figure 15. IB4 labelling in cultured trigeminal neurons. Brightfield and fluorescent images of two small diameter neurons labelled positively for IB4-488. Note that the IB4 labelling is specific of a set of cultured neurons, the non-peptidergic nociceptive neurons.

Tetrodotoxin (TTX) sensitivity

TTX is a voltage-gated sodium channel blocker (McCleskey and Gold, 1999; Waxman et al., 1999; Baker and Wood, 2001) that was used to distinguish nociceptive neurons that are resistant to TTX from TTX-sensitive neurons. In a specific set of electrophysiological experiments, APs and MA currents were measured in control conditions and the AP was then measured again during continuous superfusion of 1 μM TTX (Tocris Bioscience, Minneaopolis, MS, USA). Finally, the AP was recorded after washout of the TTX to check that the cell was still healthy.

Capsaicin and Cinnamaldehyde sensitivity

In calcium imaging recordings the TRPV1 activator **Capsaicin** (Sigma-Aldrich, St Louis, MO, USA) and the TRPA1 activator **Cinnamaldehyde** (Sigma-Aldrich, St Louis, MO, USA) were used to distinguish nociceptive neurons from non-nociceptive neurons. These activators were dissolved in extracellular solution A and used at a final concentration of 100 nM (Capsaicin) and 100 μM (Cinnamaldehyde).

3.8 Pharmacological testing

In order to determine the pharmacological sensitivity of the mechanically gated current, 8 μM **Gadolinium** (Gd^{3+}) (Sigma-Aldrich, St Louis, MO, USA), a blocker of stretch activated channels was applied. The selective TRPA1 antagonist **HC-030031** (10 μM ; Tocris Bioscience, Minneaopolis,MS, USA) was used to study the effect of TRPA1 blockade on the mechanically gated current. The experimental procedure involved first applying the mechanical stimulus in control conditions, followed by a second mechanical protocol in the presence of the substances. Finally, a third mechanical stimulus after wash out was used to test the recovery from inhibition.

3.9 Molecular biology techniques

3.9.1 RNA extraction

Dissected trigeminal ganglia were harvested in dry ice and their total RNA was isolated using PureLink RNA Mini Kit (Ambion, USA), according to the manufacturer's protocol. The concentration and quality of the RNA was assessed by Nanodrop (Labtech International, Ringmer, UK).

3.9.2 cDNA synthesis

To eliminate genomic DNA, the total RNA was incubated with DNAse I (Life Technologies, Carlsbad, CA, USA) at 37°C for 30 min. This RNA (1 µg) was incubated for 5 min at 65 ºC with 150 ng of random primers (Life Technologies, Carlsbad, CA, USA) and 0.5 mM of dNTP (Life Technologies, Carlsbad, CA, USA), and then on ice for 5 min. Thereafter, 1X Superscript buffer, 10 mM DTT (Life Technologies, Carlsbad, CA, USA) and 2 U/µl RNAse OUT (Life Technologies, Carlsbad, CA, USA) were added and the mixture was incubated for 2 min at room temperature. Finally 10 U/µl Superscript™III reverse transcriptase (Life Technologies, Carlsbad, CA, USA) was added, incubated for 10 min at room temperature and then for 1 hour at 50ºC and finally for 15 min at 70ºC.

3.9.3 Polymerase chain reaction (PCR)

The cDNAs generated were then used as templates for semi-quantitative PCR using GoTaq Flexi DNA Polymerase (Promega) using a reaction mix that contained the following components in a final volume of 25 µl (see Table 3).

Table 3. PCR protocol for a semi-quantitative PCR

Reagents	Concentration
Go Taq buffer	1X
$MgCl_2$	2.5 mM
dNTPs	0.4 mM
Forward Primers	0.4 µM
Reverse Primers	0.4 µM
cDNA	1µg
Go Taq Polymerase	5U/µl
H_2O	Final volume 25 µl

PCR amplification was performed using the following conditions:

Polymerase activation step at 95° C for 3 min;

35 cycles:

- 95° C for 30 seconds
- 60-65° C, for 30 seconds (in function of the melting temperature of the primers; see Tables 4 and 5)
- 72° C for 30 seconds

The reaction was cooled to 4ºC.

Primers were designed using the primer-BLAST programme (NCBI) and β-Actin was amplified as a control housekeeping gene. Housekeeping genes are genes that are involved in the regulation of basic and ubiquitous cellular functions required for the survival of most cell types. Due to its presumptive invariable expression, β-Actin can be used as an internal positive control. In order to detect potential contamination, two negative controls were used: one for the reverse transcription (where instead of the enzyme H_2O was added); and another for the PCR amplification (where instead of the cDNA, the same volume of H_2O was added).

Table 4. Forward and reverse sequences and melting temperatures of the different primers used for the PCR

Gene	Forward	Reverse	Tm (ºC)	Size(bp)
TRPA 1	TTGGCTTGGCGGTTGGGGAC	CCGTAGCATCCTGCCGTGCC	65	182
TRPC5	CTATGAGACCAGAGCTATTGATG	CTACCAGGGAGATGACGTTGTATG	60	221
TRPC3	ACCTTGTAGCAGGCTGGGGAAGA	TTGGCAGCGTGGTGATGCCT	60	137
ASIC 3	TCCTGCCAGCAACAGCAACTGA	CGTGTAGTGGCGCACGGGTT	60	320
TRPV1	TGGAAGCTGCAGCGAGCCATC	CTTCCGGCTGGGTGCTATGCC	65	343
NaV1.8	ATCTGATGCTGGCCACTGCC	ATTTCACCCTGGGTCTTCTCTCA	60	452
TRPV2	CCGATGAGTTCTACCGAGGC	CAGTGACACTCGGACAGGAC	60	554
Piezo 2	GCCTGGCAGTAGCATGTGCGT	GGTCACCACGACCTTGCCCG	64	632
B-Actin	GACCCAGATCATGTTTGAGACCTT	CAGCTCAGTAACAGTCCGCC	65	791

3.9.3.1 Gel electrophoresis

Agarose gel electrophoresis was used to separate the DNA fragments by size. The 2% agarose gels were prepared by dissolving agarose (Sigma-Aldrich, St Louis, MO, USA) in TAE 1X buffer (40mM Tris-acetate, 1mM EDTA). After cooling, 1X SYBR safe stain (Life Technologies, Carlsbad, CA, USA) was added, a fluorescent dye that binds to nucleic acid, and then set into a gel tray. 8-10 µl of each sample was loaded into wells, alongside the molecular weight marker TrackIt (Life Technologies, Carlsbad, CA, USA).

A power pack supplying 80-120 volts was used to separate the bands which were then visualised using a UV-transilluminator, the Alphalmager 2200 system, and a picture was taken.

3.9.5 Single cell RT-PCR

Individual neurons were aspirated into a large-diameter glass electrode (resistance of 300 KΩ and with a diameter from 10 to 15µm) containing 2-3 µl RNase-free PBS. The cell lysates were ejected into a sterile PCR tube and rapidly frozen on dry ice (–78ºC), which were stored at –80ºC for subsequent reverse transcription. The membrane was disrupted by thermic shock: at 65ºC for 3 min and then the cell was cooled on ice for 2 min.

cDNA synthesis

For the reverse transcription, the procedure and components used were similar to those used for the cDNA synthesis from the entire ganglia, except for the adjustment to the concentration of the random primers (0.25 ng/µl) and DTT (5mM).

PCR reaction

The cDNAs generated was divided into six or seven 3-µl aliquots that were used in separate PCRs. To increase the fidelity of the PCR reaction, as well as the specificity of the products amplified, Nested PCR was used. This is a variation of the PCR protocol in which the cDNA is amplified with two pairs of primers instead of one pair. The first pair of PCR primers (see Table 4) amplify a fragment similar to that obtained in the standard PCR, while the second pair of primers, called nested primers (see Table 5), bind to sequences within this first PCR product to amplify a second shorter PCR product (Figure 16).

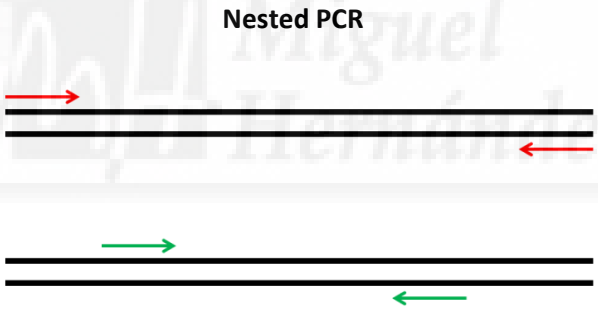

Figure16. Primer design for the Nested PCR. The arrows represent the reverse and forward primers and the double lines represent the DNA. The red arrows represent the primers for the 1st round of amplification, while the green arrows represent the 2nd round (nested) primers.

Table 5. Forward and reverse primer sequences and melting temperatures of the different primers used for the second round of nested PCR.

Gene	Forward	Reverse	Tm (ºC)	Size(bp)
TRPA 1	ATTGCTGAGGTCCAGAAGCAT	TGGACCTCTGATCCACTTTGC	60	118
TRPC5	AACTGCAAGGGGATCCGATG	GTCGGGCCTTCACATTGGTA	60	127
TRPC3	CCTTGTAGCAGGCTGGGGAAG	ATCTGTCCGAGGCGTTGAATAC	60	112
ASIC 3	GCCTGTGAGTCACGCTATGT	ACAAGTGTCCTTTCGCAGCA	60	141
TRPV1	TGCTTCAGGGTGGATGAGGT	GTTTCTCCCTGAAACTCGGC	60	138
NaV1.8	CGTTCCTCTCACTGTTCCGT	GAGCGAGGTTGTGTCAATGC	60	293
TRPV2	CGCTTCTTCCAAAAGCACCAA	GATCACCAGCGCACTGTTCT	60	216
Piezo 2	TGGGCTCTCCTTTGTCTACCTTTCT	GCCGGCATCAGCTCCCTTCA	60	267
B-Actin	ACCCACACTGTGCCCATCTA	GCCACAGGATTCCATACCCA	65	342

The components for single cell RT-PCR amplification were similar to the used for the tissue extracts except for the adjustment to the concentration of primers and cDNA (see Table 6).

PCR amplification was performed using the same conditions as described above, but in the second round, 38 cycles at 95ºC for 30 seconds, were used instead of 35 cycles. Similarly, the reaction was finally cooled to 4ºC. β-Actin was used as an internal control. In order to control for contamination, a negative control for the PCR amplification was used (where instead of the cDNA the same volume of H_2O was added). The resulting PCR products were then visualized on 2% agarose gels with 1X SYBR safe stain (Life Technologies, Carlsbad, CA, USA), as described above.

Table 6. PCR protocols for the first and second round of nested PCR

Reagents	Concentration 1st round nested PCR	Concentration 2st round nested PCR
Go Taq buffer	1X	1X
$MgCl_2$	2.5 mM	2.5 mM
dNTPs	0.4 mM	0.4 mM
Forward Primers	0.2 µM	0.4 µM
Reverse Primers	0.2 µM	0.4 µM
cDNA	~3 µl	5 µl of 1st PCR
Go Taq Polymerase	5U/µl	5U/µl
H_2O	Final volume 25 µl	Final volume 25 µl

4. Results

At the outset of these studies, a decision was taken to perform the work in newborn and adult mice. This choice was made based on strong evidence that during the first three weeks of postnatal development, changes in electrophysiological properties occur that are linked to the process of myelination. Accordingly, during this period a heterogeneous population of unmyelinated and myelinated primary sensory neurons exists, this latter state being characteristic of adult animals (Djouhri et al. 1998). These changes may also be associated to the functional specialization of adult neurons (Cabanes et al. 2002), which may affect their mechanosensory properties.

4.1 Characterization of mechanosensitive neurons by calcium imaging

Previously, distinct approaches have been used to characterize the mechanosensory properties of DRG neurons. Indeed, calcium measurements have been made in the soma of dissociated sensory neurons in response to a variety of mechanical stimuli, including suction, poking with a polished pipette, or stretch due to changes in osmolarity (Cho et al., 2002; Drew et al., 2002; Gotoh and Takahashi, 1999; McCarter et al., 1999). Trigeminal neurons have been shown to respond to both, hypotonic solutions and radial stretching by increasing their intracellular calcium concentration (Viana et al., 2001; Bhattacharya et al., 2008). All these studies indicate that TG and DRG neurons are mechanosensitive, although the mechanical properties and the molecular machinery underlying mechanosensitivity of TG neurons have been poorly studied.

Hence, the first part of these studies focused on characterizing mechanosensitive TG neurons using calcium imaging to study dissociated cells following two different mechanical stimuli: exposure to a hypoosmotic solution (210 mosmol Kg^{-1}), which causes membrane stretching, and static indentation using a polished pipette. Both stimuli were applied on the same neuron and the responses were analysed in order to identify different subpopulations of primary afferent neurons responding to different stimuli.

4.1.1 Mechanical stretch and static indentation revealed distinct populations of mechanosensitive TG neurons

Fluorimetric measurements of intracellular calcium concentration were made on cultured TG neurons from newborn (n=65) and adult mice (n=62).

Dissociated mouse TG neurons were visible by transmitted light and when loaded with FURA2-AM, they could be detected by fluorescence microscopy in control solution, in the hypoosmotic solution (210 mosmol Kg^{-1}) and after static indentation (Figure 17 A). After exposure to the control solution (1 minute), perfusion was switched to an isotonic solution (90 mM NaCl) for 2 min and then to a 30% hypotonic solution for 4-5 min, before switching perfusion back to the control solution until the calcium baseline was recovered. Subsequently, I recorded the responses of individual neurons to repetitive indentation stimulus of increasing amplitude, some of which had responded to the hypoosmotic solution and other that had not. In these studies, the probe was positioned near to the cell body (see lower left panel of figure 17 A), and it was moved forward in steps of 1 μm for 250 ms and then withdrawn, with an interval of 10 sec between each stimulus. The resulting time course of the $[Ca^{2+}]_i$ response to hypotonic solution (left panel) and to static indentation (right panel) of the neuron (see arrow in figure 17 A) was plotted (Figure 17 B), allowing the mechanical threshold to be determined, that is the minimum force at which neurons respond with an increase in the $[Ca^{2+}]_i$. This average threshold was 8.5 ± 0.6 μm (n=48) and 9.0 ± 0.5 μm (n=44) in newborn and adult mice, respectively.

A

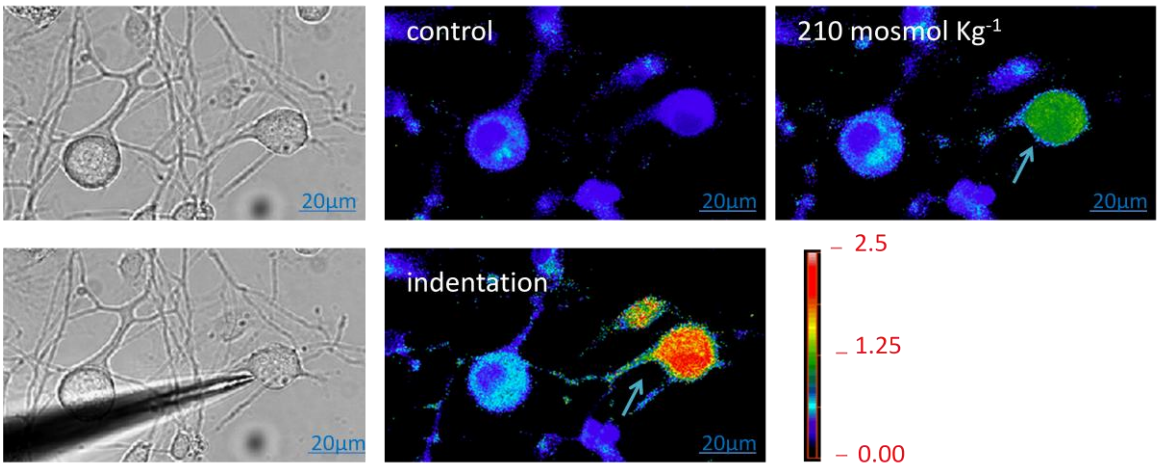

B

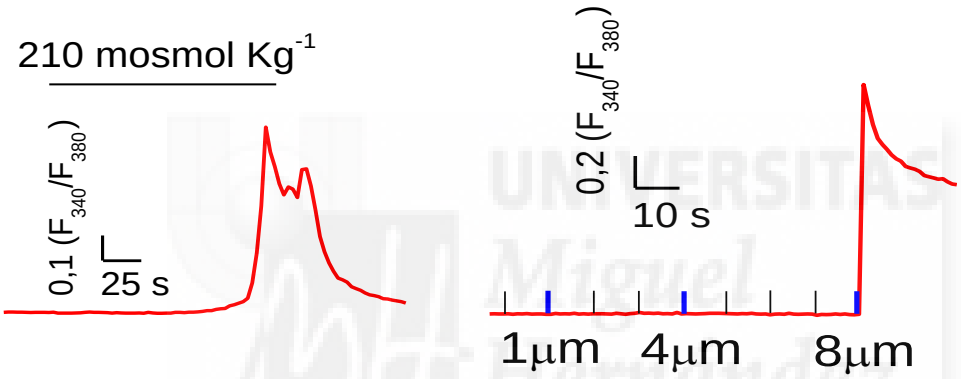

Figure 17. Hypoosmotic and static indentation stimuli increase the intracellular calcium concentration in TG neurons. (A) Representative pseudocolour images of adult trigeminal neurons showing ratiometric $[Ca^{2+}]_i$ responses to the control solution, 210 mosmol Kg^{-1} and static indentation. Changes in $[Ca^{2+}]_i$ are reflected by the ratio of fura-2 emission at 340 to 380 nm excitation wavelength (see color bar). Scale bar, 20 µm. (B) Time course of the changes in calcium during exposure to a 210 mosmol Kg^{-1} solution and to static indentation of the neuron indicated by the arrows in A.

The results showed that the overlap between hypotonic and mechanical touch responses was not absolute. Not all neurons responded to both stimuli and thus, three mechanical sensitive populations of neurons were indentified: i) neurons that responded to the hypoosmotic solution only, 14% of newborn neurons (n=9/65) and 18% of adult neurons (n=11/62); ii) neurons that responded to the indentation only, 43% of newborn neurons (n=28/65) and 37% of adult neurons (n=23/62); and neurons that responded to both stimuli, 31% of newborn neurons (n=20/65) and 34% of adult neurons (n=21/62). In addition, 12% of newborn neurons (n=8/65) and 11% of adult neurons (n=7/62) did not respond to either of the mechanical stimuli

(Figure 18). All the analysed neurons responded with an increase in calcium to a depolarization produced by a brief application of elevated extracellular K^+ (30 mM) at the end of the experiment (data not shown).

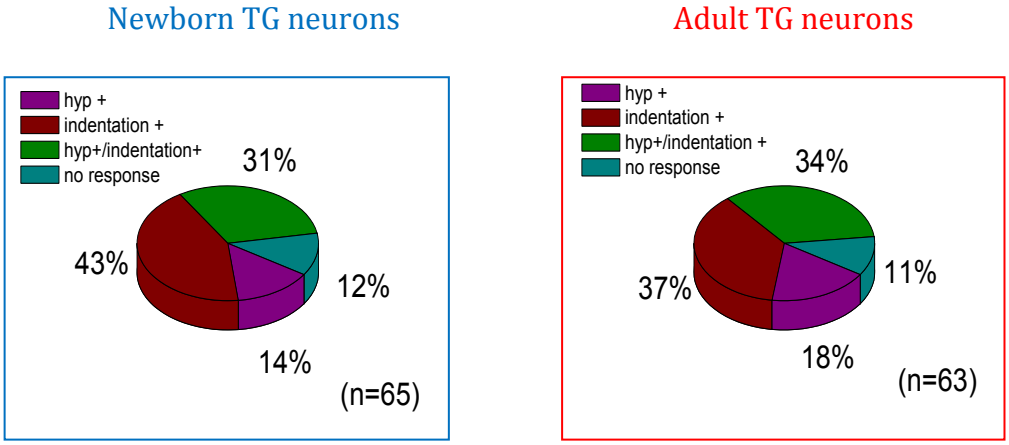

Figure 18. Identification of three mechanically sensitive populations of trigeminal neurons responding to hypoosmosis, indentation or both stimuli. Pie chart showing the proportion of newborn and adult TG neurons responding to hypoosmosis, indentation or both stimuli. A small part of neurons were insensitive to mechanical stimuli.

4.1.2 Non-nociceptive and nociceptive mechanosensitive neurons

Next, I asked whether mechanical responses differed between nociceptive and non-nociceptive neurons. To classify the populations of mechanosensory neurons into nociceptive and non-nociceptive neurons, I employed two criteria:

- ✓ Response to chemical irritants
- ✓ Size of the cell soma

Response to chemical irritants

The TRPV1 channel is sensitive to noxious heat, protons and the irritant vanilloid capsaicin. TRPV1 is highly expressed in a subset of peptidergic and IB4-binding nociceptive neurons, and, the response to capsaicin is normally used to identify unmyelinated polymodal nociceptors (Caterina et al., 1997; Caterina et al., 2000). TRPA1 is another channel activated by pungent chemicals, such as cinnamaldehyde (CA) and allyl isothiocyanate (mustard oil) (Story et al., 2003; Bandell et al., 2004; Jordt et al., 2004; Bautista et al., 2006). This channel is also

expressed in a subset of nociceptors and CA can also be used to identify nociceptive neurons.

The sequence of images in Figure 19 shows the changes in fluorescence intensity in adult TG neurons under control, hypoosmotic condition, static indentation, CA 100 µM, Cap 100 nM and KCl 30 mM. One of the two cells that responded to the hypoosmotic solution was then stimulated with the mechanical probe in the same sequence as explained in Figure 17 A. After calcium recovery to the baseline values, the perfusion solution was changed to a solution of 100 µM CA for 2-3 min, and after washing out this solution for 4 min, 100 nM Cap solution was applied for 2-3 min. Finally, 30 mM KCl was applied in order to check the health of neurons, as was performed at the end of the protocol in all the experiments performed. In the specific example shown in Figure 19, the neuron responded to all the stimuli applied.

A

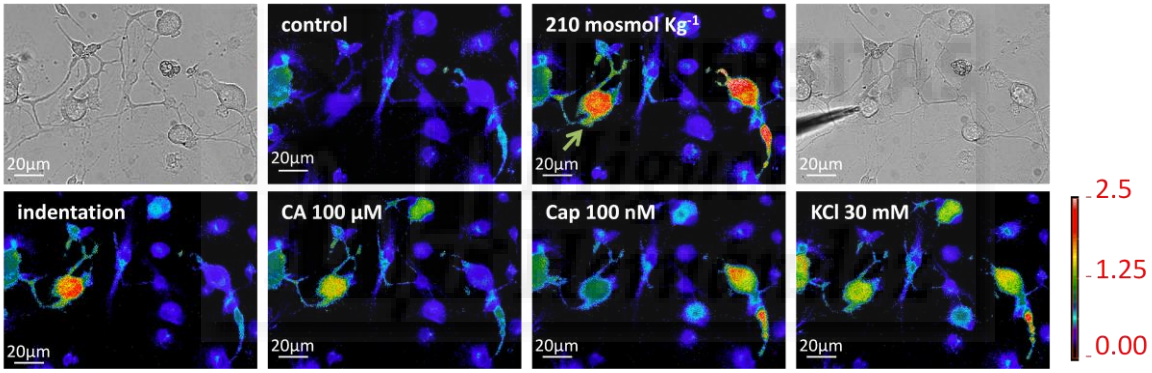

B

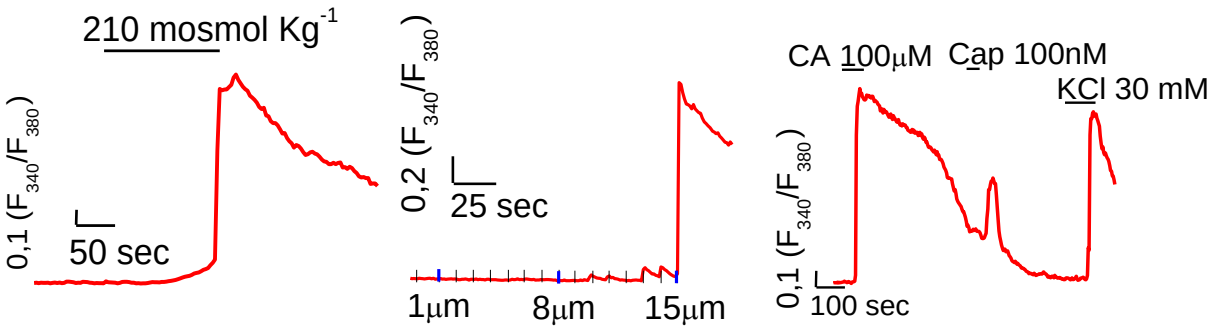

Figure 19. Mechanosensitive TG neurons responded to noxious stimuli, by increasing their intracellular calcium concentration. (A) Representative pseudocolor images of adult trigeminal neurons showing ratiometric $[Ca^{2+}]_i$ responses to 210 mosmol Kg^{-1}, static indentation, capsaicin 100 nM (Cap), cinnamaldehyde 100 µM (CA) and KCl 30mM. Colored bar shows the pseudocolour scale, with the lowest calcium concentration at the base. (B) Time course corresponding to the images in A.

When the entire population of neurons was analyzed CA and Cap activated 10% (n=25/261) and 12% (n=34/266) of the newborn neurons, respectively. The proportion of neurons responding to chemical noxious stimuli increased in adult mice, being statistically significant for responses to CA (29%; n=57/195) and to Cap (20%; n=40/200; Figure 20).

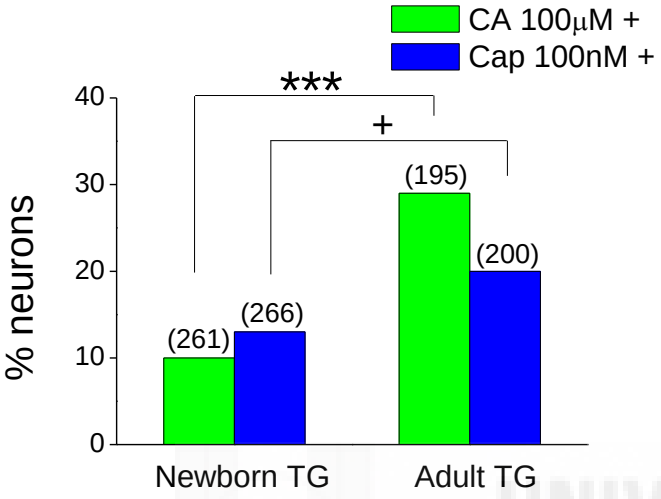

Figure 20. Proportion of neurons responding to noxious stimuli in newborn and adult mice, after applying mechanical stimuli. Histograms summarizing the proportion of newborn and adult neurons responding to the noxious chemical stimuli cinnamaldehyde 100 μM or capsaicin 100 nM. The value on top of the bars indicate the number of neurons recorded in each group ($^{***}p < 0.001$, $^{+}p < 0.05$; F-test).

It is known from literature that TRPA1 is expressed exclusively within a subset of TRPV1-positive sensory neurons (Story et al. 2003), thus the proportion of neurons that respond to Cap should be higher that the response to CA. However, as it is shown in figure 20, I obtained a higher proportion of neurons that respond to CA. This discrepancy could be due to a decrease of the healthiness of neurons during the experiment caused by the application of several stimuli previously to the exposure to Cap. To confirm that this was the case, I performed a new set of experiments using a different protocol where only Cap and CA, but none mechanical stimuli, were applied to newborn and adult neurons. The histogram of figure 21 shows that CA and Cap activated 7% (n=7/104) and 26% (n=27/104) of the newborn neurons, respectively. The proportion of neurons responding to chemical noxious stimuli significantly increased in adult mice, being 30% (n=29/96) and 47% (n=45/96) for CA and Cap, respectively. Thus, I also confirm that the proportion of neurons that responds to Cap is higher than the proportions of neurons that respond to CA.

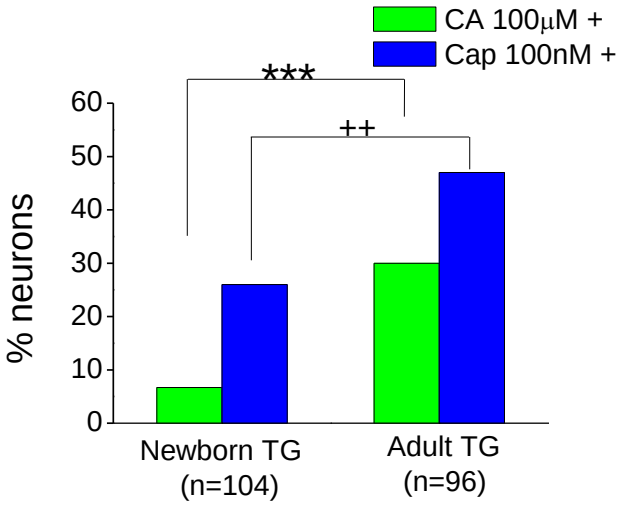

Figure 21. The proportion of neurons responding to noxious stimuli in newborn and adult mice. Histograms summarizing the proportion of newborn and adult neurons responding to the noxious chemical stimuli cinnamaldehyde 100 µM or capsaicin 100 nM. The value on top of the bars indicate the number of neurons recorded in each group ($^{***}p < 0.001$, $^{\#\#}p < 0.01$; F-test).

The increase in nociceptive neurons in adult mice was also observed in the mechanosensitive (MS) neurons. Among these neuron populations in newborn mice that responded to mechanical stimuli, 2% (n=1/55) and 13% (n=7/55) responded to CA and Cap, respectively. By contrast, 21% (n=12/56) and 12.5% (n=7/56) of adult MS neurons that responded to both mechanical stimulation also responded to CA and Cap, respectively (Figure 22).

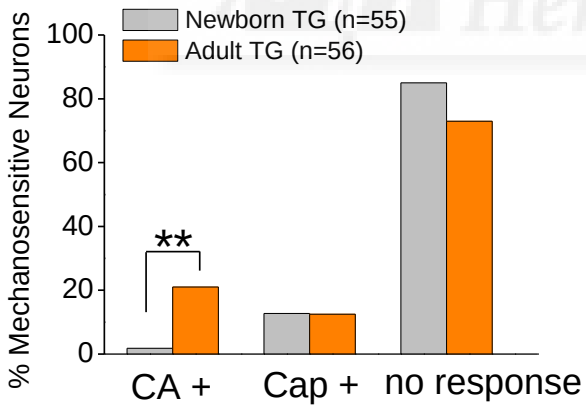

Figure 22. The proportion of MS neurons responding to CA increases in adult mice. Histograms summarizing the proportion of MS neurons responding to noxious chemical stimuli in newborn and adult neurons ($^{**}p < 0.01$, Z-test).

In summary, I found that responses to CA were more common in adult TG neuron populations that responded to either mechanical stimulus. The very low proportion of neurons responding to CA in newborn neurons was consistent with previous studies on dissociated DRG neurons (Hjerling-Leffler et al., 2007), suggesting a lower expression of TRPA1 in newborn neurons, compared to adult

neurons. In these cells, the responses to CA at 7 postnatal days indicated that functional TRPA1 channels appear in the first postnatal week, while the response to Cap appears before, at embryonic day 12.5. Moreover, the detection of TRPV1 and TRPA1 mRNA in these DRG cells was closely correlated with the appearance of functional responses.

In order to confirm that TRPA1 was more weakly expressed in newborn TG mice than in adult TGs, semi-quantitative PCR was performed on cDNA synthesized from mRNA extracted from the whole trigeminal ganglia isolated from newborn and adult mice to detect TRPA1 transcripts. When the products of this semi-quantitative PCR amplification from different numbers of amplification cycles (28 and 31) were analysed in a SYBR-safe-stained agarose gel (Figure 23), the lower expression of TRPA1 in newborn TG neurons when compared to that in adult mice was clear. In all these experiments negative controls were included in which the cDNA template was replaced with water (H_2O) or the mRNA that was not subjected to reverse transcription (RT–).

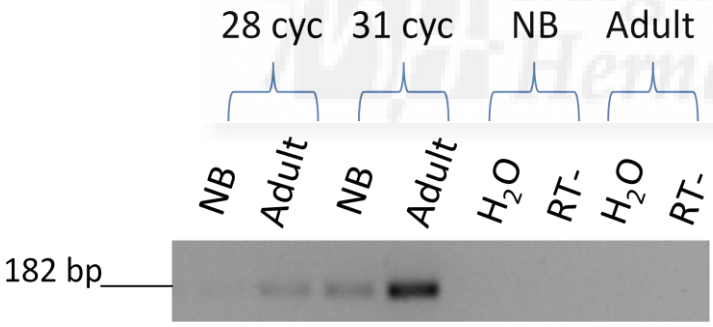

Figure 23. TRPA1 mRNA expression in newborn neurons compared with adult animals. RT-PCR (n=3) after 28 and 31 cycles show the onset of TRPA1 mRNA expression in newborn (NB) and adult TG neurons.

Size of different subclasses of TG neurons

Sensory neurons with a cell soma of small-diameter have a strong probability of being nociceptors, whereas low threshold mechanosensitive neurons are thought to have a bigger soma (Lawson, 2002).

Thus, I measured the soma size of MS neurons classified as nociceptive and non-nociceptive on the basis of their responses to capsaicin and/or cinnamaldehyde. The soma size was measured in the three populations of neurons that responded to static indentation, hypoosmotic solution or to both stimuli.

The mean soma size of mechanosensory newborn neurons was 183 ± 27 μm^2 in the population of nociceptive neurons and 260 ± 18 μm^2 in the non-nociceptive neurons. In neurons from adult mice, the mean soma size was 321 ± 32 μm^2 for nociceptive and 460 ± 36 μm^2 for non-nociceptive neurons. The difference in size between nociceptive and non-nociceptive neurons was not significant in newborn animals, whereas the soma of neurons in newborn mice were significantly smaller than those in the adult, both for the nociceptive and non-nociceptive neurons subpopulations of (Figure 24). These results suggest that probably the evolution of the properties of neurons with age is associated with a parallel increase in the surface area of the soma, which may explain the differences in the mean soma size between nociceptive and non-nociceptive neurons from adult animals, which is not observed in newborns.

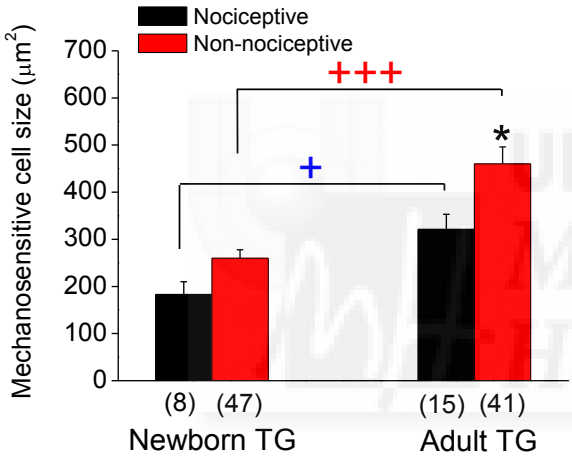

Figure 24. Mean soma size of nociceptive and non-nociceptive MS neurons in newborn and adult mice. The number of cells recorded is given below each bar. + denotes statistical significance between cells in the conditions indicated ($^{+}p < 0.05$, $^{+++}p < 0.001$, *p<0.05; Student's *t*-test).

4.2 Electrophysiological characterization of mechanosensitive neurons

In the past decade, several techniques have been developed that have opened up new pathways to study the molecular and cellular aspects of mechanotransduction. Among these techniques the mechano-clamp allows forces to be applied to the surface of cultured cells via an electrically driven glass probe while performing patch clamp recordings. Accordingly, this technique was used for the electrophysiological characterization of the mechanical properties of TG neurons.

4.2.1 Electrophysiological properties of TG neurons

Electrophysiological recordings were made in the soma of sensory TG neurons using the patch clamp technique in the whole cell configuration. Recordings were obtained from 182 neurons from newborn mice and 157 neurons from adult mice. These neurons had a mean resting membrane potential of -55±1 mV and -56±1 mV in newborn and adult mice, respectively. Initially, these recordings were started in current clamp mode and then subsequently, they were switched to voltage clamp mode. The following electrical properties of TG neurons were analyzed: the membrane potential, rheobase current, firing pattern, and action potential shape. The presence of TTX-resistant voltage-gated sodium channels was also studied and all these parameters are summarized below for the entire population of neurons studied. Indeed, later on, some of these classification criteria will be used to establish different populations of mechanosensitive neurons. I compared results obtained in newborn and adult animals.

Rheobase

The rheobase is the minimum current that is required to generate an action potential and it is a measure of membrane excitability. To calculate the rheobase current, the resting membrane potential was held at -80mV and a series of incremental current steps (20 or 50 pA increments) were injected for 200 ms. The rheobase of newborn and adult neurons was 173 ±9 pA (n=182) and 289 ± 15 pA (n=157), respectively. These values indicated a significantly higher excitability of

newborn neurons in comparison to those from adult mice (***p< 0.001, Rank sum test).

Firing pattern of TG neurons

The firing pattern has been used to distinguish nociceptive from low-threshold MS neurons. Low-threshold mechanoreceptors have a phasic response *in vivo*, since they respond to the ramp phase of the stimulus but not to the static phase. Conversely, mechano-nociceptors have a tonic response, since they respond to the static phase of the stimulus (Lewin and Moshourab, 2004; Johnson, 2001). I used this feature to distinguish between non-nociceptive and nociceptive neurons although I have to consider that the firing pattern *in vivo* depends also on other factors, including support cells and specialized terminal structures (Hao and Delmas, 2010).

TG neurons presented two different patterns in response to injection of depolarizing current. "Phasic" neurons had a very low rate of firing followed by a silence, whereas "Tonic" neurons continued the discharge of action potentials throughout the entire duration of the depolarizing pulse. The firing patterns of a "phasic" and a "tonic" adult neuron are shown in Figure 25, where a series of depolarizing current steps (20 pA increments) were applied, from a membrane potential artificially set to −80 mV. In newborn mice, 57% (n=98) of TG neurons presented a phasic response and 43% (n=73) responded with a tonic response. In adult mice, the proportion of neurons that responded with a phasic pattern increased significantly to 76% (n=119; ***p< 0.001, Z-test), whereas only 24% (n=37;***p< 0.001, Z-test) of neurons responded with a tonic response.

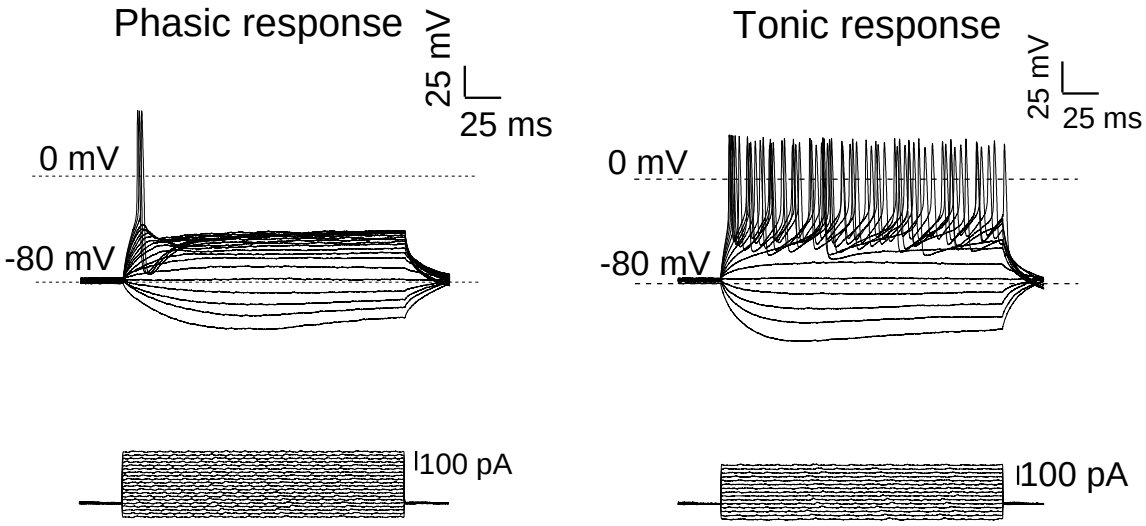

Figure 25. Firing patterns of adult TG neurons. Effect of depolarizing current commands and typical recordings from "phasic" and "tonic" neurons.

Action potential shape

It has been shown that mechanosensory neurons can be reliably classified as nociceptive or non-nociceptive through their characteristic action potential shape (Koerber et al., 1988; Lawson, 2002). Nociceptors have wide APs with an inflection on the falling phase of the AP (Koerber et al., 1988; Traub and Mendell, 1988; Gold et al., 1996). By contrast, low threshold mechanoreceptive neurons display a very narrow spike with no inflection on the falling phase of the AP (Koerber et al., 1988; Djouhri et al., 1998).

Thus, when the shape of APs was analyzed to distinguish nociceptive and non-nociceptive neurons, 80% (n=136) of the newborn neurons analyzed displayed a hump in the falling phase of action potential and only 20% (n=35) had a narrow AP. Similar data were observed with adult TG neurons, with a hump detected in 88% (n=137) and only 13% (n=19) with a narrow AP, suggesting that the majority of neurons were nociceptive.

Tetrodoxin-resistant voltage-gated Na^+ channels

Nociceptive neurons differ from most other neurons in that they express TTX resistant voltage-gated sodium channels NaV1.8 and NaV1.9 (McCleskey and Gold, 1999; Waxman et al., 1999; Baker and Wood, 2001), generally in conjunction with TTX-sensitive (TTX-S) sodium channels. Conversely, non-nociceptive neurons predominantly express TTX-S sodium channels and barely TTX-R channels (Kostyuk et al., 1981; Caffrey et al., 1992). Thus, the sensitivity of AP generation to 1 μM TTX was used to distinguish between nociceptive TTX-resistant and TTX-sensitive neurons. The firing pattern of tonic neurons from a newborn mouse was assessed in response to a series of depolarizing current steps in control solution (A) and in the presence of 1 μM TTX (B) (Figure 26). When depolarizing currents activated APs in the presence of the drug, the cells could be considered to be nociceptive neuron (Figure 26B). By contrast, recordings were also obtained from phasic newborn neurons sensitive to 1μM TTX, a phenotype expressed in low threshold neuron (Figures 26C and D). As shown in these specific examples, the TTX-resistant neuron displays a tonic discharge pattern, whereas the TTX-sensitive neuron displays a phasic discharge pattern. However this distribution is by no means exclusive as the tonic and phasic discharges are present in both subpopulations of TTX-resistant and TTX-sensitive neurons, both in newborn as well as in adult neurons.

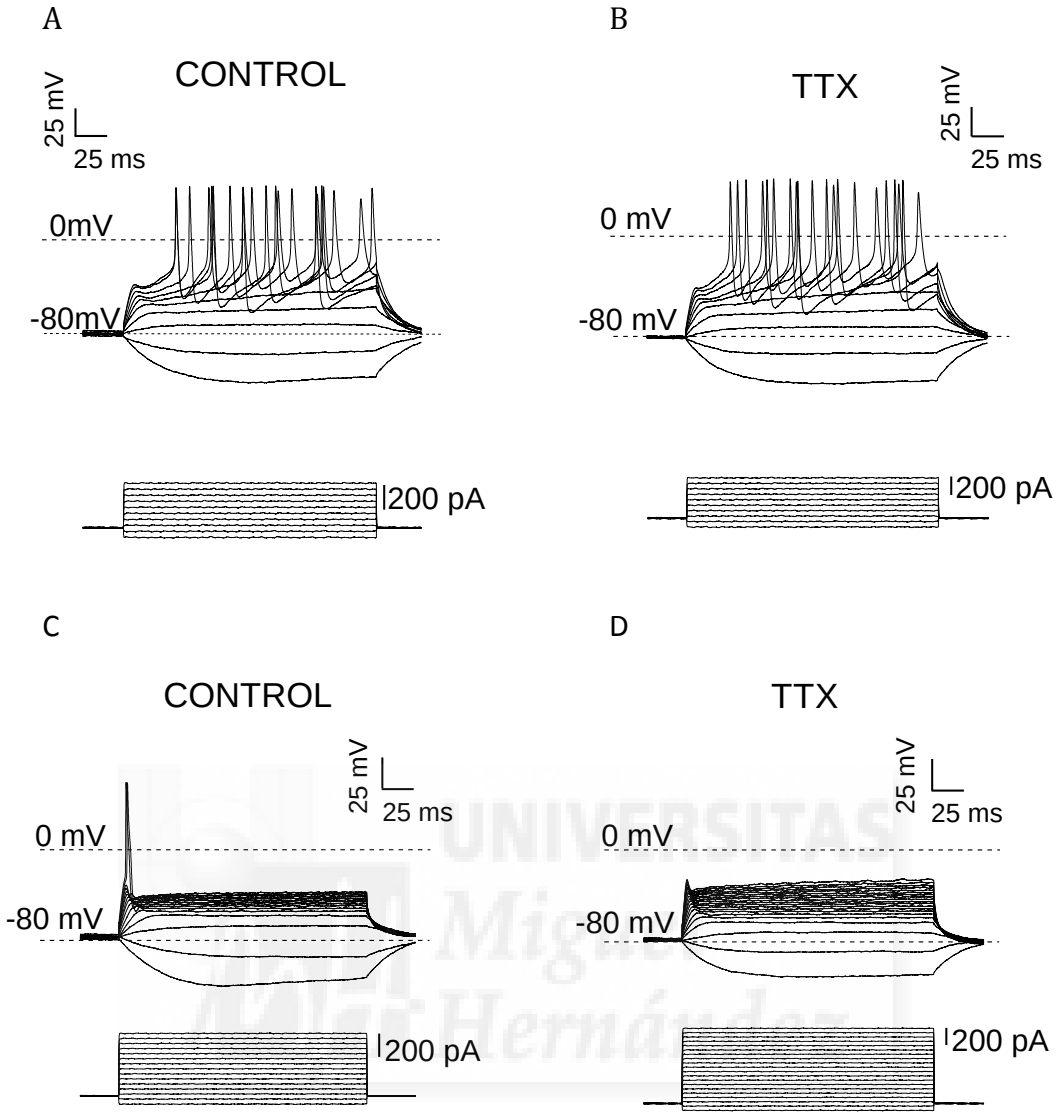

Figure 26. Action potential discharges before and after application of TTX. Recordings of action potentials in control solution (A and C) and during application of TTX 1μM (B and D), indicating the nociceptive (TTX-resistance, B) or the low threshold (TTX-sensitivity, D) phenotype of neurons.

IB4 labelling

Another way to distinguish specific subpopulations of nociceptive neurons is by labelling with the membrane-bound lectin IB4. In fact small diameter sensory neurons can be divided into two major neurochemical subtypes (Nagy and Hunt, 1982). Firstly, there is the so-called peptidergic population of neurons that contain neuropeptides, such as substance P and CGRP, and that express TrkA, the NGF receptor (Snider and McMahon, 1998). By contrast, the second population lacks the neuropeptides but binds the plant lectin IB_4 (Caterina and Julius, 2001). Thus, I used IB4 labelling to identify a population of non-peptidergic nociceptive small neurons

positive for IB4, and IB4 negative neurons that include nociceptive as well as non-nociceptive neurons.

Both IB4+ and IB4– neurons could be recorded at a holding potential of -60 mV and stimulated by mechanical indentation.

4.2.2 Mechanically activated neurons

After characterizing the electrical properties of the TG neurons in the current clamp mode, the activation of ionic currents by mechanical stimulation was studied using the voltage clamp configuration at a holding potential of –60 mV. The mechanical probe was positioned near the cell without touching it and the probe was then moved forward 0.5 μm, before 1 μm increments were applied at 10 sec interval up to a total distance of 15 μm (see methods).

Static indentation evoked inward currents in 79% (144/182) of newborn and 59% (93/157) of adult neurons at a holding potential of –60 mV (Figure 27), indicating a significant decrease in the proportion of adult neurons that responded to the static indentation (**p=0.003, Z-test). These data are in accordance with previous studies performed on newborn (90%: Drew et al., 2002; Lechner et al., 2009) and adult neurons (68%: Hu and Lewin, 2006; Hao and Delmas, 2010; Vilceanu and Stucky, 2010).

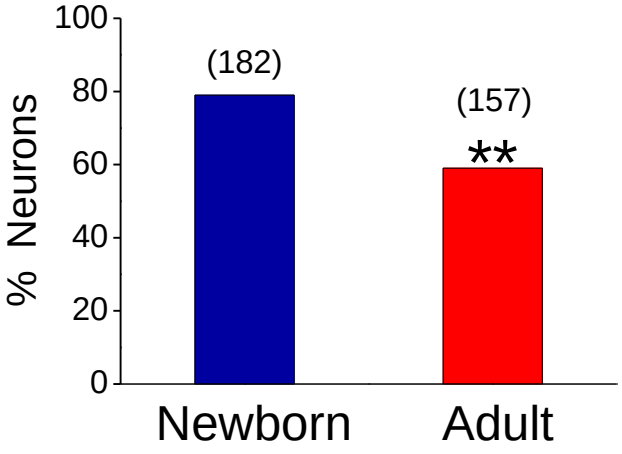

Figure 27. Response to static indentation in newborn and adult neurons. The values in parenthesis on each bar indicate the number of neurons recorded in each group. (**p<0.01, Z-test).

Mechanosensory neurons had a variable mechanical threshold ranging from 2 to 10 μm. There was no difference in the mean threshold between newborn (5.7 ± 0.3 μm) and adult neurons (5.8 ± 0.3 μm).

In order to measure the amplitude of the inward currents, the first MA current elicited by a mechanical stimulus in each neuron was selected. I used this criterion for two reasons: first, because in many neurons the recording was lost after the first mechanical stimulation and second, because I found a considerable variability in mechanical thresholds meaning that the same stimulus intensity in different neurons may correspond to big differences in current amplitude. The mean current amplitude in the population of mechanosensitive neurons recorded, was similar in newborn (147 ± 10 pA; n=144) and adult neurons (166 ± 20 pA; n=93).

The current density was also measured to correct for the size factor of the neurons and, accordingly, the current density of mechanosensitive neurons was 6.9 ± 0.5 pA/pF and 7.9 ± 1.2 pA/pF in newborn and adult neurons, respectively. These values are not significantly different. (p=0.719, Mann-Whitney Rank-Sum test).

MA currents exhibited graded increases in amplitude in response to increases in the magnitude of indentation, in newborn and adult mice (Figure 28). For the specific neuron shown in the figure, the mechanical threshold was 3 μm and the amplitude of the response augmented as the intensity of the stimulus increased.

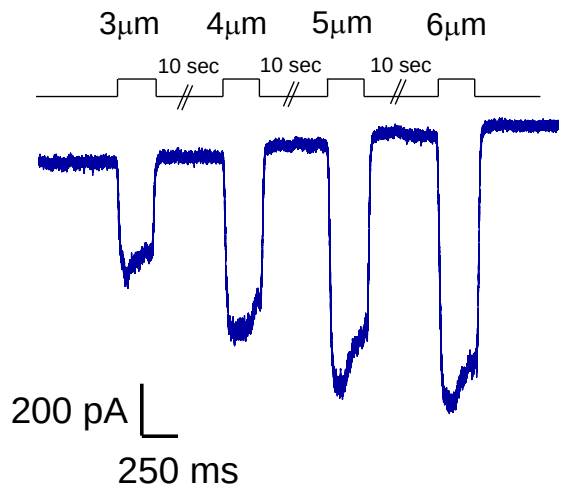

Figure 28. Mechanically activated currents measured using the mechano-clamp technique in a newborn TG neuron. Series of mechanically gated currents with increasing amplitude elicited by a series of more intense mechanical stimuli. Black trace shows the mechanical protocol. (V_{hold}= -60 mV)

I examined the electrophysiological properties of mechanosensitive and mechano insensitive neurons, looking for possible differences between them. The mean values of soma size, cell capacitance, input resistance, membrane potential and rheobase current are summarized in table 7 for newborn and table 8 for adult neurons.

The **soma size** of adult MS neurons (361 ± 10 μm²) was significantly higher than that of mechano insensitive neurons (328 ± 10 μm²). This difference was also reflected in the capacitance values that increased from a mean value of 26 pF in mechanoinsensitive neurons to 29 pF in MS neurons. As observed in calcium imaging experiments, in both subpopulations of neurons the mean soma size of neurons from newborn mice was significantly smaller than that of adult ones. Conversely, there was no difference in soma size and capacitance between MS and touch negative neurons from newborn mice.

The resting membrane potential was recorded in current clamp mode. In neurons from newborn mice, MS neurons had a significantly lower resting membrane potential (–53 ± 1 mV) than touch negative neurons (–61 ± 2 mV). This difference was not observed in adult neurons, whose membrane potential was quite similar in both subpopulations of neurons (–55 ± 1 mV).

The **rheobase** current of MS adult neurons was significantly higher than that in non-mechanosensitive neurons, indicative of a decrease in the excitability of MS neurons. In newborn neurons these differences were not observed.

Table 7

	Soma size (μm²)	Cell capacitance (pF)	Input resistance (MΩ)	Membrane potential (mV)	Rheobase current (pA)	Number of recorded cells
Mechano positive	279± 6	28 ± 1	467 ± 24	-53 ± 1$^{\#\#}$	183 ± 12	144
Touch negative	256 ± 11	27 ± 3	497 ± 49	-61 ± 2	138 ± 15	38

Table 8

	Soma size (µm²)	Cell capacitance (pF)	Input resistance (MΩ)	Membrane potential (mV)	Rheobase current (pA)	Number of recorded cells
Mechano positive	361 ± 10$^{###}$ ***	29 ± 2$^{\#}$	392 ± 20$^{\#\#}$	-55 ± 1	329 ± 19 ***	93
Touch negative	328 ±10 **	26 ± 2	454 ± 40	-55 ± 1.6	251 ± 24 ### **	64

Tables 7 and 8. Properties of mechanosensitive and touch negative trigeminal neurons from newborn and adult mice, respectively. # denotes statistical significance between mechanosensitive and touch negative neurons, in newborn (Table 7) or adult (Table 8) mice. The red asterisks denote statistical significance between newborn and adult neurons in the same subpopulations of neurons (***p < 0.001; ###p< 0.001; ##p< 0.01; #p< 0.05, Student's *t*-test).

4.2.3 Different classes of mechanosensitive currents

In order to characterize and classify the mechanically activated currents, I used the kinetic properties of the currents. For that, the decay phases of the currents were fitted with single exponential function and a time constant for current inactivation (τ) was calculated. Following the frequency distribution represented in Figure 29, mechanosensitive currents with a τ between 0.1 and 10 ms were classified as rapidly adapting (RA) currents. Mechanosensitive currents with a τ between 11 and 39 ms were classified as intermediately adapting (IA) currents and finally, currents with a τ > 40 ms were classified as slowly adapting (SA) currents that inactivated only marginally during the 250 ms stimulus. For some currents with very slow inactivation kinetics it was not possible to fit their decay phases reliably with an exponential function and they were included as SA currents. Some mechanosensitive currents, characterized by intermediate inactivation kinetics, were fitted by double exponential currents because they first present a faster decay phase followed by a slower second decay phase; for classification only the faster decay was considered.

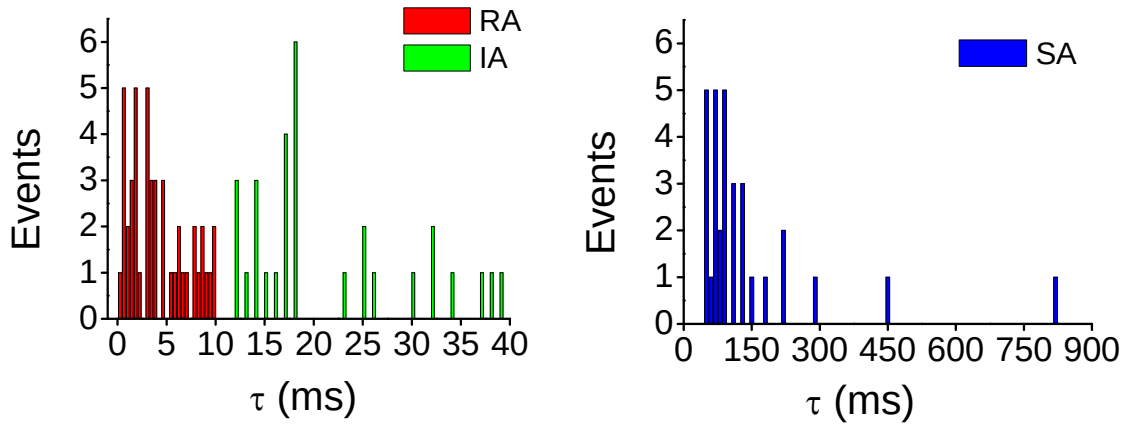

Figure 29. Frequency distribution of inactivation time constants in TG neurons from newborn mice. Data collected from 110 TG neurons voltage clamped at -60 mV and stimulated with a standard mechanical stimulus. The bin width was 0.4, 1 and 10 ms for RA, IA and SA currents, respectively.

Figure 30 shows sample traces of the three different types of mechanically gated currents obtained: rapidly adapting (A), intermediately adapting (B) and slowly adapting (C) currents recorded from three different adult TG neurons stimulated with the same mechanical protocol, forward increased movements of 1 μm for 250 ms. The number above the trace indicated the intensity of the applied mechanical stimulus.

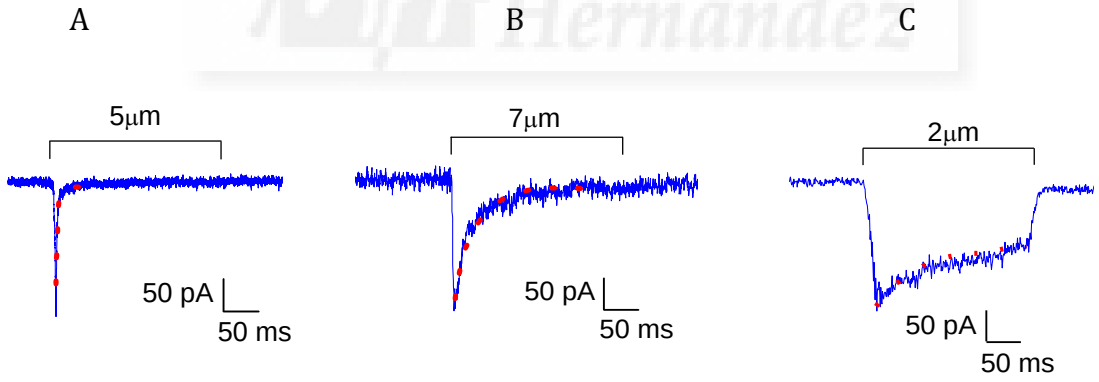

Figure 30. Static indentation activates three different inward currents in TG neurons. Examples of a rapidly adapting current with a τ of 10 ms (A), an intermediately adapting current with a τ of 23 ms (B) and a slowly adapting current with a τ of 127 ms (C). The information above the traces of each current indicates the duration and intensity of the mechanical stimulus applied. The red lines indicate the single exponential functions calculated to fit the decay phases of MA currents.

The distribution of the different mechanically activated currents was similar in neurons from newborn and adult mice. 52% (n=75/144) of newborn neurons exhibited SA currents, 32% (n=46/144) RA and 16% (n=23/144) IA currents; while

41% (n=38/93) of neurons from adult mice exhibited SA currents, 35% (n=33/93) RA currents and 24% (n=22/93) IA currents (Figure 31).

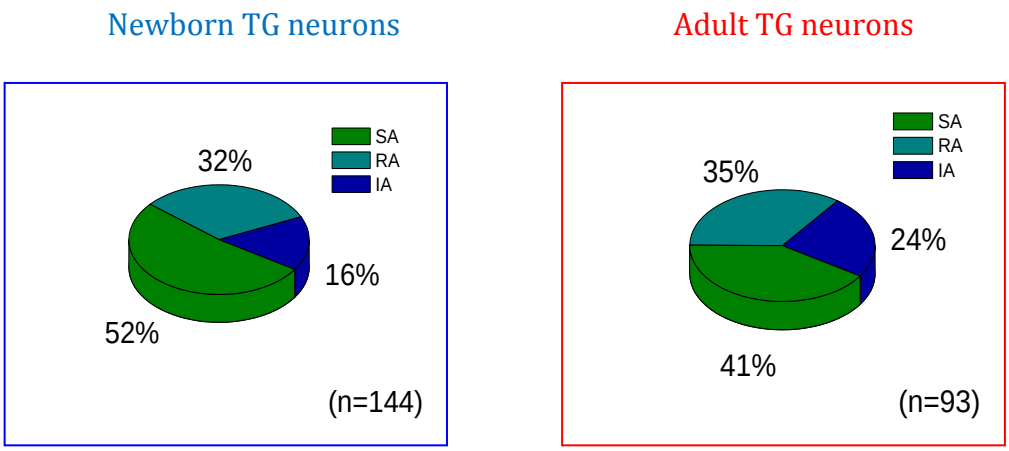

Figure 31. Distribution of the three mechanically gated currents in the total population of neurons from newborn and adult mice studied. The pie charts show the proportion of neurons from newborn and adult mice responding to mechanical stimulation with RA, IA or SA currents.

In neurons from newborn as well as adult mice, all three types of MA currents exhibited graded increases in amplitude in response to increasing the magnitude of indentation. Figure 32 shows mechanically gated currents with increasing amplitude evoked by a series of 1 µm incremental mechanical steps in the three different types of TG neurons, whose mechanical thresholds and decay phase differed. In all the three examples, application of a stronger stimulus activated currents with a larger amplitude. This degree of sensitivity to discriminate between different grades of mechanical forces is one of the properties of mechanotransducers.

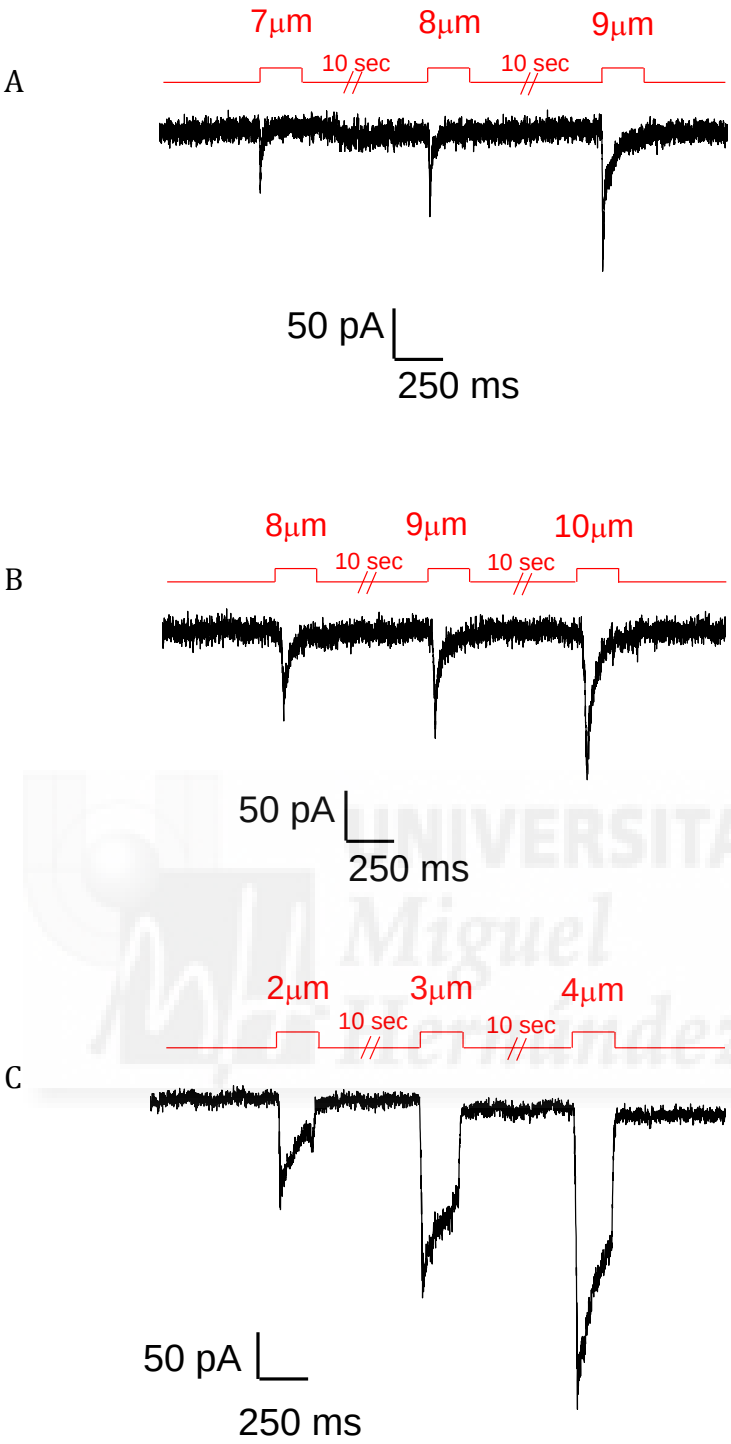

Figure 32. Examples of the subtypes of mechanically gated currents evoked in trigeminal neurons. The three general subtypes of mechanical currents were observed: (A) Rapidly Adapting, (B) Intermediate Adapting and (C) Slowly Adapting. Red traces indicate the mechanical protocol to increase the mechanical stimulus in 1 μm increments. All three mechanically gated currents exhibit graded increases in current amplitude in response to stronger mechanical stimulus. (V_{hold}= -60 mV).

4.2.3.1 Properties of TG neurons expressing different mechanosensory currents

After performing a general classification of the MA currents, the *soma size*, *mechanical threshold*, *latency*, *current amplitude* and *current density* of the neurons from newborn and adult mice displaying RA, IA and SA currents were analyzed. The current amplitude and current density between the neurons from newborn and adult mice were also compared.

I found that there were no significant differences in soma size, cell capacitance and latency time among neurons from newborn mice in cells displaying RA, IA or SA responses. By contrast, neurons with IA currents had a significantly higher mechanical threshold than RA currents (Table 9), while both the amplitude and density of the currents in cells with SA responses was significantly higher than in those with RA and IA (Table 10).

Table 9

	Soma size (μm^2)	Inactivation τ (ms)	Threshold (µm)	Latency Time (ms)	Number of cells
RA cells	276 ±10	4.0 ± 0.4	5.8 ± 0.4	1.2 ± 0.2	46
IA cells	273 ± 14	16.3 ± 0.9	6.5 ± 0.6$^{\#}$	0.9 ± 0.4	23
SA cells	278 ± 8	103 ± 19	5.0 ± 0.3	2.2 ± 0.2	75

Table 10

	Current amplitude (pA)	Current density (pA/pF)	Number of cells
RA cells	133 ± 21$^{\#\#}$	6.0 ± 1.0$^{\#}$	46
IA cells	99 ± 10 $^{\#\#\#}$	4.5 ± 0.7$^{\#}$	23
SA cells	171 ± 14	7.8 ± 0.8	75

Table 9 and 10. Properties of mechanosensitive currents in neurons from newborn mice. # denotes significant differences between the three RA, IA or SA subpopulations of neurons. ($^{\#}p< 0.05$; $^{\#\#}p < 0.01$; $^{\#\#\#}p < 0.001$; Student's *t*-test).

In the adult neurons, RA currents were observed in neurons with a soma significantly larger compared with cells with IA currents (Table 11), whereas there were no significant differences in the mechanical threshold, latency, amplitude and density of the current between the RA, IA and SA current types (Table 12).

Table 11

	Soma size (µm²)	Inactivation τ (ms)	Threshold (µm)	Latency Time (ms)	Number of cells
RA cells	402 ± 20# ***	4.3 ± 0.6	5.3 ± 0.4	2.1 ± 0.3 *	33
IA cells	336 ± 17 *	21 ± 2.2	6.2 ± 0.4	2.6 ± 0.2 **	22
SA cells	366 ± 15 **	158 ± 38	5.8 ± 0.4	2.7 ± 0.2	38

Table 12

	Current amplitude (pA)	Current density (pA/pF)	Number of cells
RA cells	153 ± 30	8.3 ± 2.6	33
IA cells	135 ± 25	6.7 ± 1.7	22
SA cells	196 ± 50	7.2 ± 1.8	38

Table 11 and 12. Properties of mechanosensitive currents in neurons from adult mice. # denotes significant differences between the three RA, IA or SA subpopulations of neurons. The red asterisk denotes statistical significance between the same RA, IA or SA subpopulations of neurons from newborn and adult mice (*p < 0.05; **p < 0.01; ***p < 0.001; #p< 0.05, Student's *t*-test).

I found significant differences in the mean soma size of the populations of neurons showing three current types, both in newborn and adult mice. This result was expected as at birth, most sensory axons are unmyelinated but become myelinated during the first three postnatal weeks, increasing their soma size. Another difference is the latency of the RA and IA currents in adult neurons that were significantly higher than in those from newborn mice (see Table 11).

So far, I had not observed differences in mechanical threshold between the three types of current that could clearly correlate them with low-and-high threshold neurons, with the exception of the IA current in neurons from newborn mice. This

finding suggests that the mechanical threshold at the level of soma, may not be an appropriate criterion to establish the functional phenotype of the neuron.

4.3 Properties of mechanosensitive currents in nociceptive and non-nociceptive neurons

To determine whether the different types of MA currents found in TG neurons from newborn and adult mice correlated with specific neuronal phenotypes, I classified neurons according to the different properties described previously, *i.e.* firing pattern and action potential shape, sensitivity to tetrodotoxin and IB4 labelling (see above). Previous studies have shown that these parameters discriminate between non-nociceptive and nociceptive mechanosensitive neurons (Drew et al., 2004; Drew et al., 2002; Hu and Lewin, 2006; Vilceanu and Stucky, 2010; Koerber et al., 1988; McCleskey and Gold, 1999).

4.3.1 Firing pattern and action potential shape

Neurons from newborn mice respond to a sustained suprathreshold depolarizing current pulse with either a phasic or a tonic firing. Analyzing the group of mechanosensitive neurons that express RA, IA or SA MA currents, no differences were found in the proportion of neurons with a phasic or tonic discharge pattern: phasic responses were present in 57% (n=25/44), 52% (n=11/21) and 53% (n=36/68) of RA, IA and SA cells, respectively (Figure 33A).

In neurons from adult mice on the other hand, phasic discharge pattern was more prevalent than the tonic pattern in neurons displaying the three types of MA currents: RA (88%, n=29/33), IA neurons (76%, n= 16/21) and SA (84%, n=32/38: $^{###}p < 0.001$; Figure 33B), compared with the proportion of neurons displaying tonic pattern. In addition, the proportion of neurons that expressed SA and RA currents and that presented a phasic discharge pattern was significantly higher than that in neurons from newborn mice, suggesting a change in the firing pattern during development.

The number of cells with a well-defined hump in the falling phase of the spike was analyzed and these cells were identified as probable nociceptors (Koerber et al., 1988; Lawson et al., 1997; Stucky and Lewin, 1999; Hu and Lewin, 2006).

The presence of APs with a hump was more common than narrow APs in all three types of MA currents in neurons form newborn and adult mice ($^{###}p < 0.001$; Z-test).

In neurons from newborn mice the hump was present in 82% (n=36/44), 91% (n=19/21) and 79% (n=54/68) of RA, IA and SA cells, respectively (Figure 33C). These proportions were quite similar in neurons from adult mice, which were 82% (n=27/33), 86% (n=18/21) and 92% (n=35/38) of RA, IA and SA cells, respectively (Figure 33D).

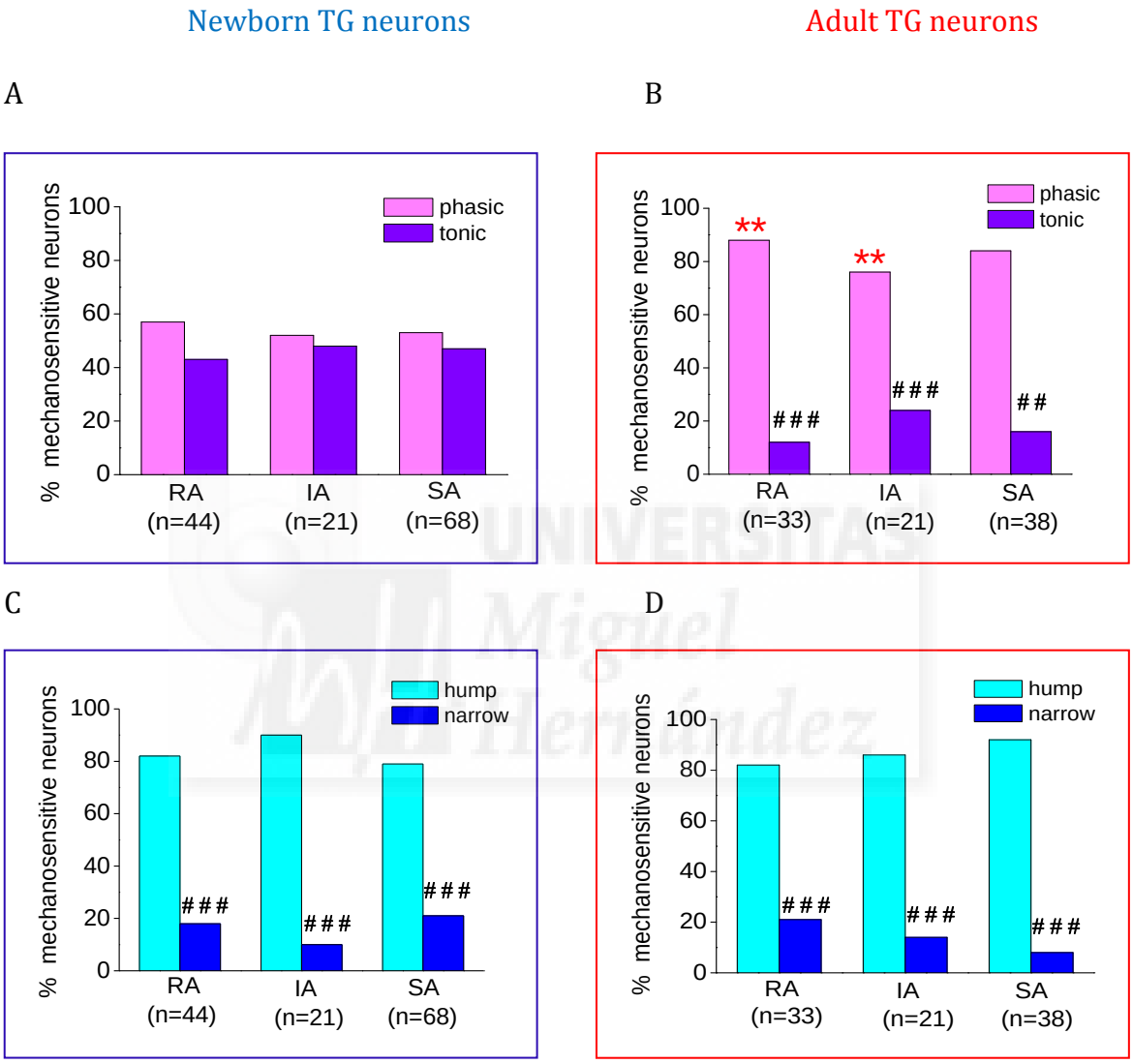

Figure 33. Discharge pattern and action potential shape in the three subtypes of RA, IA and SA neurons from newborn and adult mice. The discharge pattern in neurons from newborn (A) and adult mice (B). In adult mice there was a significant increase in phasic discharge, when compared to newborn mice. The majority of trigeminal neurons had a hump in the falling phase of the AP, in neurons from both newborn (C) and adult (D) mice. The values below the bars indicate the number of neurons recorded in each group. The # denotes statistical significance between the phasic vs.tonic or hump vs. narrow subpopulations of neurons, from the newborn or adult mice. The red asterisk denotes statistical significance between neurons from newborn and adult mice, in the same subpopulations of RA, IA or SA neurons ($^{###}p < 0.001$; $^{**}p < 0.01$; Z-test).

4.3.2 The presence of tetrodoxin-resistant voltage-gated Na^+ channels in mechanosensitive neurons

TG neurons from newborn mice were characterized using the voltage-gated Na^+ channels blocker TTX (see example in Figure 34). In the example shown, tonic firing behaviour in the control solution in current clamp mode (A) and when the mechanically activated current was monitored in voltage-clamp mode (B). Finally, the current clamp protocol was repeated during superfusion of 1 μM TTX and the firing of an AP indicated that this neuron is resistant to TTX, therefore showing a nociceptive phenotype (C).

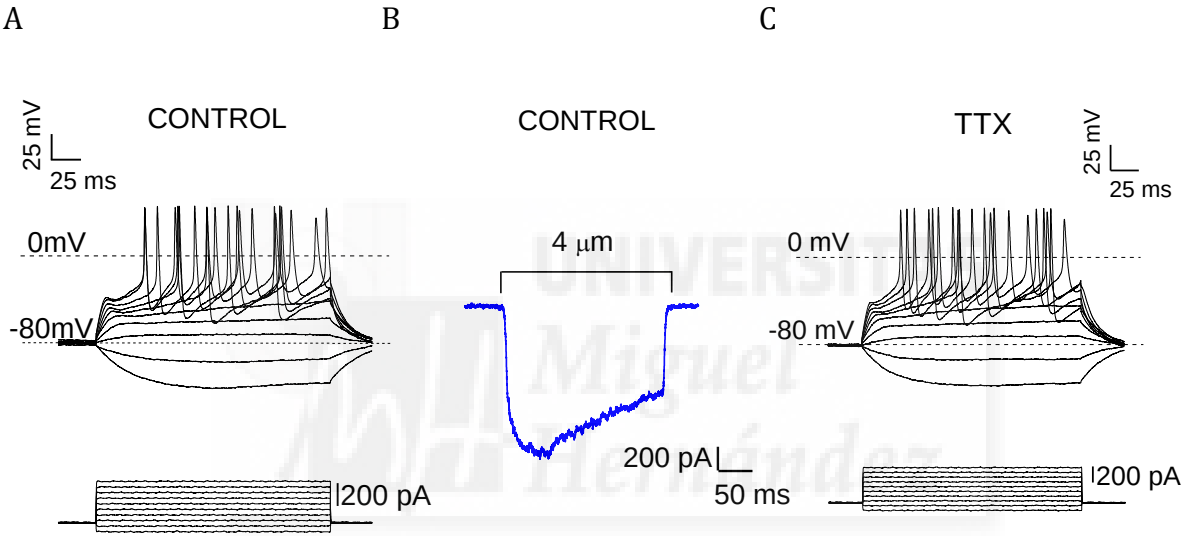

Figure 34. Entire sequences of electrophysiological protocols applied using TTX. After assessing the excitability of the neurons in current clamp mode (A), the protocol was switched to voltage clamp to record mechanically gated currents (B). This particular example correspond to a SA neuron with a mechanical threshold of 4μm. Finally, the current clamp protocol was again applied in the presence of TTX 1μM to assess the TTX-resistance of neurons (C).

Similar protocols were applied to 31 neurons from newborn mice and 19 adult neurons.

More heterogeneity was observed when the incidence of the three types of mechanosensitive currents were analysed in the TTX-resistant or TTX-sensitive neurons. In TTX-sensitive neurons from newborn mice, 12% (n=1/9), 44% (n=4/9) and 44% (n=4/9) responded with a RA, IA and SA currents, respectively. By contrast, the majority of TTX-resistant neurons from newborn mice responded with a SA

current (73%; n=16/22; ***p < 0.001, Z-test), and only 18% (n=4/22) and 9% (n=2/22) responded with RA and IA currents, respectively (Figure 35A).

In TTX-sensitive adult neurons, 55% (n=6/11), 9% (n=1/11) and 36% (n=4/11) responded with a RA, IA and SA currents, respectively (not significantly different), whereas in TTX-resistant adult neurons 25% (n=2/8), 37.5% (n=3/8) and 37.5% (n=3/8) responded with a RA, IA and SA currents, respectively (Figure 35B). There was no significant difference in the proportion of RA, IA and SA currents in the TTX-resistant or TTX-sensitive neurons from newborn and adult mice, indicating that there is heterogeneity in the distribution of the three MA currents in the different subsets of studied neurons.

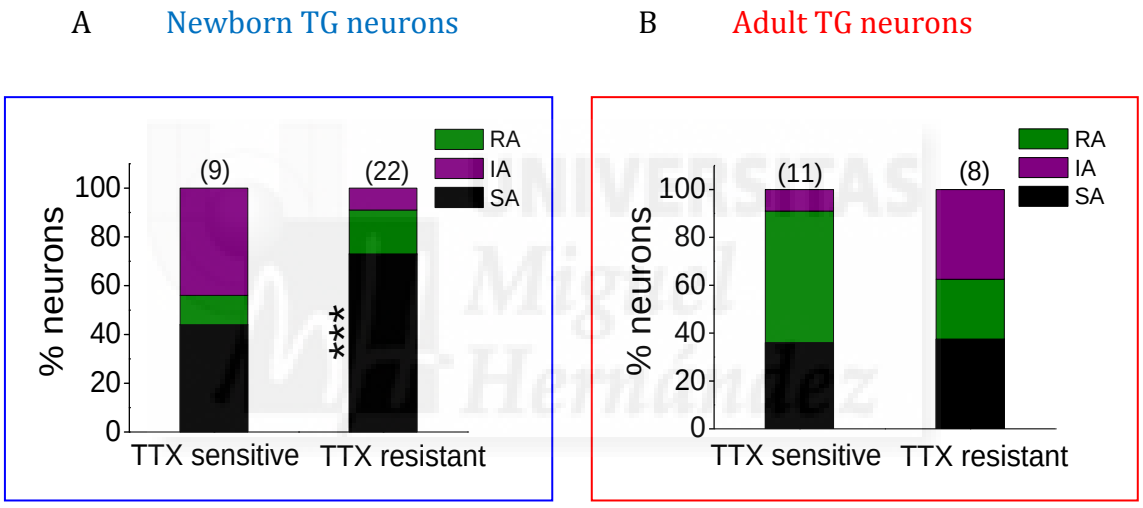

Figure 35. The distribution of mechanosensitive currents among the two subpopulations of TTX-resistant or TTX-sensitive neurons. Histograms summarize the proportion of TTX resistant or TTX sensitive neurons from newborn (B) and adult (C) mice that responded to mechanical stimulation with RA, IA or SA currents. The values above the bars indicate the number of neurons recorded in each group. The asterisks denote significant differences between the proportion of RA, IA or SA neurons among the TTX resistant neurons from newborn mice (***p < 0.001; Z-test).

4.3.3 IB4 labelling

IB4 staining was used to identify non-peptidergic nociceptive neurons and, when the incidence of the three mechanosensitive currents was analyzed in the two subpopulations of IB4 positive and negative neurons, there was also heterogeneity in the mechanosensitive response with no significant differences. Accordingly, in IB4 positive neurons from newborn mice 43%, 17% and 40% responded with RA, IA and SA currents, respectively (Figure 36A). Among the IB4 negative neurons from

newborn mice 41%, 11% and 48% responded with RA, IA and SA currents, respectively (Figure 36C).

In adult IB4 positive neurons 33%, 21% and 46% responded with RA, IA and SA currents, respectively (Figure 36B), whereas RA, IA and SA currents were detected in 40%, 35% and 25% IB4 negative adult neurons, respectively (Figure 36D).

When newborn and adult mice were compared, there were no differences between RA, IA and SA currents among the IB4 positive and IB4 negative neurons.

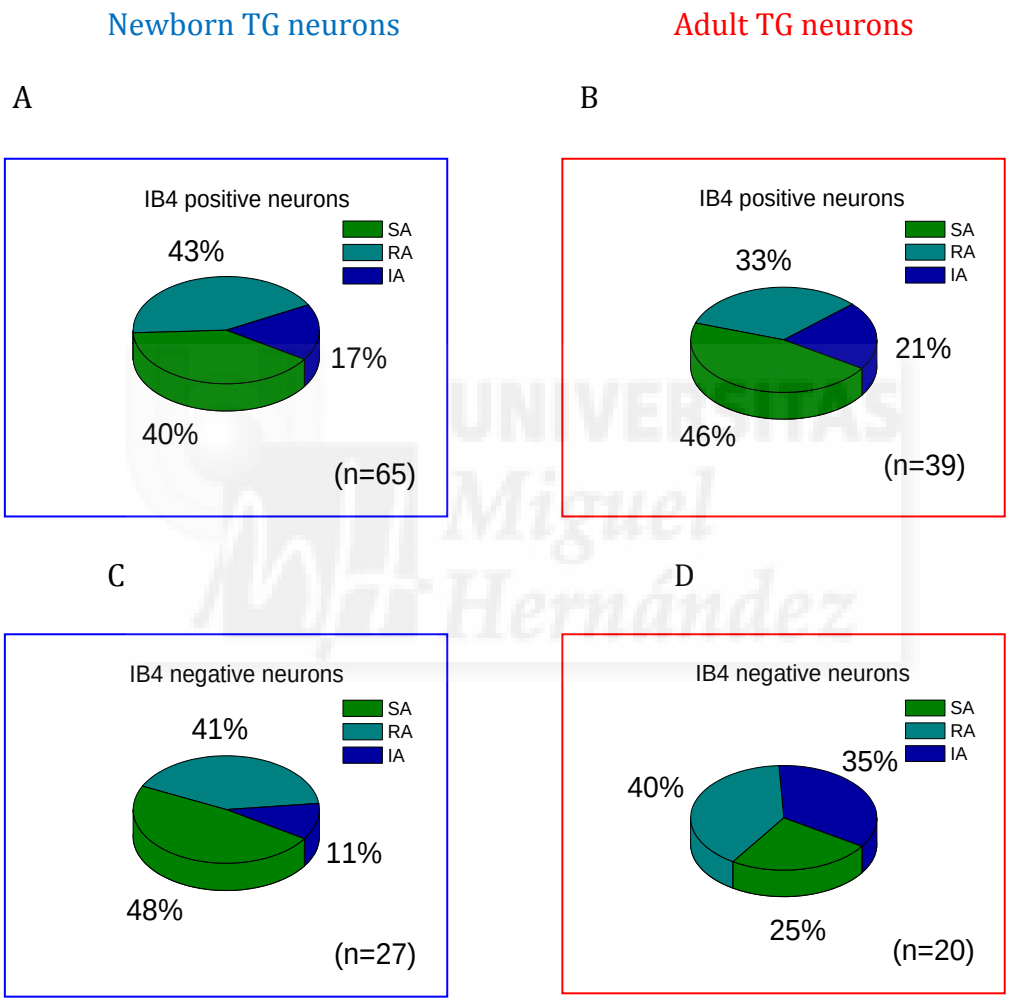

Figure 36. Distribution of mechanosensitive currents among the two subpopulations of IB4 positive and IB4 negative neurons. Proportion of RA, IA or SA currents in IB4 positive neurons from newborn (A) and adult (B) mice and IB4 negative neurons from newborn (C) and adult (D) mice.

4.3.4 Expression of the mechanically gated currents in nociceptive and non-nociceptive neurons from newborn and adult mice

I used a combination of different criteria, to classify neurons as non-nociceptive and nociceptive, and I associated these with the expression of the different types of MA currents.

Neurons were classified as nociceptive if they were IB4 positive or were resistant to TTX. In contrast, lacking a specific marker for non-nociceptive neurons, several parameters were used to identify them. I considered their TTX sensitivity, the soma size, the firing pattern and the action potential shape to define these latter neurons.

Several properties were analyzed for the population of nociceptive and non-nociceptive mechanosensitive neurons (See Table 13 and 14, for neurons from newborn and adult mice, respectively).

In neurons from newborn mice, non-nociceptive neurons had a significantly larger soma (333 ±17 μm^2; $^{\#\#}p = 0.005$) than nociceptive neurons (277 ±6 μm^2), while no differences were detected in any of the other parameters. Surprisingly, the mean soma size of non-nociceptive neurons from adult mice was similar to that of nociceptive ones, although this maybe due to a technical limitation of the difficulty to record the largest neurons with the patch clamp technique.

Table 13

	Soma size (μm^2)	Current amplitude (pA)	Current density (pA/pF)	Threshold (µm)	Latency Time (ms)	n
Mechano-Nociceptive neurons	277 ± 6	131 ± 13	5.0 ± 0.6	5.6 ± 0.3	2.5 ± 0.3	80
Mechano-non-nociceptive neurons	333 ± 17 ##	158 ± 47	8.7 ± 2.8	7.0 ± 1.0	1.1 ± 0.7	9

Table 14

	Soma size (μm^2)	Current amplitude (pA)	Current density (pA/pF)	Threshold (µm)	Latency Time (ms)	n
Mechano-nociceptive neurons	359 ±12 ***	134 ± 29	4.9 ± 0.8	5.7 ± 0.4	2.5 ± 0.2	45
Mechano-non-nociceptive neurons	373 ± 31	212 ± 47#	7.0 ± 1.9	6.0 ± 0.5	1.9 ± 0.5	21

Table 13 and 14. Kinetic properties of mechanosensitive currents recorded in mechano-nociceptive and non-nociceptive neurons, from newborn and adult mice, respectively. The values on the "n" column indicate the number of neurons in each group. # represents statistically significant differences between the two subpopulations of neurons, nociceptive and non-nociceptive neurons from the newborn (Table 13) or adult (Table 14) populations. The red asterisks represent a statistically significant difference between neurons from newborn and adult mice within the same subpopulation, mechano-nociceptive or non-nociceptive neurons (***$p < 0.001$; ##$p < 0.01$; #$p < 0.05$, Student's *t*-test).

When neurons from newborn and adult animals were compared no significant differences other than the larger soma of the nociceptive neurons from adult mice (***$p < 0.001$) were observed.

Both populations of neurons displayed the three types of currents at different proportion in newborn and adult mice (Figure 37). Apparently, there was an increase in the proportion of RA currents and a decrease of IA currents in non-nociceptive neurons from adult mice compared to those from newborn mice, although these trends were not statistically significant. This could be due to the low number of non-nociceptive neurons identified from newborn animals. In conclusion, these results indicate that it is not possible to associate a specific MA current to a subpopulation of neurons.

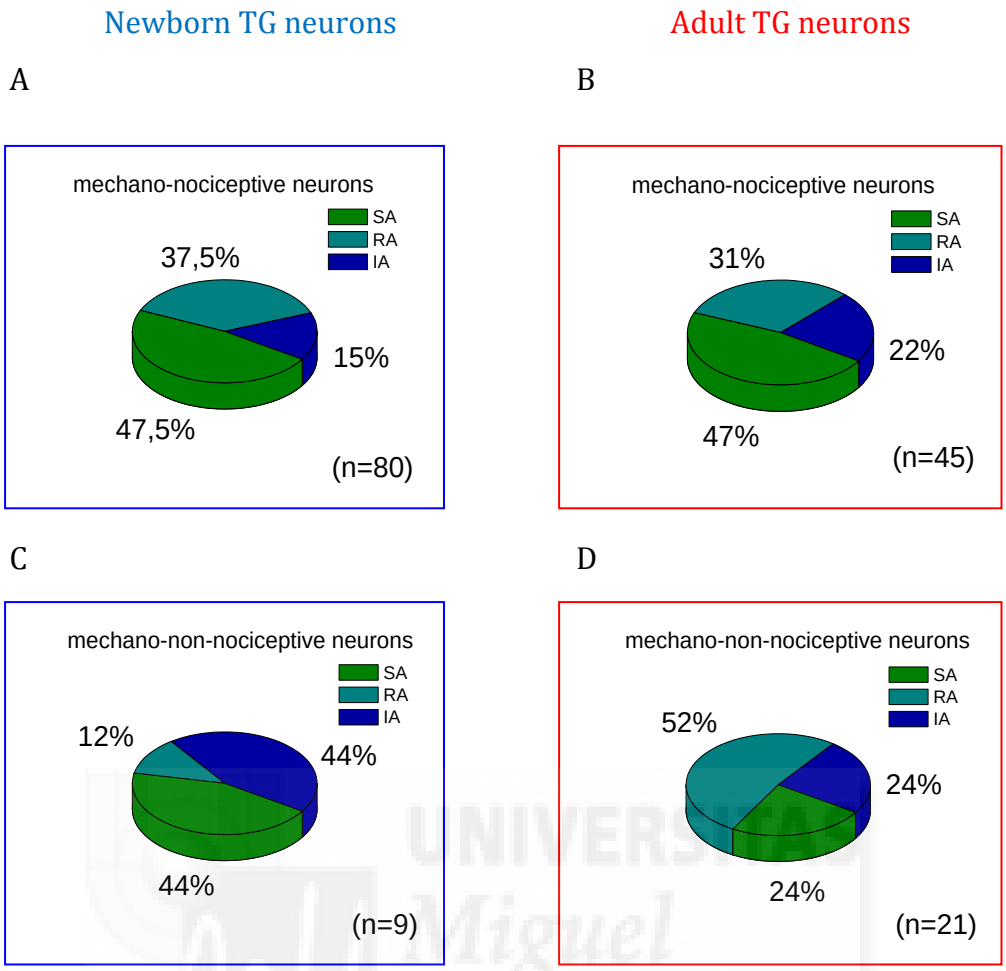

Figure 37. Distribution of mechanosensitive currents among the two subpopulations of nociceptive and non-nociceptive MS neurons. Proportion of RA, IA or SA currents in mechano-nociceptive neurons from newborn (A) and adult (B) mice, and mechano-non-nociceptive neurons from newborn (C) and adult (D) mice.

4.4 Mechanotransducer channel properties of the RA, IA and SA mechanosensitive currents

An open question is whether the different kinetic properties of mechanosensitive currents reflect the activation of distinct populations of ion channels. To address this question, I analyzed the reversal potential of the three MA currents and I studied the pharmacological sensitivity of MA currents using the trivalent ion gadolinium, a blocker of stretch activated channels (McCarter et al., 1999; Drew et al., 2002; Hu and Lewin, 2006; Cho et al., 2002; McCarter and Levine, 2006; Viana et al., 2001).

4.4.1 Current-voltage relationship in RA, IA and SA currents

The reversal potential is the potential at which the net ionic current is zero and it is important because it gives the voltage that acts on channels permeable to that ion and it allows to know the ion channel selectivity. Thus, I measured the reversal potential of RA, IA and SA currents evoked by stimulating the cell soma of neurons from newborn mice.

The mechanical stimulus was delivered with the membrane command voltage set to different membrane potentials between −80 mV and +40 mV. For each cell, the MA current was activated at four to six holding potentials, as evident in the graphs on the left column of Figure 38 that show representative traces of RA, IA and SA mechanosensitive currents recorded in three different neurons from newborn mice that were evoked by different mechanical intensities and that depended on the mechanical threshold of each neuron. Once a neuron responded to a mechanical stimulus, the same stimulation was repeated at different voltage potentials. The right column of Figure 38 shows the mean peak current amplitude plotted against the membrane potential for neurons responding with RA (n=4), IA (n=1) and SA (n=8) currents. The mean reversal potentials, calculated as the mean of the reversal potential of each cell, were 6.5 ± 2.5 mV, −2 mV and −2.2 ± 1.4 mV for RA, IA and SA currents, respectively (values ranged from −3.4 to +9 mV). These values are positive or close to 0 mV, indicating that the currents in TG neurons are non-selectively carried by cations.

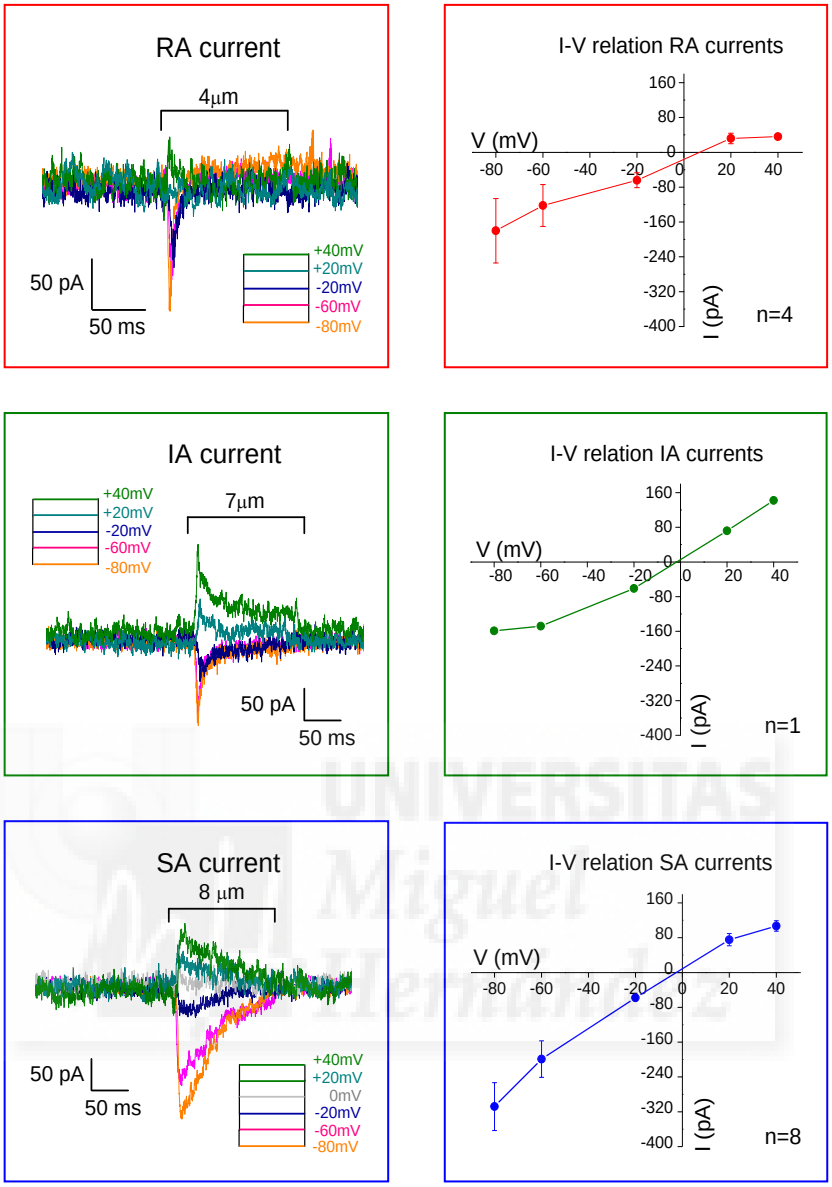

Figure 38. The mechanically gated currents are non-selective cation currents. (Left column) Representative traces of RA, IA and SA currents, each evoked by identical mechanical stimuli and manually changing the membrane potentials between −80 mV and +40 mV. (Right column) Current-voltage relationships for the mechanically activated currents recorded in whole-cell configuration. The means reversal potential indicates that the RA current reverses at about +6.5 mV, whereas IA and SA currents reverse at about −2 mV.

4.4.2 Effect of Gadolinium on the mechanically gated currents in newborn and adult mice

In order to determine the pharmacological sensitivity of mechanically gated currents, the trivalent ion gadolinium (Gd^{+3}) was used. Studies carried out over two decades ago in *Xenopus laevis* show that Gd^{+3} blocks stretch activated channels (SACs: Yang and Sachs, 1989; Hamill and McBride, Jr., 1996) and thus, it has been widely adopted as a tool to study mechanogated channels. Exposure to 10μM Gd^{3+} is sufficient to largely block cation SACs and thus, to inhibit mechanosensitive processes (Hamill and McBride, Jr., 1996; Morris, 1990) and mechanically gated currents elicited by static indentation (McCarter et al., 1999; Drew et al., 2002; Hu and Lewin, 2006).

In neurons recorded in whole cell configuration at −60 mV, the effect of Gd^{3+} was assessed on RA and SA mechanically activated currents (representative examples shown in Figure 39A, B). After trying different concentrations of Gd^{+3}, I decided to use 8 μM, rather than a higher concentration, because neurons recovered better after drug washout. Neurons that responded to mechanical indentation were perfused with Gd^{+3} (8 μM) and a second protocol of mechanical indentation was applied in the presence of the drug. After wash out of Gd^{3+}, a third mechanical stimulus was applied to test the recovery of the inhibition. The traces of RA mechanical activated currents evoked by 6 μm indentation of a neuron from a newborn mouse are superimposed in control conditions (black trace), in the presence of the drug (red trace) and after washout of the drug (gray trace: Figure 39A). A similar example of a SA current can be seen when evoked by 4 μm indentation in a neuron from a newborn mouse in control conditions (black trace), in the presence of the drug (red trace), and after washout of the drug (gray trace: Figure 39B).

I found that Gd^{+3} (8μM) was effective in reversibly inhibiting both RA and SA currents. IA currents were not recorded in this set of experiments.

The effect of Gd^{3+} on the MA currents was expressed as the proportion of current inhibition with respect to the control response as summarised in histograms. In neurons from newborn mice, Gd^{+3} blocked 95 ± 4% of the RA currents (n=3) and 80 ± 7.5 % of the SA currents (n=4: Figure 39C). By contrast Gd^{+3} blocked 58 ± 8 % of the RA currents (n=5) and 72 ± 12 % of the SA ones in adult neurons (n=4: Figure

39D). Thus, gadolinium blocked all the MA currents significantly, except the RA currents in adult mice. In these neurons Gd^{+3} also appeared to reduce the amplitude of the current but this trend was not statistically significant.

Full recovery of the current amplitude was not observed after drug washout with control solution for 5 minutes, and some inhibition of RA currents (36 ± 15 % and 32 ± 11 % in newborn and adult mice, respectively) and of SA currents (32 ± 16 % and 39 ± 16 % in newborn and adult mice, respectively) persisted.

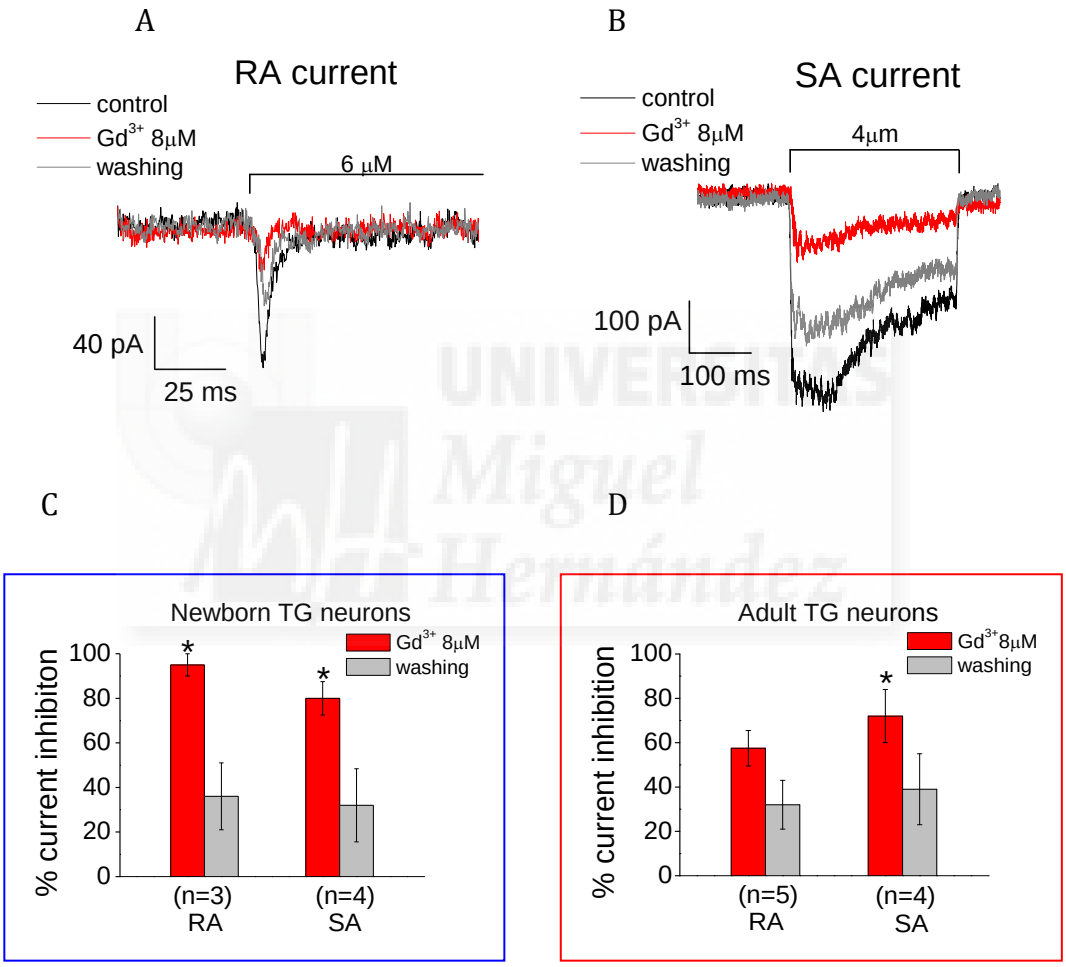

Figure 39. Pharmacological inhibition of RA and SA mechanosensitive currents by gadolinium in neurons from newborn and adult mice. Sample traces from neurons of newborn mice with a RA (A) and a SA current (B) in control solution, as well as during and after application of gadolinium. Gadolinium has an inhibitory effect on mechanosensitive currents. (V_{hold}= -60 mV). Histograms showing the effect of 8 μM gadolinium on mechanosensitive currents in mechanosensitive TG neurons from newborn (C) and adult (D) mice. The figures below the bar indicate the number of neurons tested in each group. (*$p < 0.05$; Mann-Whitney Rank-Sum test).

4.5 Identification of mechanotransducer channels in newborn and adult neurons

The next objective of this Thesis was to identify the expression of specific mechanotransducer channels in the different populations of MS TG neurons, looking for possible correlations between a MS phenotype and the expression pattern of specific receptors. To achieve this, I performed semi-quantitative PCR on single neurons (see methods) that had been electrically and mechanically characterized prior to identifying the presence of mRNAs encoding putative mechanotransducers. In these studies, a nested PCR amplification strategy was employed in order to increase the fidelity of the PCR reaction and the specificity of the product amplified.

4.5.1 Expression of mechanotransducer channels in trigeminal neurons

Several ion channels proposed as putative mechanotransducers were selected (see introduction section): **TRPA1** (Vilceanu and Stucky, 2010; Brierley et al., 2011); **TRPC5** (Gomis et al., 2008); **Piezo2** (Coste et al., 2010; Coste et al., 2010; Bae et al., 2011); **TRPC3** (Quick et al., 2012); **ASIC3** (Price et al., 2001); and **TRPV2** (Muraki et al., 2003; Beech et al., 2004). The aim was to assess the expression of these channels with the populations of nociceptive and non-nociceptive mechanosensory neurons already characterized. Therefore, as well as using the criteria previously described to distinguish nociceptive from non-nociceptive neurons, I also analyzed the mRNA expression of the nociceptive markers: **TRPV1** (Caterina et al., 1997; Caterina et al., 2000); **NaV1.8** (McCleskey and Gold, 1999; Waxman et al., 1999; Baker and Wood, 2001) and **TRPA1** (Story et al., 2003; Bandell et al., 2004; Jordt et al., 2004; Bautista et al., 2006). β-actin was used as a control housekeeping gene. As indicated, TRPA1 was also used as a putative mechanotransducer channel.

TG neurons have been shown to express all the channels selected, with the exception of Piezo2, both by PCR and immunocytochemistry (Akopian et al., 1996; Gomis et al., 2008; Story et al., 2003; Lingueglia, 2007; Vandewauw et al., 2013; Ichikawa and Sugimoto, 2002). Nevertheless, to confirm these data and to test the efficacy of the designed primers, the expression of these channels in trigeminal ganglia from newborn and adult mice was tested.

The expression of the distinct mRNAs was assessed by RT-PCR using cDNA synthesized from the mRNA extracted from whole TG ganglia as the template. All the genes tested were detected in TG ganglia using the set of primers shown in Table 4 (see Materials and Methods). Two SYBR-safe-stained agarose gels are shown (Figure 40) that were loaded with the products of semi-quantitative PCR amplification from cDNA generated from the mRNAs extracted from the trigeminal ganglia of an adult mouse, using primers for the **first round** nested PCR. The first and last lanes of each gel showed the molecular weight markers and the H_2O labelled lanes are negative controls of PCR amplification, whereas the lanes labelled (-) are negative controls of reverse transcription. The expression of mRNAs encoding all the channels studied was also detected in newborn mice.

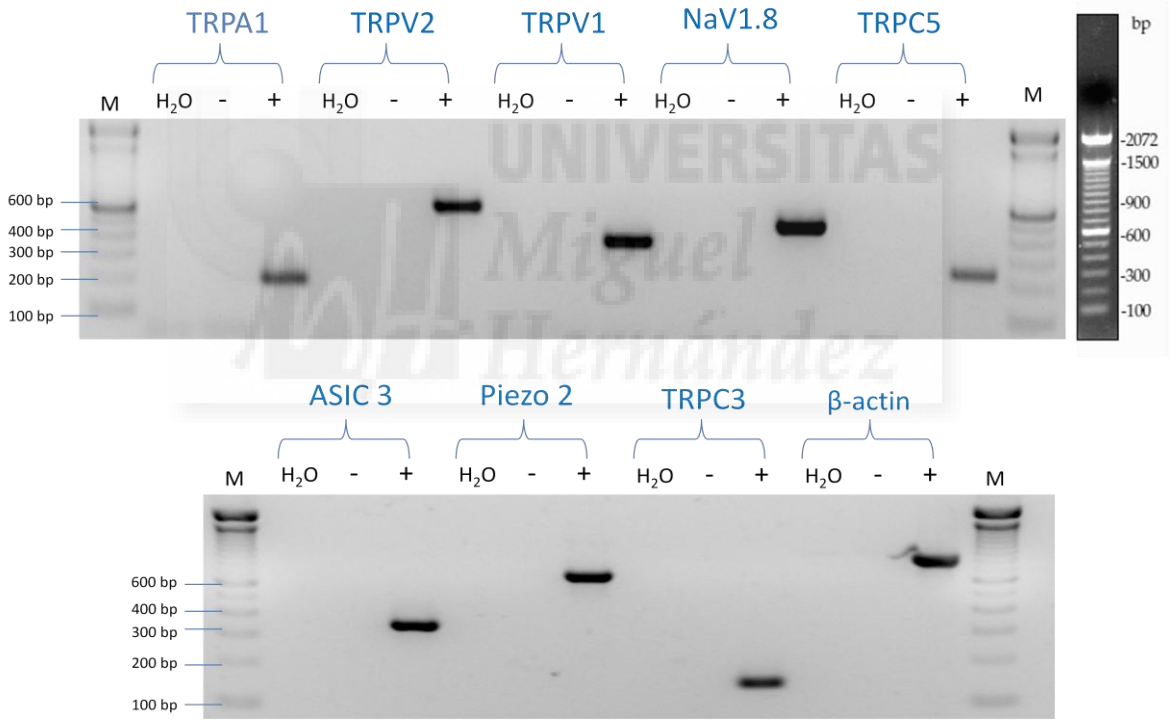

Figure 40. mRNA expression of the indicated proteins in the adult TG tissue. The primers used for the RT-PCR correspond to those to be used in the first round of the nested PCR. The two gels are from the same RT-PCR experiment. Predicted product sizes for TRPA1 (182 bp), TRPV2 (554 bp), TRPV1 (343 bp), NaV1.8 (452 bp), TRPC5 (221 bp), ASIC3 (320 bp), Piezo2 (632 bp), TRPC3 (137 bp) and β-actin (791 bp). The sizes of the molecular weight marker are shown on the left. (n=4)

The agarose gels shows in Figure 41 were loaded with products of a similar semi-quantitative PCR amplification but using the primers shown in Table 5 that will be used for the **second round** of the nested single cell PCR. All the mRNAs tested

were also detected with these primers and again, the same results were obtained in newborn mice.

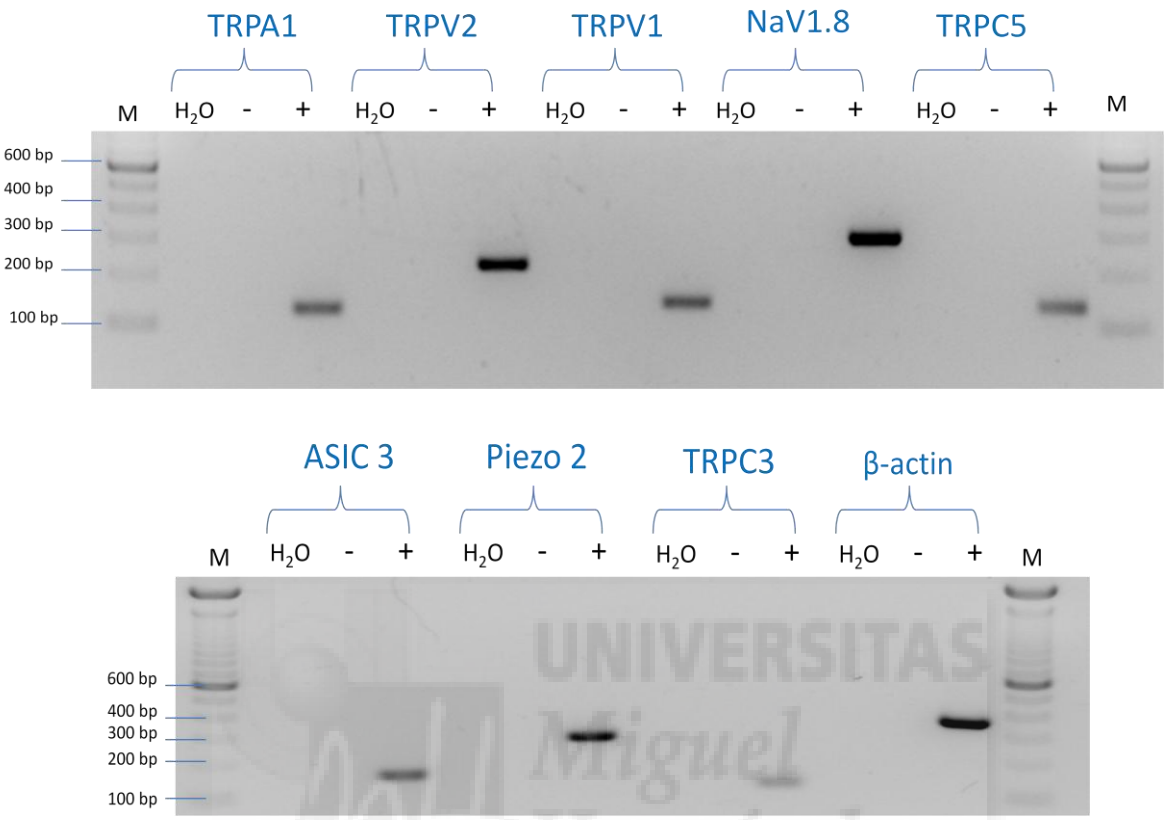

Figure 41. mRNA expression of the indicated proteins in the adult TG tissue. The primers used for the RT-PCR correspond to those to be used in the second round of the nested PCR. The two gels are from the same RT-PCR experiment. Predicted product sizes for TRPA1 (118 bp), TRPV2 (216 bp), TRPV1 (138 bp), NaV1.8 (293 bp), TRPC5 (127 bp), ASIC3 (141 bp), Piezo2 (267 bp), TRPC3 (112 bp) and β-actin (342 bp). The size of the molecular weight marker are shown on the left. (n=4)

4.5.2 Detection of mechanotransducer channels in neurons from newborn and adult mice

The expression of the candidate mechanotransducers was analysed in 18 neurons from newborn and 23 neurons from adult mice, collected after characterizing their electrical, mechanical and nociceptive properties. Amplification of β-actin was detectable in 39 of the 41 tested neurons, indicating a high efficiency in the successful collection of the cells and cDNA synthesis.

The complete characterization of a single TG neuron from a newborn mouse, positive for IB4 (a hallmark of nociceptors), with a soma size of 235 μm^2 is show in

Figure 42. Electrophysiological recordings in current clamp mode highlighted a tonic firing behavior (Figure 42A, left panel). The mechanically activated currents were monitored in this neuron in voltage-clamp mode and they showed a mechanical threshold of 7 μm. Moreover, when the decay phase of this current was fitted by a single exponential function the time constant for current inactivation (τ) was 1.3 ms, reflecting RA kinetics (Figure 42A right panel). After this characterization, the neuron was collected into a PCR tube, the membrane was broken by thermic shock and cDNAs were synthesized from the total mRNA. The population of cDNAs synthesized were divided into six ~3-μl aliquots that were used in a first PCR reaction. Given the small amount of cDNA available from each neuron, it was not possible to assess the expression of more than six or seven genes. The product of this PCR amplification was then run again in a second round of PCR using different (nested) primers in order to analyze the expression of the selected mechanotranducer channels (for more details see the Materials and Methods). The expression of TRPC5, Piezo2 and TRPC3 was clearly evident in this specific neuron (Figure 42B). Indeed, while the products of the first (larger PCR product) and additional nested (smaller) amplification were detected for TRPC5 and Piezo2, a product from the second amplification alone was detected for TRPC3. As a positive control of the PCR, β-actin from the whole trigeminal ganglia was amplified, as evident in the lane "β-actin tissue".

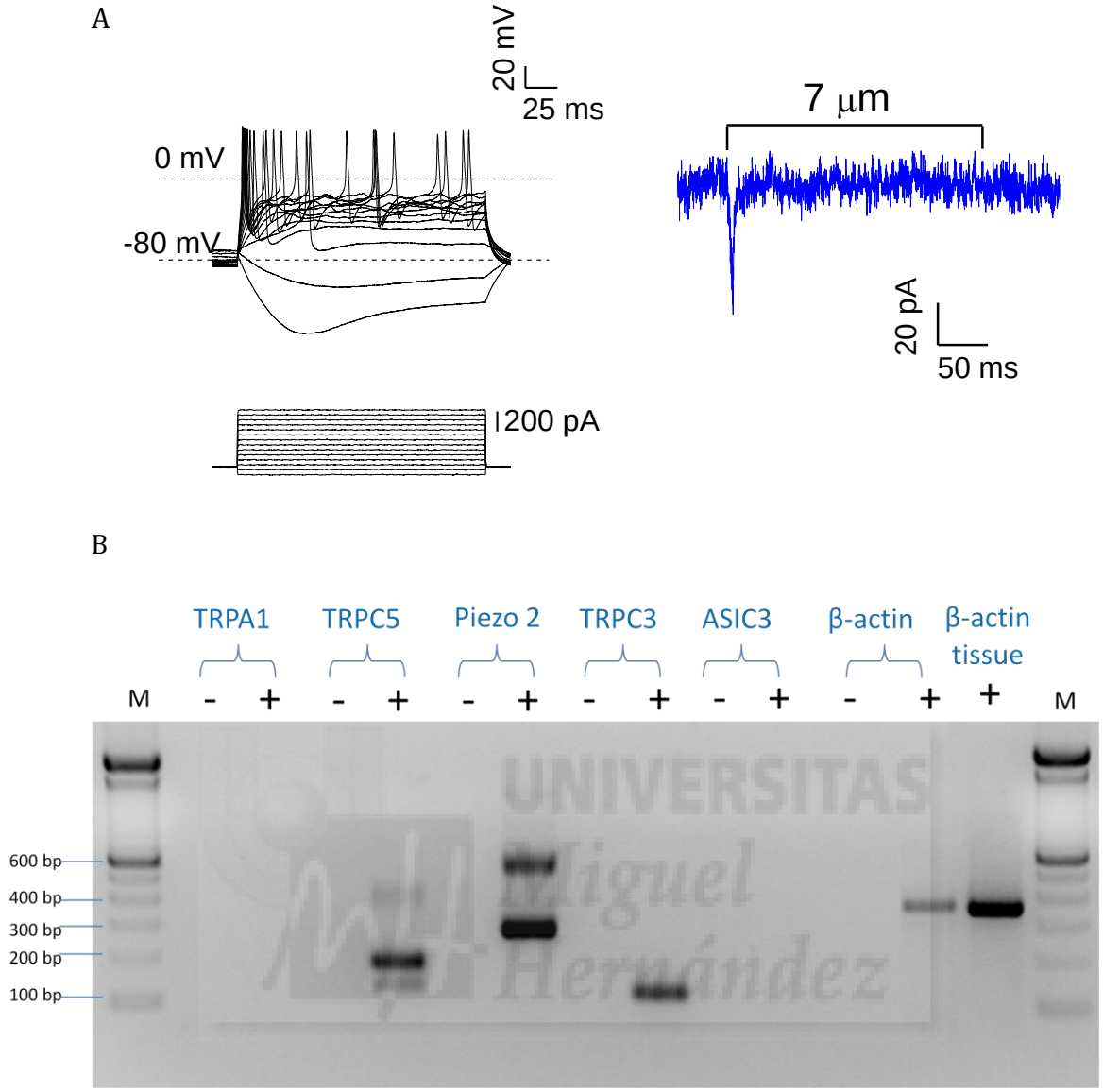

Figure 42. Expression of candidate mechanotransducer channels detected by single cell RT-PCR in a trigeminal neuron from a newborn mouse. (A) Firing discharges and mechanically activated currents recorded by current and voltage clamp, respectively. (B) Detection of TRPC5 (expected products 221 bp and 127 bp), Piezo2 (expected products 632 bp and 267 bp), TRPC3 (expected product 112 bp) mRNA expression, and that of the housekeeping β-actin (expected product 342 bp). As negative controls, the same amount of H_2O was added instead of the cDNA (lane -).

4.5.3 Heterogeneity in the expression of mechanotransducer channels in different subpopulations of neurons from newborn and adult mice

To try to correlate the mechanotransducer channel expression with specific subpopulations of neurons, two different analyses were carried out. First, I associated the three types of the MA currents displayed by the neurons (RA, IA and SA) with the expression of the mechanotransducers studied. In the second analysis I assessed the expression of the mechanotransducers in nociceptive and non-nociceptive

mechanosensory neurons, using the criteria established previously to classify neurons a nociceptive or non-nociceptive (see section 4.3). The mRNA expression for TRPV1 and NaV1.8 was not always tested due to limitations in the availability of the samples. Moreover, the expression of the SA or RA current were not considered as a criterion of nociceptive and non-nociceptive neurons because my results showed such kinetics are not exclusive to these populations of neurons.

The results showed that TRPA1 (16/18 in neurons from newborn and 12/23 from adult mice), TRPC5 (18/18 newborn and 18/23 adult) and Piezo2 (14/18 newborn and 13/23 adult) are expressed in the majority of the neurons recorded. This is particularly evident in the histograms showing the proportions of mechanosensory neurons from newborn and adult mice displaying RA, IA or SA currents that express TRPA1, TRPC5, Piezo2, TRPC3 and ASIC3 (Figures 43A and B). The data show that significant fewer RA neurons from adult mice express TRPC5 compared to those displaying SA currents ($*p < 0.05$; Z-test). Similarly, the proportion of nociceptive and non-nociceptive neurons from newborn and adult mice that expressed TRPA1, TRPC5, Piezo2, TRPC3 and ASIC3 are also shown in histograms (Figures 43C and D). NaV1.8 expression was tested in the initial experiments performed in adult mice but it was then decided not to include this channel in the analysis of newborn animals. Therefore, I reduced the number of channels tested in order to increase the volume of the PCR reaction available. The results obtained showed there were no differences in the proportion of neurons that expressed a specific channel.

In summary, the expression of putative mechanotransducer channels is heterogeneous and it was not possible to associate their expression to a specific group of neurons. This may suggests that the final response of neurons might depend on the contribution of different ion channels, with different properties and kinetics.

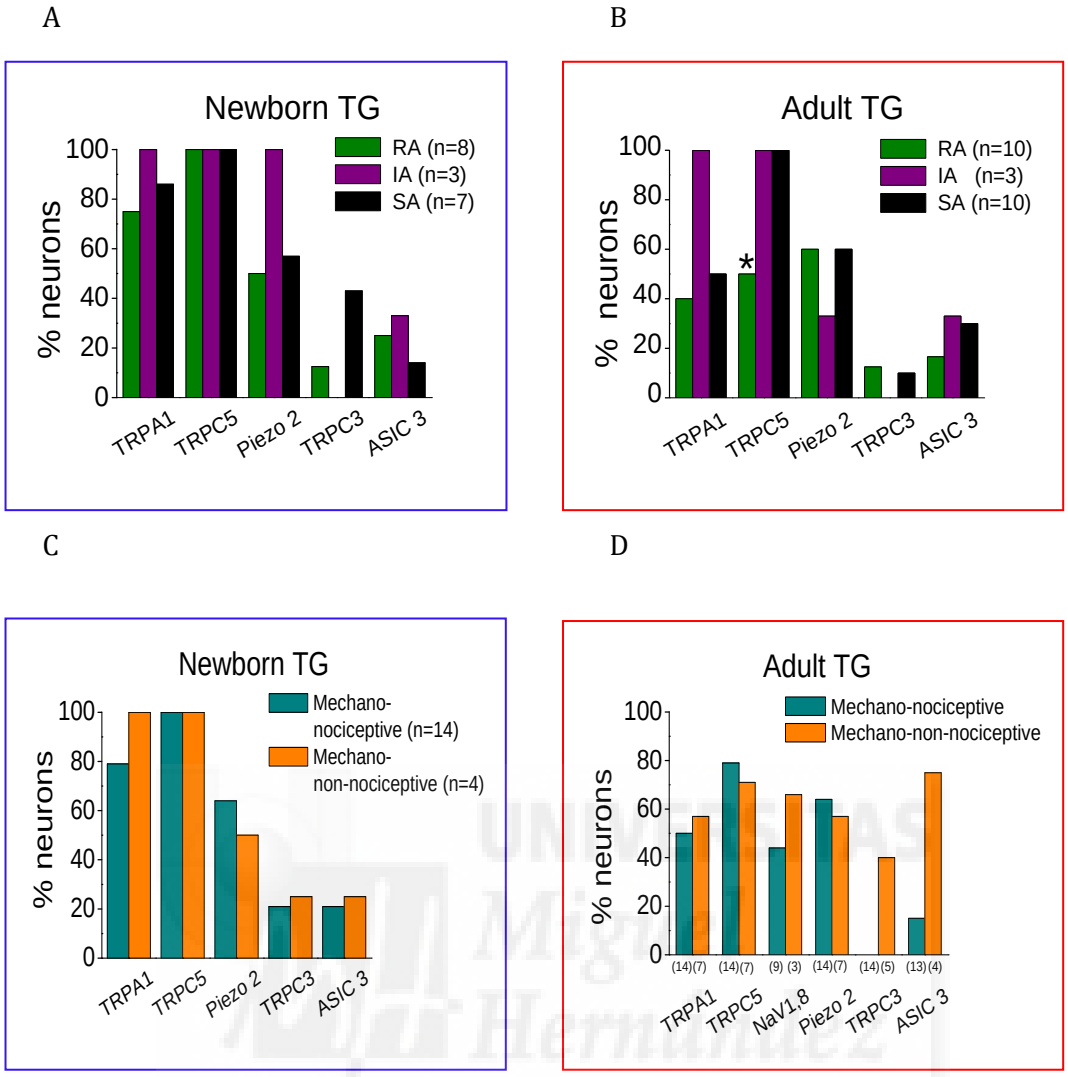

Figure 43. Proportion of mechanosentive TG neurons that express different candidate channels for mechanotransduction . (A-B) Histograms summarizing the proportion of RA, IA and SA neurons from newborn and adult mice that express the channels indicated. (C, D) Histograms summarizing the proportion of mechano-nociceptive and mechano-non-nociceptive neurons from newborn and adult mice that express the channels indicated. The numbers of cells analyzed in each group are indicated in the legend, except for (D), where the number of neurons studied in each group shown below each bar. (*p < 0.05; Z-test).

4.5.4 Co-expression of TRPA1, TRPC5 and Piezo2 in different populations of neurons

Based on the results described above, the majority of the TG neurons recorded expressed the channels TRPA1, TRPC5 and Piezo2. Thus, I performed a new analysis of the data correlating the development of RA, IA and SA currents with the combinatorial expression of TRPA1, TRPC5 and Piezo2 channels. The expression of a combination of TRPA1, TRPC5 and Piezo2 was also analysed in nociceptive and non-nociceptive neurons. Accordingly, the number of RA, IA or SA in neurons from

newborn and adult mice that express the pool of indicated channels was defined (Figure 44A, B) from which no clear pattern was evident. However adult neurons that express Piezo2 but not TRPA1 or TRPC5 always responded with RA currents, and the expression of Piezo2 was significant stronger in neurons displaying RA currents (*p = 0.034; Z-test).

In addition, the number of nociceptive or non-nociceptive mechanosensory neurons from newborn and adult mice that express the indicated pool of genes was examined (Figure 44C, D) and interestingly, TRPA1, TRPC5 and Piezo2 co-expression was significantly higher in mechano-nociceptive neurons from adult mice than in mechano-non-nociceptive neurons (*p=0.034; Z-test). The results also indicate that neurons displayed variation in the expression of TRPA1, TRPC5 and Piezo2, suggesting that these neurons might exhibit different sensory profiles.

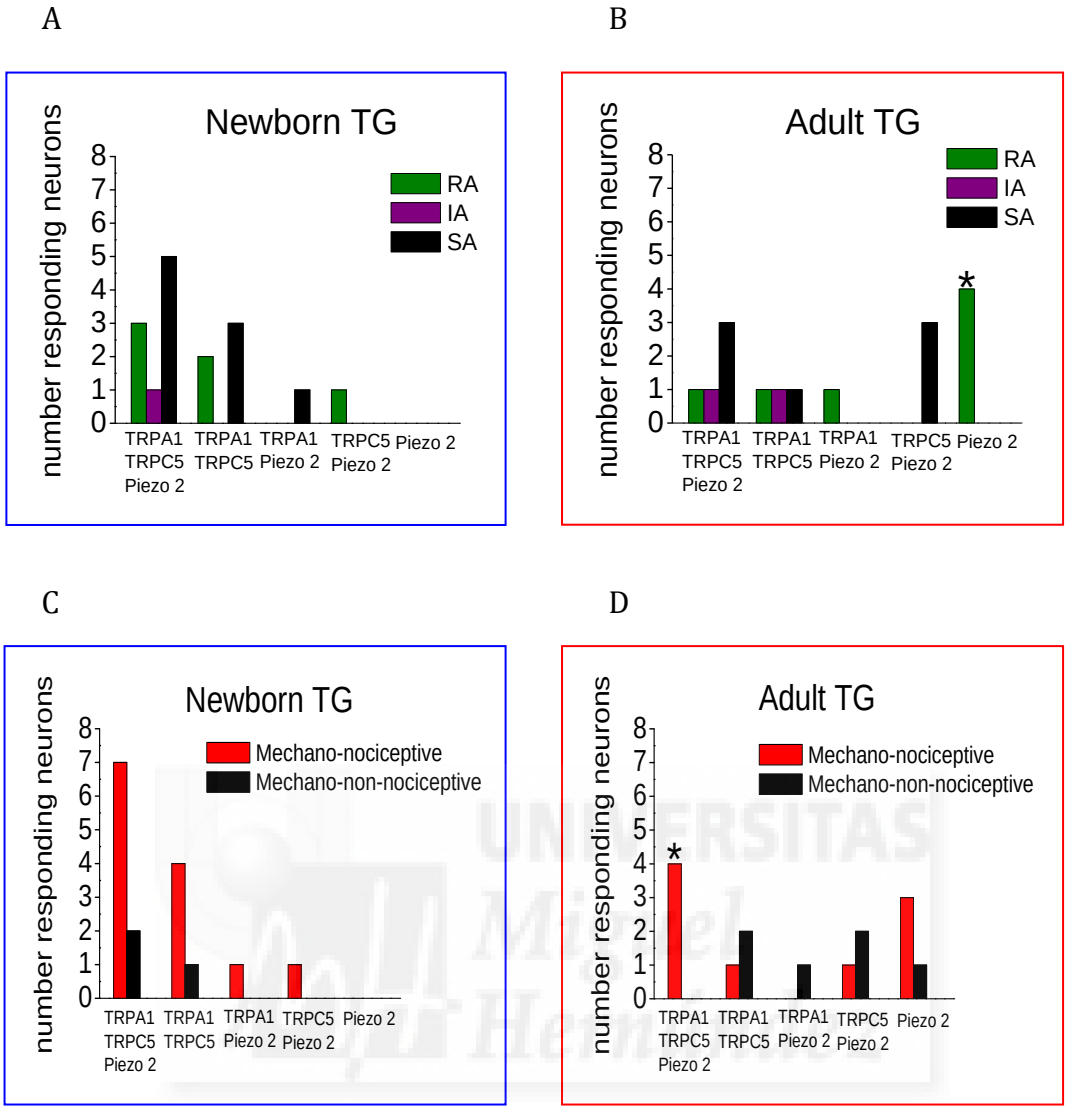

Figure 44. Different populations of neurons from newborn and adult mice co-express TRPA1, TRPC5 and Piezo 2. (A, B) The histogram represents the number of RA, IA or SA neurons from newborn and adult mice that co-express the genes indicated on the abscissa. (C, D) The histograms represent the number of mechano-nociceptive or mechano-non-nociceptive neurons from newborn and adult mice that co-express genes indicated on the abscissa (*p < 0.05; Z-test).

4.6 The contribution of TRPA1 channels to mechanosensory currents

As reviewed in the introduction, several candidates for mechanotransduction have been proposed in mammalian cells, including some members of the TRP channel family. One of these candidates is the TRPA1 channel.

It has been hypothesized that the 18 ankyrin repeats in the N terminal region of TRPA1 channel can interact with the intracellular cytoskeleton and could act as a spring to open the channel under mechanical stress (Corey et al., 2004; Sotomayor et al., 2005). Recent studies have shown that genetic ablation or pharmacological inhibition of TRPA1 in dissociated DRG neurons reduces SA and IA currents, suggesting that TRPA1 may be the molecular correlate of these currents (Vilceanu and Stucky, 2010; Brierley et al., 2011). Moreover, single cell RT-PCR has shown TRPA1 to be widely expressed in different subpopulations of MS neurons. For all these reasons, I sought to record mechanically-activated currents of trigeminal neurons in mice lacking TRPA1, to determine whether the absence of TRPA1 alters the properties of TG mechanically activated currents. The results from newborn and adult TRPA1 knock-out mice are presented separately, in order to compare each population with the corresponding wild-type mice.

4.6.1 Characterization of mechanosensory neurons from newborn TRPA1 knock-out mice

Electrophysiological recordings were made at the soma of sensory TG neurons using the patch clamp technique in whole cell configuration. Recordings from 57 neurons from newborn mice indicated a mean membrane potential of −56 ± 1 mV, a value similar to that of the neurons from wild type newborn.

As for the neurons from wild type mice, the rheobase current, the firing pattern and the AP shape were analyzed. Moreover, the presence of TTX resistant voltage-gated sodium channels and IB4 labelling was studied. These properties were also studied in more detail for the different populations of TG neurons.

4.6.1.1 Mechanically activated neurons from TRPA1$^{-/-}$ newborn mice

After characterizing their electrical properties, the neurons were stimulated at the soma to record the mechanically activated currents, through mechanical stimulation with the probe using the same protocol as that used for neurons from wild type animals (see section 4.2.2). As with wild type neurons, MS TG neurons responded to static indentation at different mechanical thresholds and the mechanosensitive currents exhibited graded increases in current amplitude in response to increasing the magnitude of indentation.

The total proportion of TG neurons from newborn TRPA1$^{-/-}$ mice that responded to static indentation was 75% (n=43/57), not significantly different from the proportion of MS neurons from wild type mice (79%; n=144/182).

The electrophysiological parameters described in section 4.2.1 were also used to analyze all the TG MS neurons recorded and to distinguish the differences between neurons from wild type and knock-out mice (see Table 15 for a comparison of the properties of the recorded TG MS neurons from TRPA$^{-/-}$ and wild type mice). No significant differences were evident between wild type and knock-out newborn mice.

Table 15

	Soma size (μm²)	Input resistance (mΩ)	Membrane potential (mV)	Rheobase current (pA)	Number of cells
WILD TYPE	279± 6	467 ± 24	-53 ± 1	183 ± 12	144
TRPA1 KO	282 ± 8	550 ± 74	-55 ± 1.4	208 ± 21	43

Table 15. Properties of mechanosensitive TG newborn neurons from wild type and knock-out mice. The mean soma size, input resistance, membrane potential and rheobase are shown.

4.6.1.2 Different classes of mechanosensitive currents in TRPA1 KO

TG mechanosensitive neurons were classified using the same criterion applied to wild type neuron, namely the kinetics of current decay.

Soma stimulation induced the activation of the three distinct types of mechanosensitive currents: rapidly adapting currents (RA, 4.4 ± 1.6 ms, n=13),

intermediately adapting currents (IA, 19.0 ± 1.8 ms; n=11) and slowly adapting currents (SA, 113 ± 37 ms; n=19). Samples traces of a RA (A), IA (B) and SA (C) currents recorded in different TG sensory neurons from mice lacking TRPA1 are shown in Figure 45, obtained using the mechanical protocol used in wild type animal. The mechanical threshold is shown above each current trace.

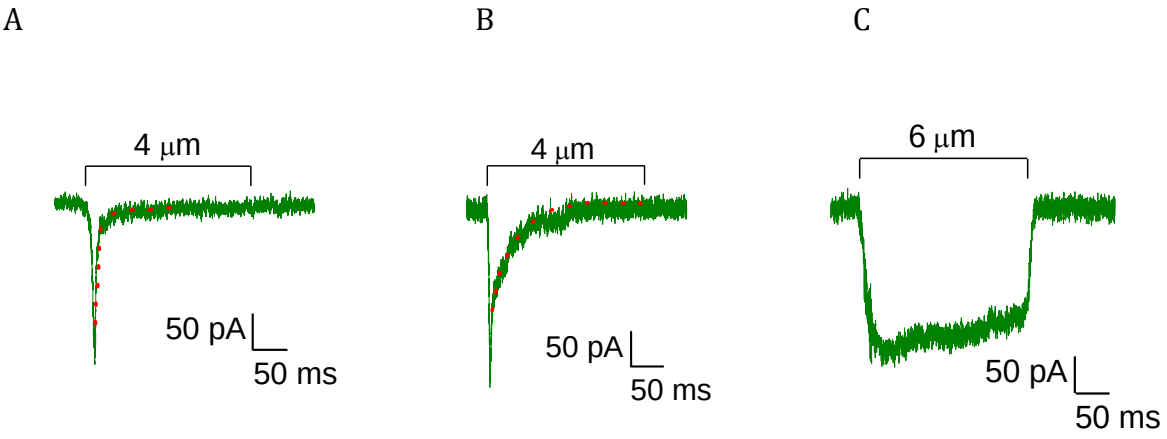

Figure 45. Examples of the subtypes of mechanically-activated currents evoked in neurons from newborn TRPA1$^{-/-}$ mice. Examples of a rapidly adapting current with a τ of 4 ms (A), an intermediately adapting current with a τ of 24 ms (B) and a slowly adapting current (C). Red lines in A and B indicate the single exponential functions calculated to fit the decay phases of RA and IA currents, respectively. It was not possible to calculate the decay phase of current in C because it only marginally inactivates over 250 ms.

Analysis of the expression of the different types of mechanically activated currents in TG neurons from TRPA1$^{-/-}$ mice (Figure 46) showed no differences compared with the neurons from wild type mice (for comparison, see Figure 31). This result was expected considering the very low or absent expression of TRPA1 in newborn animals. Nevertheless, the results confirm that TRPA1 does not participate in the kinetics of the MA currents in TG neurons from newborn animals.

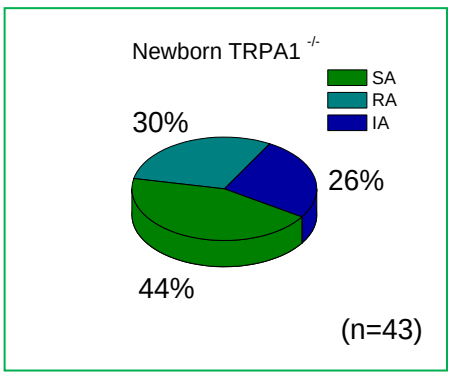

Figure 46. Distribution of the three mechanically gated currents in the total population of neurons from newborn TRPA1 $^{-/-}$ mice studied. Pie charts show the proportion of neurons responding to mechanical stimulation with RA (30%), IA (26%) and SA (44%) currents.

4.6.1.3 Properties of TG neurons expressing different mechanosensory currents

The parameters of mechanical threshold and latency were analyzed for each subtype of mechanically activated currents, namely RA, IA and SA cells (see Table 16).

As in the wild type mice, IA currents were associated with a slightly higher mechanical threshold (6.4 ± 0.7 µm) than RA (4.4 ± 0.4 µm; $^{\#}p = 0.020$) and SA (5.6 ± 0.5 µm) currents in KO mice. Indeed, the kinetic properties and current amplitude of neurons from TRPA1$^{-/-}$ and wild type mice expressing RA, IA and SA currents were similar (see Table 9). The only significant difference detected was the lower mechanical threshold of RA currents in neurons from TRPA1$^{-/-}$ mice.

Table 16

	Inactivation τ (ms)	Threshold (µm)	Latency Time (ms)	Number of cells
RA cells	4.4± 1.6	4.4 ± 0.4*	2.9 ± 0.5	13
IA cells	19 ± 1.8	6.4 ± 0.7#	3.1 ± 0.1	11
SA cells	113 ± 37	5.6 ± 0.5	2.0 ± 0.6	19

Table 16. Properties of mechanosensitive currents in neurons from newborn TRPA1$^{-/-}$ mice. # denotes statistical significance between the three subpopulations of neurons, RA, IA or SA cells, in the newborn TRPA1$^{-/-}$ population. The red asterisk denotes statistical significance between wild type (see Table 9) and knock-out neurons in the same subpopulations of RA, IA or SA neurons (*p < 0.05, $^{\#}p< 0.05$; Student's *t*-test).

As for wild type neurons, I analyzed the values of the first MA current elicited by a mechanical stimulus in each neuron. Current amplitude and density were analyzed for each type of mechanically activated current (see table 17), and a significant increase in the amplitude of SA neurons (229 ± 39 pA) was evident compared to both RA (111 ± 18 pA; $^{\#}p=0.026$) and IA cells (101 ± 20 pA; $^{\#\#}p=0.006$). This difference was also observed for the current density, where SA currents had a significantly larger current density than IA currents ($^{\#}p=0.025$). No differences were evident in either the amplitude or density between neurons from TRPA1$^{-/-}$ and wild type mice (see table 10 for comparison).

Table 17

	Current amplitude (pA)	Current density (pA/pF)	Number of cells
RA cells	111 ± 18	6.3 ± 2.1	13
IA cells	101 ± 20	4.0 ± 1.0	11
SA cells	229 ± 39#	9.4 ± 1.8#	19

Table 17. Magnitute of the mechanosensitive current in TG neurons from newborn TRPA1$^{-/-}$ mice. # denotes statistical significance between the three subpopulations of neurons, RA, IA or SA cells, in the TRPA1$^{-/-}$ newborn population ($^{\#}p< 0.05$, $^{\#\#}p< 0.01$; Student's *t*-test).

4.6.2 Distribution of the mechanically gated currents in nociceptive neurons from newborn TRPA1 $^{-/-}$ mice

When studying the mechanical gated currents I only analysed the population of nociceptive neurons as the number of recordings obtained from non-nociceptive neurons was very low. When the soma size, current amplitude, current density, mechanical threshold and latency for mechano-nociceptive neurons were compared between neurons from newborn TRPA1 knock-out (See Table 18) and wild type mice (see Table 13), no differences in any of these properties were found.

Table 18

	Soma size (µm^2)	Current amplitude (pA)	Current density (pA/pF)	Threshold (µm)	Latency Time (ms)	n
Mechano-nociceptive neurons	289 ± 9	115 ± 16	6.9 ± 1.3	5.6 ± 0.4	2.8 ± 0.5	35

Table 18. Kinetic properties of MA currents recorded in mechano-nociceptive neurons from TRPA1 $^{-/-}$ mice. The n column indicates the number of neurons studied.

The expression of the three types of MA currents in the mechano-nociceptive was similar in these knock-out neurons, where 20% (7/35), 28% (10/35) and 52% (18/35) responded with RA, IA and SA currents, respectively (Figure 47).

There were no significant differences in the proportion of RA, IA and SA when compared with neurons from wild type mice.

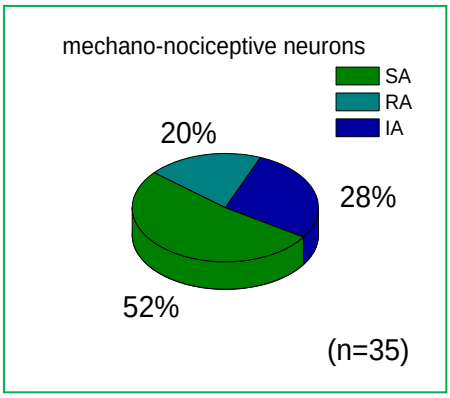

Figure 47. Distribution of MA currents in the subpopulation of mechano-nociceptive TRPA1 $^{-/-}$ neurons. Proportion of RA, IA or SA currents in nociceptive neurons.

In conclusion, all these results are consistent with my previous calcium imaging data that demonstrated a reduced response to cinnamaldehyde in neurons from newborn mice compared to adult neurons, indicating that expression levels of TRPA1 in TG neurons from newborn mice are low or absent. Moreover, these data corroborate previous studies in which poor TRPA1 mRNA expression and functional responses were demonstrated in DRG neurons from newborn mice compared to adult mice (Hjerling-Leffler et al., 2007).

4.6.3 Characterization of mechanosensory neurons from adult TRPA1$^{-/-}$ mice

Electrophysiological recordings were made on the soma of 50 sensory TG neurons from knock-out mice using the patch clamp technique in the whole cell configuration. These neurons had a mean membrane potential of –49 ± 1 mV, a value significantly more depolarized than in neurons from wild type adult (***$p<0.001$; Rank-Sum test). Thus, the depletion of TRPA1 may affect the resting membrane potential of neurons, making them more depolarized.

As for the populations of TG mechanosensitive neurons studied previously, electrical properties of TG neurons were analyzed (rheobase current, firing pattern and AP shape), as well as the presence of TTX resistant voltage sodium channels and IB4 labelling.

4.6.3.1 Mechanically activated neurons from TRPA1 $^{-/-}$ adult mice

The proportion of neurons from adult TRPA1 $^{-/-}$ mice that responded to static indentation was no different from that in wild type mice, with 64% (n=32/50) of neurons from TRPA1$^{-/-}$ mice responding to static indentation.

The properties of the recorded TG MS neurons from TRPA1$^{-/-}$ and wild type adult mice were compared (Table 19) and as for the entire population of TG neurons from adult TRPA1$^{-/-}$ mice, MS neurons presented a more depolarized membrane potentials than neurons from wild type mice (–50 ± 1.5 mV; **p=0.002).

Table 19

	Soma size (µm²)	Input resistance (mΩ)	Membrane potential (mV)	Rheobase current (pA)	Number of cells
Wild Type	361 ± 10	392 ± 20	-55 ± 1	329 ± 19	93
TRPA1 KO	375 ± 13	373 ± 42	-50 ± 1.5**	373 ± 32	32

Table 19. Properties of mechanosensitive TG neurons from adult wild type and knock-out mice. The red asterisk denotes statistical significance between wild type and TRPA1$^{-/-}$ neurons, (**p < 0.01; Student's *t*-test).

4.6.3.2 Different classes of mechanosensitive currents

Soma stimulation induced the activation of the three distinct types of mechanosensitive currents in TG neurons from adult TRPA1$^{-/-}$ mice: RA currents (6.3 ± 1 ms, n=19; Figure 48A), IA currents (31 ± 11 ms, n=2; Figure 48B) and SA currents (124 ± 32 ms, n=11; Figure 48C). The mechanical protocol used was that applied to wild type neurons and the mechanical threshold is shown above each current trace.

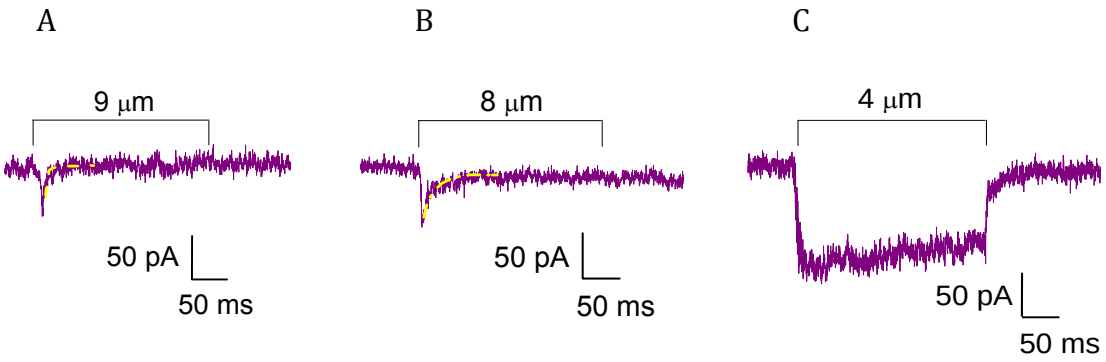

Figure 48. Examples of the subtypes of mechanically-activated currents evoked in adult TRPA1$^{-/-}$ neurons. Examples of a rapidly adapting current with a τ of 6 ms (A), an intermediately adapting current with a τ of 20 ms (B) and a slowly adapting current (C). Yellow dotted lines in A and B indicate the single exponential functions calculated to fit the decay phases of RA and IA currents, respectively. It was not possible to calculate the decay phase of current in C because it inactivates only marginally over the 250 ms.

The expression of the three types of mechanically activated currents was analysed in the TRPA1$^{-/-}$ adult mice, showing that the proportion of neurons responding with an IA current was remarkably smaller (6%) than in from wild type mice (24%: *p=0.05; Z-test).

Moreover, there was a significant increase of RA currents from 35% in wild type to 60% in knock-out mice (*p=0.023; Z-test). Thus, the majority of MS neurons responded with RA currents (60%; n=19/32), whereas only 34% (11/32) and 6% (2/32) of neurons from knock-out mice responded with SA and IA currents, respectively (Figure 49B).

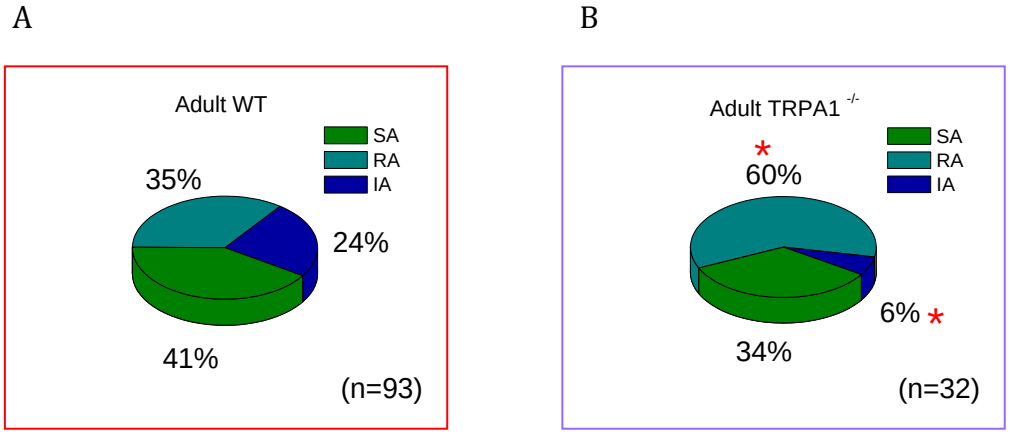

Figure 49. Differences in the distribution of the three mechanically gated currents among the neurons from adult wild type and TRPA1$^{-/-}$ mice. Pie charts show the proportion of adult neurons from wild type (A) and TRPA1 $^{-/-}$ (B) mice responding to mechanical stimulation with RA, IA or SA currents. There was a significant increase in the proportion of TRPA1$^{-/-}$ neurons that respond with RA currents, and a significant reduction in IA currents (*p<0.05; Z-test). "n" values indicate the number of neurons studied.

4.6.3.3 Properties of TG neurons from adult TRPA $^{-/-}$ mice expressing different mechanosensory currents

The parameters of mechanical threshold and latency time were analyzed for each subtype of mechanically activated currents, the RA, IA and SA cells (see Table 20).

In the neurons from adult TRPA1$^{-/-}$ mice there were no significant differences in latency of current activation between the neurons expressing the different types of MA currents.

Comparing the neurons expressing RA, IA and SA currents in TRPA1$^{-/-}$ and wild type mice (see Table 11) indicated a similar soma size, inactivation time of currents and mechanical threshold. However, the latency time of RA cells was significantly slower in the neurons from knock-out mice (3.3 ± 0.1 ms; *p=0.024; Student's *t*-test) than that in wild type mice (2.1 ± 0.3 ms).

Table 20

	Inactivation τ (ms)	Threshold (µm)	Latency Time (ms)	Number of recorded cells
RA cells	6.3 ± 1.0	6.4 ± 0.4	3.3 ± 0.1 *	19
IA cells	31 ± 11	8.5 ± 2.5	/	2
SA cells	124 ± 32	5.8 ± 0.7	3.0 ± 0.8	11

Table 20. Properties of mechanosensitive currents in neurons from adult TRPA1$^{-/-}$ mice. Values in the n columns indicate the number of neurons in each group. The red asterisk denotes statistical significance between neurons from wild type and knock-out mice of the same subpopulations of RA, IA or SA neurons (*p < 0.05; Student's *t*-test).

I analyzed the amplitude and the current density values from the first MA current elicited by a mechanical stimulus in each responding neuron. The current amplitude of all mechanosensitive neurons studied was significantly smaller (70 ± 7 pA; ***p<0.001) in the neurons from the KO mice than in those from wild type mice (166 ± 20 pA), as was the current density (3 ± 0.2 pA/pF; *p=0.013).

Current amplitude and current density were also analyzed for each subtype of mechanically activated currents, the RA, IA and SA cells and there were no differences in the current amplitude nor in the current density between RA, IA and SA neurons.

Comparing neurons from wild type (see Table 12) and knock-out mice, I found a significant reduction in the current amplitude of neurons responding with RA (from 153 pA in wild type to 63 pA in TRPA1$^{-/-}$ neurons; *p=0.015) and IA currents (from 135 pA in wild type to 40 pA in TRPA1$^{-/-}$ neurons; *p=0.025: Figure 56). The current amplitude in SA cells also appeared to be reduced (from 196 pA in wild type to 87 pA in TRPA1$^{-/-}$neurons), but not significantly (Figure 50).

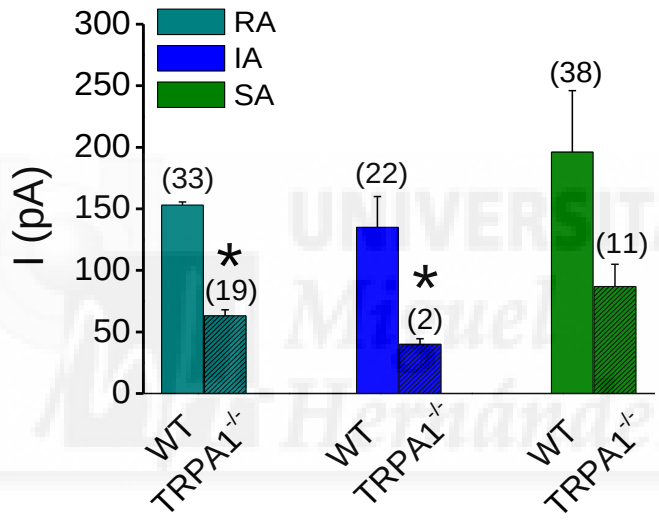

Figure 50. Deficits in mechanotransduction occur in RA and IA currents of adult neurons from TRPA1$^{-/-}$ mice. Histograms summarizing the mean current amplitude of RA, IA and SA neurons in adult wild type and TRPA1$^{-/-}$ mice. The values above the bars indicate the number of neurons responding in each group. There was a significant decrease in current amplitude of RA and IA neurons from knock-out mice compared to wild type neurons. (*p < 0.05, Mann-whitney rank-sum test).

Consequently it seems that the absence of TRPA1 not only alters the inactivation kinetics of neurons, accelerating this parameter, but also it significantly decreases the amplitude of RA and IA currents. Moreover, these data corroborate those from previous studies where a significant reduction in the current amplitude of IA currents was also seen in TRPA1$^{-/-}$ mice (Brierley et al., 2011).

4.6.4 Distribution of the mechanically gated currents in nociceptive neurons from adult TRPA1 $^{-/-}$ mice

As above, I only studied the population of nociceptive neurons in adult TRPA1$^{-/-}$ mice due to the limited number of non-nociceptive neurons identified from these mice. Nociceptive neurons were identified through the TTX resistance and IB4 labelling.

The soma size, current amplitude, current density, mechanical threshold and the latency time were analyzed in this subpopulation of nociceptive neurons (see Table 21).

Compared to the wild type (see Table 14), the current of nociceptive neurons from the knock-out mice had a significantly smaller amplitude (reducing from about 134 pA in wild type to about 71 pA in TRPA1$^{-/-}$ neurons; *p=0.035), as was the current density (reducing from about 4.9 pA in the wild type to about 3.1 pA in TRPA1$^{-/-}$ neurons; *p=0.038).

Table 21

	Soma size (µm²)	Current amplitude (pA)	Current density (pA/pF)	Threshold (µm)	Latency Time (ms)	n
Mechano-nociceptive neurons	384 ± 14	71 ± 8*	3.1 ± 0.5*	6.1 ± 0.4	2.9 ± 0.4	28

Table 21. Kinetic properties of mechanosensitive currents recorded in adult mechano-nociceptive TRPA1$^{-/-}$ neurons. The values in the n column indicate the number of neurons studied. The red asterisk denotes statistical significance between adult wild type and TRPA1$^{-/-}$ neurons. (*p < 0.05, Mann-whitney rank-sum test).

In TRPA1$^{-/-}$ mechano-nociceptive neurons 61% (17/28), 7% (2/28) and 32% (9/28) responded with RA, IA and SA currents, respectively (Figure 51 B). Thus, there was a significant increase in the proportion of neurons that responded with RA currents in TRPA1$^{-/-}$ nociceptive neurons compared to the neurons from wild type mice (Figure 51 A-B).

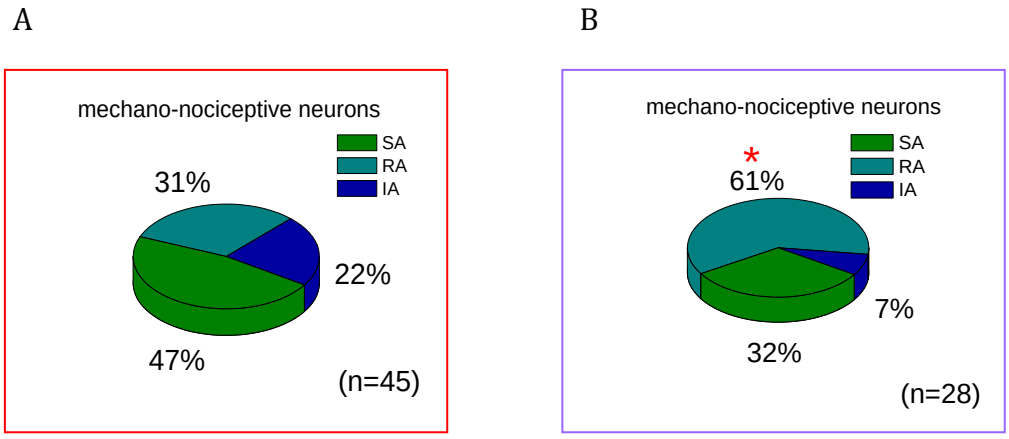

Figure 51. Differences in the distribution of the three mechanically gated currents among the nociceptive neurons from adult wild type and TRPA1$^{-/-}$ mice. Proportion of RA, IA or SA currents in nociceptive neurons from wild type (A) and TRPA1 $^{-/-}$ (B; *p<0.05, Z-test). "n" values indicate the number of neurons studied.

To better understand which subtypes of mechano-nociceptive neurons were most affected by TRPA1 deletion, the current amplitude in the three subtypes of RA, IA and SA neurons was analyzed, in neurons from wild type and knock-out mice. Comparing wild type and knock-out mice, there appeared to be a decrease in the mean current amplitude of all three subtypes of RA, IA and SA neurons, although this was only significant in the IA neurons (*p=0.041, Figure 52), indicating that TRPA1 principally affects IA nociceptive neurons.

The mean current amplitude of adult nociceptive neurons responding with RA currents was 100 ± 24 pA and 62 ± 6 pA in those from wild type and TRPA1 $^{-/-}$ mice, respectively. The mean current amplitude of nociceptive neurons responding with IA currents was 201 ± 73 pA and 40 ± 5 pA in the neurons from adult wild type and TRPA1$^{-/-}$ mice, respectively. Finally in nociceptive SA neurons the mean current amplitude was 164 ± 59 pA and 95 ± 22 pA in neurons from adult wild type and TRPA1$^{-/-}$ mice, respectively.

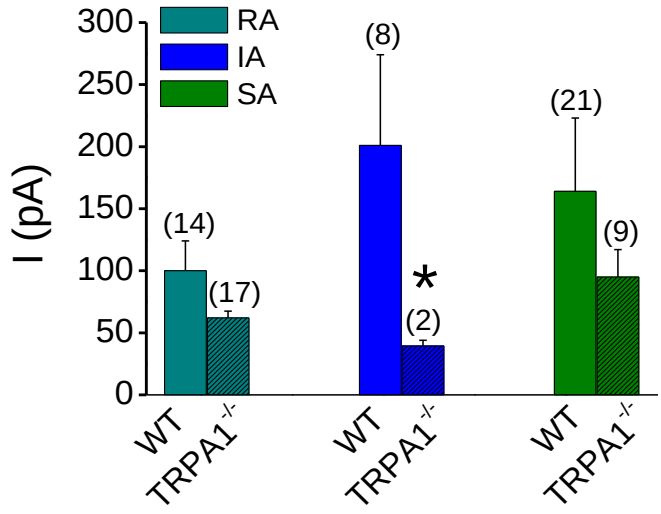

Figure 52. Deficits in mechanotransduction occur in IA currents of mechano-nociceptive neurons from adult TRPA1$^{-/-}$ mice. Histograms summarizing the mean current amplitude of RA, IA and SA neurons from adult wild type and TRPA1$^{-/-}$ nociceptive mice. The values above the bars indicate the number of the responding neurons in each group. There was a significant decrease in the current amplitude of IA neurons in knock-out mice when compared to wild type neurons. (*$p < 0.05$; Student's *t*-test).

In conclusion, my results provide evidence that TRPA1 plays a key role in the mechanosensory function of trigeminal neurons, contributing on one hand to RA and IA currents in the total populations of neurons and on the other hand, affecting the IA currents in nociceptive neurons.

4.6.5 Effect of the selective TRPA1 antagonist HC-030031 on the mechanically gated currents in adult mice

The data present here suggest that TRPA1 mediates a significant fraction of the RA and IA currents in the total population of TG neurons studied. To corroborate the contribution of the TRPA1 channel to the activation of mechanically activated currents, wild type neurons were exposed to a pharmacological blocker of TRPA1 that inhibits TRPA1 channel function while leave the TRPA1 protein expressed at the membrane intact. TRPA1 in adult TG neurons from wild type mice was blocked pharmacologically with the synthetic compound HC-030031, a selective inhibitor of TRPA1 (McNamara et al., 2007). These neurons were recorded in whole cell configuration at –60 mV and those that responded to mechanical indentation were

perfused for 3 minutes with HC-030031 (10 μM) before a second protocol of mechanical indentation was applied in the presence of the drug. After wash out of the compound, a third mechanical stimulus was applied to test the recovery of the inhibition. Representative examples of the effect of HC-030031 on the three different mechanically activated currents, the RA, IA and SA currents, and the following recovery of the currents are shown in Figure 53A-C. These neurons were activated at different mechanical intensities as indicated above the traces.

The effect of HC-030031 on current amplitude was also expressed as the proportion of current inhibition respect the control response (Figure 53D). This selective TRPA1 antagonist reduced the amplitude of the RA, IA and SA currents to 65%, 32% and 33%, respectively. In particular the RA currents were significantly reduced ($p=0.038$, Student's *t*-test). Full recovery of the current amplitudes was not observed after drug washout with control solution for 5 minutes and in fact, inhibition of RA (~50 %), IA (~13%) and SA (~28 %) currents persist. Thus, while HC-030031 significantly reduced the amplitude of RA currents (*$p < 0.05$; Student's *t*-test), it had no significant effect on IA and SA currents, although there was a trend towards a decrease in the IA and SA currents. In conclusion, whereas the amplitude of RA and IA currents were reduced in TRPA1$^{-/-}$ mice, inhibition of TRPA1 with HC-030031 in wild type neurons only altered the amplitude of RA currents but not that of the IA and SA currents.

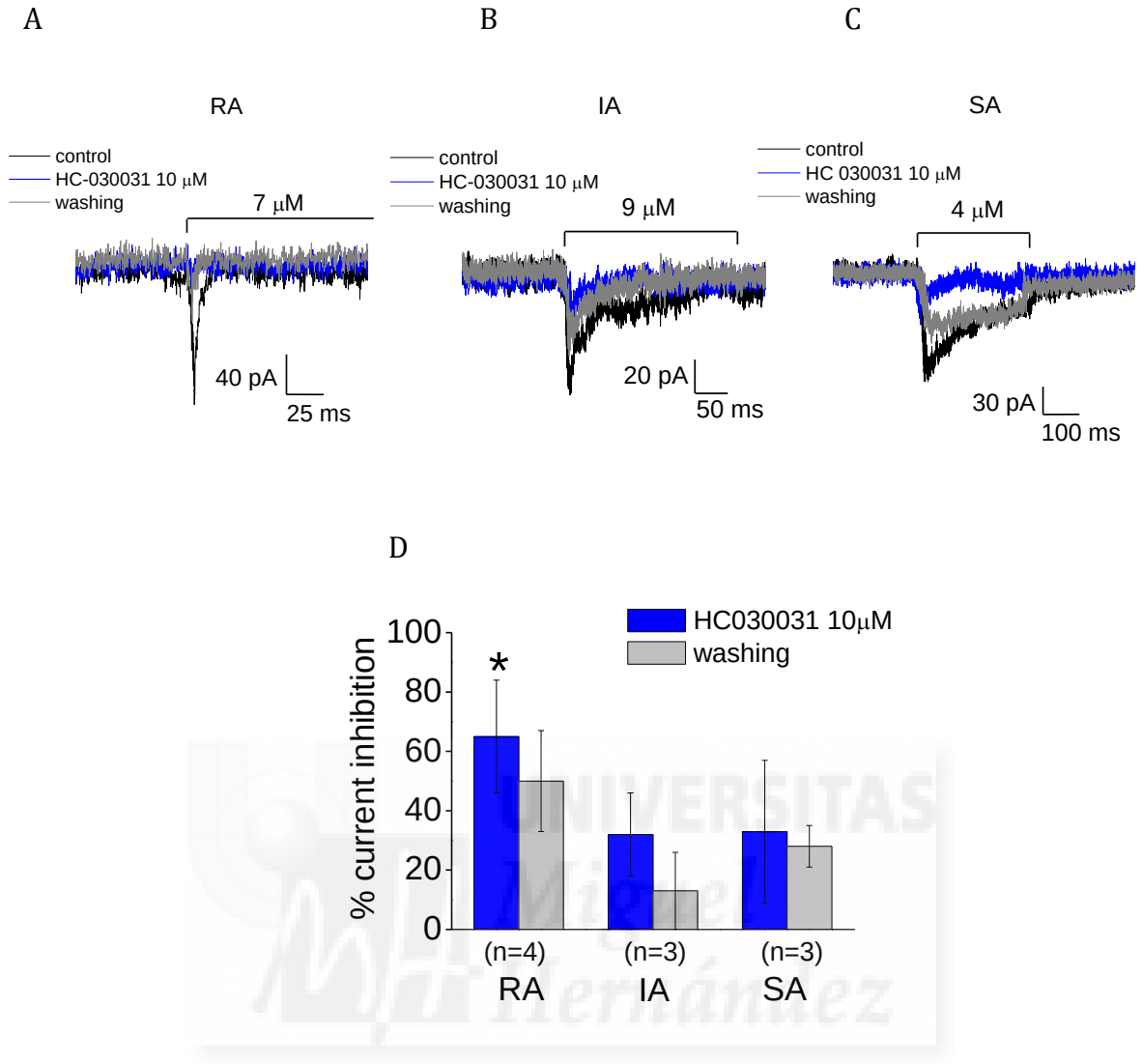

Figure 53. Pharmacological inhibition of the three mechanosensitive currents by HC-030031 in adult neurons. Sample traces of a RA (A), IA (B) and SA (C) current in control solution before and after application of HC-030031. The TRPA1 antagonist has an inhibitory effect on mechanosensitive currents. Summary histogram shows the effect of 10μM HC-030031 on the three types of mechanosensitive currents. The values below the bars indicate the number of neurons tested in each group. (*$p < 0.05$; Student's *t*-test).

UNIVERSITAS
Miguel
Hernández

5. Discussion

Over recent years, it has become more and more evident that mechanical stress contributes critically to a broad range of physiological processes, such as hearing, proprioception, tissue homeostasis and muscle regeneration (Waters et al., 2002; Li et al., 2005; Mikuni-Takagaki, 1999). A key question remains the characterization of the cellular mechanism and the identification of the molecules responsible for mechanotransduction. Accordingly, specific properties of mechanotransducer currents in different subsets of mechanosensory DRG neurons have been defined in rodents, although the molecular mechanisms underlying these remain unclear. TG neurons also responded to mechanical stimulation during an hypotonic stimulus (Viana et al., 2001) and to radial stretching (Bhattacharya et al., 2008), although their mechanically activated currents have yet to be described.

In this Thesis, I focused my research on the characterization of TG neurons from newborn and adult mice that respond to changes in osmolarity and the indentation stimulus. I also described the properties of different types of mechanically activated currents provoked through the indentation stimulus. In addition, I detected the expression of several mechanosensory proteins in non-nociceptive and nociceptive neurons. One of these proteins is the TRPA1 channel and hence, I studied the role of this channel in the mechanosensitive TG neurons using TRPA1 knock-out mice and a specific antagonist of this cationic channel. I characterized these mechanosensitive neurons using two different approaches, calcium imaging and electrophysiological recordings.

Even if the physiological unit of transduction is the sensory ending, recordings were obtained from the soma of the neurons. The soma of cultured sensory neurons has been used extensively as a model of transduction as there are close similarities between the properties of the cell bodies in culture and those of their central and peripheral terminals, the latter of which are currently inaccessible to patch-clamping (Julius and Basbaum, 2001). Moreover, *in vivo* the channels are synthesized in the soma and then transported along the axon to the terminals. Hence, I performed this study on the soma as a surrogate given that they express transducer channels.

5.1 Mechananosensory TG neurons in newborn and adult mice

In the first section of this study I combined cell calcium imaging with exposure to a hypoosmotic solution or static indentation to examine the responses of cultured TG sensory neurons to these mechanical stimuli. Although both these forms of mechanical stimuli produce membrane deformation they also present experimental differences. The use of a hypoosmotic solution permits the delivery of the stimulus and the monitoring of the responses in a large number of cells, although there is still some debate as to whether cell swelling is an appropriate mechanical stimulus. Indeed, it has been proposed that cell swelling would change the effective concentrations of signalling components which could affect many types of chemical reactions within the cytoplasm (Sachs, 2010). However, this stimulus has been used widely to identify mechanosensitive cells *in vitro* (Viana et al., 2001; Alessandri-Haber et al., 2003; Haeberle et al., 2008; Gomis et al., 2008). Deformation of the plasma membrane using the mechano-clamp presents some similarities with the mechanical depression of the skin. This technique allows certain parameters of the stimulus to be controlled and the recording of membrane currents although it is not possible to directly quantify the force applied (Hao and Delmas, 2011).

My results define three mechanically sensitive populations of neurons in newborn and adult mice, responding to a hypoosmotic solution, to indentation or to both stimuli. By contrast, a small proportion of neurons are insensitive to these stimuli. The lack of a complete overlap in the responses to hypotonic stress and indentation suggests that the deformation evoked by these two different stimuli probably acts through distinct mechanisms.

Pooling the cells that respond to hypoosmotic stimulation and hypoosmotic plus indentation, I obtained the same proportion of mechanosensitive neurons described in an earlier study (Bhattacharya et al., 2008). In this study the authors showed that 48% of newborn TG neurons stimulated by varying magnitudes of radial stretch respond to the highest stretch stimuli, increasing the concentration of intracellular calcium. Moreover, all the stretch sensitive neurons were also activated by a hypotonic stimulus (220 mosmlkg^{-1}), which suggested that the population of neurons

activated by radial stretch is the same population of neurons activated by hypoosmotic stress and hypoosmotic plus indentation.

However, my data show that 45% of neurons respond to hypotonic solution which does not completely fit with that obtained previously in TG neurons from newborn animals, which 80% of newborn TG neurons responded to hypotonic solution (210 mosml kg^{-1}) with an increase in intracellular calcium concentration (Viana et al., 2001). This discrepancy could be due to experimental bias such as the signal resolution of the calcium recording system, to differences in the criterion used to define a positive response or due to the loss of the largest MS neurons in my cell cultures.

It is also noteworthy that the proportion of mechanosensitive neurons was the same in newborn and adult mice, suggesting that the mechanical sensitivity of TG neurons, as detected by calcium imaging, is not modified during development.

The total population of TG neurons studied by calcium imaging was divided in non-nociceptive and nociceptive neurons in function of their cinnamaldehyde (CA) and capsaicin (Cap) sensitivity. The proportion of mechanically activated neurons that respond to CA (an activator of TRPA1) increases in adult mice, which is consistent with the weak expression of TRPA1 detected in TG newborn neurons.

These data are consistent with previous studies on newborn TG neurons (Bhattacharya et al., 2008), where a small proportion of stretch positive neurons (induced by radial stretch) responded to mustard oil (that activates TRPA1) and to Cap (that activates TRPV1). In a study of DRG neurons, a very small proportion of neurons from newborn mice responded to CA (Hjerling-Leffler et al., 2007), although responses to CA were evident at P7, indicating that functional TRPA1 appears in the first postnatal week while the response to Cap appear at E12.5. Quantitative PCR shows that the expression of TRPV1 and TRPA1 mRNA is closely correlated with the appearance of functional responses. However, since TRPA1 is probably not functional in newborn animals and given that mechanical sensitivity is similar in newborn and adult mice, TRPA1 does not appear to be essential to confer mechanosensitivity to TG newborn neurons.

TG neurons from newborn mice have a smaller soma than those from adult mice. The existence of different functional types of primary sensory neurons in newborn

rodents was suggested by morphological studies (Lawson, 1979; Coggeshall et al., 1994) in which two subpopulations of newborn DRG neurons were described in the mouse and rat with different diameters and growing rates, at different postnatal weeks. Later, the evolution of the properties of neurons with age was associated with a parallel increase in the surface area of the soma (Cabanes et al., 2002), which may explain the differences in the mean soma size between nociceptive and non-nociceptive neurons from adult animals, as opposed to newborn rodents.

These data may suggest that, although the mechanical sensitivity of TG neurons is similar in newborn and adult neurons, noxious sensitivity augment during development in the medium-small-diameter mechanical sensitive neurons, probably due to the expression of nociceptive channels.

Electrophysiological recordings of the entire population of TG neurons show that newborn neurons are more excitable than adult ones, which could reflect the variable expression of ion channels in the membrane during development as it was shown by Gallego and Eyzaguirre 1978, Fedulova et al., 1991 and Cabanes et al., 2002.

Electrophysiological recordings also highlight properties that define non-nociceptive and nociceptive neurons. For example, the firing pattern is a distinct feature of low and high threshold neurons *in vivo* (Lawson, 2002; Lewin and Moshourab, 2004). Indeed, and in accordance with previous studies (Cabanes et al., 2002), I observed a higher proportion of phasic responding neurons in adult mice compared with newborn neurons. This was probably due to the changes in the passive and active membrane properties occurring during the first 3 weeks of postnatal development (Cabanes et al., 2002).

The shape of the APs has been used to distinguish non-nociceptive and nociceptive neurons (Koerber et al. 1988; Lawson et al. 1997; Stucky and Lewin, 1999; Fang et al. 2005; Hu and Lewin, 2006) and my results reveal that the proportion of TG neurons presenting narrow or hump APs is the same in newborn and adult mice, as shown previously by Cabanes et al. 2002. These authors suggested that developmental mechanisms driving AP shape are already established at the time of birth. However, my results show that the majority of TG neurons present a hump in the falling phase of the AP while in Cabanes's work the proportion of neurons showing hump or narrow APs is similar. This discrepancy could be due to differences between the use of an intact TG ganglia as opposed to cultured neurons. Moreover, I

may have lost some low threshold neurons in culture, as it has been suggested that such neurons are those most sensitive to the culture protocols (Hao and Delmas, 2011).

In summary, the majority of newborn and adult neurons show a hump in the AP that is indicative of a higher proportion of nociceptive neurons or that this criterion alone is not good enough to identify nociceptive neurons. On the other hand, the increase in the proportion of neurons firing a phasic pattern in adult mice would indicate an increase in the non-nociceptive neurons.

These differences suggest that the firing pattern and the shape of the AP should be used with caution as an indicator of the neuron's phenotype as they probably do not fully reflect what occurs *in vivo*.

My results also indicate that there is a higher proportion of mechanosensory neurons in newborn animals, as also observed in newborn DRG neurons (Drew et al., 2002; Lechner et al., 2009). The difference in the mechanosensitivity between newborn and adult mice was not observed in calcium imaging experiments, indicating a distinct sensitivity between calcium imaging and patch clamp recordings. In patch clamp recordings the activation of mechanically gated currents is measured directly and it is possible to record small responses that may only occur in newborn neurons. In electrophysiological experiments, only the population of neurons that respond to indentation was studied and it is possible that a proportion of the calcium response observed in adult mice is due to the activation of a population of neurons that respond to hypoosmotic stress. Moreover, it is possible that I were not able to record the largest mechanosensitive neurons by the patch clamp technique.

As mentioned, soma size might be used to distinguish nociceptors and non-nociceptive neurons, since sensory neurons with a small-diameter soma are more likely to be nociceptors, whereas low threshold mechanosensitive neurons are thought to have a larger soma (Lawson, 2002). In newborn mice, non-nociceptive neurons (identified by TTX sensitivity or the lack of IB4 labelling and a narrow AP) have a significantly larger soma than nociceptive neurons, otherwise not occurring in adult mice. Conversely, data from calcium imaging experiments did not show significant differences between the size of nociceptive and non-nociceptive neurons in newborn mice. This is may reflect the technical limitation of not being able to record the largest adult neurons by the patch clamp technique. This issue might also

explain why I observe a significant difference in the size of the soma of nociceptive neurons in newborn and adult mice, but not with respect to non-nociceptive neurons.

5.2 Different types of mechanosensory currents in TG sensory neurons

Mechanosensitive currents exhibited graded increases in current amplitude as the magnitude of indentation increased. This degree of sensitivity to discriminate between different grades of mechanical forces is one of the properties of mechanotransducers. Moreover, the ability of neurons to respond to consecutive mechanical stimuli is evidence that these responses are not caused by damage to the surface membrane and that they are not artefacts of the electrode seal (Drew et al., 2002; Drew et al., 2004; Rugiero et al., 2010; Vilceanu and Stucky, 2010). I defined three types of mechanically gated currents according to their inactivation kinetics: rapidly adapting (RA), intermediately adapting (IA) and slowly adapting (SA) currents. The kinetics of these currents were very similar in newborn and adult mice, and they were consistent with previous data obtained from DRG in different laboratories (Hu and Lewin, 2006; Lechner et al., 2009; Drew et al., 2004; Coste et al., 2010).

Previous studies on DRG neurons associated soma size (Hu and Lewin, 2006), current amplitude and mechanical threshold (Drew et al., 2002) with the expression of one type of mechanically gated current. Large neurons expressing RA currents were considered to be non-nociceptive neurons and I found that the adult neurons with a larger soma express RA currents. It is also known that *in vivo*, mechanoreceptors and nociceptors are characterized by low and high mechanical thresholds, respectively (Lewin and Stucky, 2000) and indeed, I found that newborn neurons displaying IA currents have a significant higher mechanical threshold.These results suggest that RA currents might be correlated with non-nociceptive neurons and IA currents might be associated with nociceptive neurons. This difference in the mechanical threshold of TG neurons is not observed in adult mice perhaps reflecting differences in the complex machinery that confers mechanical thresholds to the terminal *in vivo*, even though recording at the cell soma has been considered as an adequate model of the peripheral terminal.

It has been proposed that expression of the different types of current is associated with non-nociceptive (RA) and nociceptive DRG adult neurons (IA and SA). In fact, large neurons expressing narrow APs generate RA currents, whereas medium-small size neurons with wide, inflected APs display distinct rates of adaptation (Drew et al., 2004). I did not detect a correlation between tonic or phasic discharges and the shape of the AP in the populations of neurons displaying the three types of MA currents in newborn and adult mice.

What apparently defines a nociceptive neuron is the expression of the TTX resistant voltage-gated sodium channels NaV1.8 and NaV1.9 (McCleskey and Gold, 1999; Waxman et al., 1999; Baker and Wood, 2001) and labelling by IB4 (Caterina and Julius, 2001; Silverman and Kruger, 1990).

The three types of MA current are found in TTX-resistant and TTX-sensitive neurons, as well as in IB4 positive and IB4 negative neurons. However, TTX-resistant newborn neurons predominantly display SA currents. These data clearly show that nociceptive and non-nociceptive mechanosensitive TG neurons exhibit the three mechanically gated currents (RA, IA and SA currents) heterogeneously in newborn and adult mice. These data are to some extent different to that obtained from adult DRG neurons where a differentially distribution of RA (non-nociceptive phenotypes) and SA currents (nociceptive phenotypes) was described, although the distribution was not exclusive to these types of currents (Drew et al., 2002; Hu and Lewin, 2006; Drew et al., 2004; Hao and Delmas, 2010). This diversity might be due to differences between DRG and TG ganglia, the latter being more heterogeneous in terms of the expression of the three MA currents. Another explanation for this difference may reside in the low number of non-nociceptive TG neurons recorded, given the difficulties in recording low threshold neurons.

Mechano-non-nociceptive neurons from adult mice present significantly larger current amplitudes compared to mechano-nociceptive neurons. This difference is not evident in newborn neurons, suggesting that MA currents are probably mediated by different mechanotransducers, each contributing to the final response. It is also possible that the density of these mechanotransducers differs in newborn and adult mice, and therefore, the specification of some mechanical properties would appear to occur during postnatal development. Moreover, it has been suggested previously that

the different MA currents recorded in DRG neurons may be mediated by the activation of different populations of ion channels (McCarter et al., 1999; Drew et al., 2002; Hao and Delmas, 2010).

My results indicate that the different types of mechanosensitive currents recorded in TG neurons are non-selectively carried by cations, so I cannot associate these currents to a specific conductance. Similarly, pharmacological results suggest that the currents are mediated by stretch activated channels, although it is not possible to distinguish between the specific ion channels involved. However, the fact that the RA currents in adult neurons are not significantly reduced by gadolinium suggests that they are the product of different mechanotransducers. The observation that mechanically gated currents are reversibly inhibited by such compounds provides additional strong support for the conclusion that the current is not purely an artefact caused by mechanical disruption of the membrane or of the electrode seal. The partially recovery of mechanically gated currents after gadolinium blockage was also observed elsewhere (McCarter et al., 1999), and it might be due to the repetitive and strong mechanical stimuli applied to the cell soma that can cause irreversible damage to the surface membrane. However, complete recovery was observed when a smaller stimulus was applied to the neurites (Hu and Lewin, 2006).

The heterogeneity of mechanosensitive currents found in TG neurons might reflect the diversity of mechanoreceptor subtypes seen *in vivo*. For the specific population of nociceptors studied, up to 20% correspond to Aβ-fibres (Djouhri and Lawson, 2004). Thus, it is tempting to propose that RA nociceptive neurons could correspond to the Aβ-nociceptors, myelinated nociceptors that respond to mechanical stimuli well into the nociceptive range and with adaptive properties that resemble SA units (Woodbury and Koerber, 2003; Djouhri and Lawson, 2004; Fang et al., 2005). IA neurons tend to be smaller than RA and SA neurons, and they have a higher mechanical threshold, which means they might correspond to the C-fibres observed *in vivo*. Finally, SA neurons could correspond to the Aδ-fibres detected *in vivo.*

Although it was possible to distinguish between nociceptive and non-nociceptive mechanosensitive neurons in this study, further sub-classification, particularly of the low threshold neurons, is currently limited by a lack of molecular

and pharmacological probes. The availability of such tools will notably improve our understanding of cellular and molecular basis of mechanosensation.

5.3 Identification of mechanotransducer channels involved in the mechanical transduction in newborn and adult neurons

Although a variety of techniques have been employed to study mechanotransduction in sensory neurons, including electrophysiology, calcium imaging and immunohistochemistry, the expression of putative mechanotransducers in specific subsets of mechanosensitive neurons has not been addressed. I used single-cell RT-PCR to identify ion channels proposed as mechanotransducers in neurons displaying the three MA currents, as well as in non-nociceptive and nociceptive neurons. This approach permits different ion channel transcripts to be measured in each neuron harvested, thereby enabling a more complete analysis of the molecular and functional properties of each neuron studied.

My data show that the expression of the mechanotransducers tested is heterogeneous which suggests that it is not possible to attribute the expression of a specific channel to the RA, SA or IA activated currents, or to nociceptive or non-nociceptive MS neurons. TRPA1 is expressed in all the three subtypes of RA, IA and SA neurons, as well as in nociceptive and low threshold neurons. Surprisingly, TRPA1 was also expressed in newborn neurons, although it was previously proposed to be only weakly expressed in such newborn neurons (Hjerling-Leffler et al., 2007), data also corroborated by my results in calcium imaging recordings. The detection of TRPA1 in these neurons probably reflects the high efficiency of the nested PCR to amplify gene transcripts, even though they are present in only very small numbers. Moreover, although the channel is expressed at the transcriptional level, the protein it encodes may not be functional.

Piezo2, a novel recently identified protein involved in mechanotransduction, contributes to RA currents in DRG neurons. Moreover, mRNA for Piezo2 was found in mechanosensory neurons, as well as in a subset of nociceptive neurons that co-express TRPV1 (Coste et al., 2010), corroborating my results in single-cell RT-PCR where Piezo's transcripts were detected in both nociceptive and non-nociceptive neurons. In contrast to other authors, I detected the expression of Piezo2 in neurons

expressing the three types of currents. However, neurons that express Piezo2 but neither TRPA1 nor TRPC5 always responded with RA currents.

Canonical TRP channels were the first mammalian homologues of the *Drosophila* TRP channel to be identified and several members of this family have been implicated in mechanotransduction. Indeed, TRPC5 and TRPC3 have been shown to participate in mechanotransduction (Gomis et al., 2008; Glazebrook et al., 2005; Quick et al., 2012). We found TRPC5 to be expressed in the RA, IA and SA neurons, as well as in nociceptive and low threshold neurons, whereas TRPC3 was only detected in RA and SA neurons. This is consistent with the clear reduction of neurons expressing RA currents in TRPC3$^{-/-}$ DRG neurons, compensated for by the increase of neurons expressing IA currents (Quick et al., 2012). Moreover, TRPC3 appears to be more strongly expressed in non-nociceptive neurons, although this difference is not statistically significant, probably due to the small number of mechano-non-nociceptive neurons recorded. Similar results were observed for ASIC3 and although the mechanosensitivity of sensory neurons is altered in ASIC mutant mice *in vivo* (Price et al., 2000; Price et al., 2001), there is no evidence that these genes are required for mechanosensitive currents in adult neurons (Drew et al., 2004). Thus, the negligible expression of ASIC3 found in the mechanosensitive neurons analyzed might suggest that ASIC3 is not necessary for mechanotransduction in TG neurons. Interestingly, in adult mice co-expression of TRPA1, TRPC5 and Piezo2 was significantly stronger in nociceptive neurons. Thus, I speculate that the co-expression of distinct mechanosensitive channels might confer the nociceptive phenotype.

Surprisingly, some ion channels that are considered markers of nociceptive neurons are also expressed in non-nociceptive neurons, as is the case for TRPA1 and NaV1.8. It has been shown that TRPA1 is not only expressed in small-diameter neurons (Story et al., 2003; Kobayashi et al., 2005; Nagata et al., 2005) but also, in medium to large-diameter DRG neurons and on large-caliber axons within nerves (Kwan et al., 2009). Similarly, while NaV1.8 is expressed by nociceptive neurons conferring them TTX-resistance, 10-30% of large-diameter DRG neurons were immunolabelled for NaV1.8 (Amaya et al., 2000; Djouhri et al., 2003), express NaV1.8 transcripts (Sangameswaran et al., 1996; Black et al., 2004) or a TTX-R Na current (Ho and O'Leary, 2011). Moreover, it was recently demonstrated that NaV1.8 is expressed in 75% of all primary somatosensory afferents, including not only

nociceptors but also C- and A- fibre low-threshold mechanoreceptors (Shields et al., 2012). Thus, my results corroborate earlier data showing that different nociceptive markers were found in non-nociceptive neurons.

Hence, it is tempting to propose that the functional specificity of a mechanical sensory neuron depends on the simultaneous activation of different transducer molecules, each of which has different properties. The diverse kinetics of mechanically activated currents and other characteristics may be accounted for by the expression of distinct but closely related ion channels, or by interactions with different membrane proteins or cytoskeletal elements that can influence the behaviour of the same channel.

5.4 The functional role of TRPA1 channels in mechanotransduction

Certain controversy surrounds the role of TRPA1 in the detection of mechanical stimuli, although recent studies in dissociated DRG neurons show that TRPA1 contributes to the SA and IA mechanosensitive currents (Vilceanu and Stucky, 2010; Brierley et al., 2011).

However, deletion of TRPA1 does not affect the electrophysiological and mechanical properties of TG neurons from newborn animals and moreover, I found the same significant differences in newborn KO mice and in wild type mice. That is, IA neurons have a higher mechanical threshold than RA and SA neurons and the SA currents have a larger amplitude than RA and IA neurons. These results suggest that IA currents might be expressed principally by nociceptive neurons in newborn neurons, in both wild type and KO mice, which is consistent with the data obtained in calcium experiments and that is compatible with TRPA1 not fulfilling a functional role in the first postnatal days. In this respect, TRPA1 is expressed only weakly at birth, although it augments strongly during the first postnatal weeks, as also confirmed by the functional responses to cinnamaldehyde (Hjerling-Leffler et al., 2007). In addition, TRPA1-mediated cold responses have failed to be detected in TG or DRG neurons isolated from newborn or young animals (Jordt et al., 2004; Bautista et al., 2006).

Adult TRPA1 KO mice present more depolarized membrane potentials in comparison to wild type mice, although other electrical properties are unaffected, such as the firing pattern and the AP shape. The role of TRPA1 was revealed in adult KO mice after differentiating the mechanically activated current type and the nociceptive phenotype through IB4 immunoreactivity and TTX resistance. The total proportion of mechanosensitive adult neurons in TRPA1$^{-/-}$ mice was similar to that in wild type mice, yet significant differences in the proportion of the three MA currents recorded were evident. As such, the proportion of neurons responding with an IA current is significantly smaller and there is a remarkably increase in the neurons displaying RA currents. Genetic ablation of TRPA1 not only leads to changes in the inactivation kinetics of currents, making them faster, but it also significantly decreases the current amplitude of RA and IA neurons.

TRPA1 also alters the proportions of the RA currents and the amplitude of the IA currents in the subpopulation of nociceptive neurons.

While two different reports recently found mechanosensory deficits in DRG neurons from TRPA1$^{-/-}$ mice, there are several discrepancies in their results (Vilceanu and Stucky, 2010; Brierley et al., 2011). The observed reduction in the amplitude of the IA current in nociceptive TRPA1$^{-/-}$ neurons shown here is in agreement of the latter of these two studies. Nevertheless, these authors did not observe differences in the proportion of the three mechanically gated currents as well as in the current amplitude of RA in KO mice as I observed here. However, as in the earlier study, I observed a reduction in the amplitude of transient currents (RA and IA currents) in neurons from TRPA1$^{-/-}$ mice.

Finally, the significantly reduction in the RA current amplitude observed by genetic elimination of TRPA1 is reproduced by blocking TRPA1 with the synthetic antagonist HC-030031. However, acute inhibition of TRPA1 with HC-030031 did not significantly alter the amplitude of IA currents, as occurred in KO mice. Yet, since I did not demonstrate functional expression of TRPA1 in the neurons exposed to this inhibitor, it is possible that not all neurons used to assess the acute inhibition of TRPA1 expressed the channel.

Taken together, these findings support the tenet that TRPA1 plays a key role in the mechanosensory function of TG neurons, although it is not essential to confer mechanosensitivity. In fact, not all neurons require TRPA1 for normal mechanosensation, as is the case for newborn neurons. However, in adult mice TRPA1 contributes on one hand to RA and IA currents in the total populations of neurons and on the other hand, it influences the nature of the IA currents in nociceptive neurons. It is possible that TRPA1 is an essential element in the structure-function of a mechanosensitive complex that mediates the IA and RA current phenotype, and that without TRPA1, neurons express attenuated IA currents and they speed up their inactivation kinetics.

The results presented here correlate well with the deficits in mechanotransduction observed in skin-based nerve-fibre afferent recordings from TRPA1$^{-/-}$ mice (Kwan et al., 2009). In these fibres, deficient mechanical responses were detected in multiple subclasses of cutaneous afferent fibres, including the low-threshold touch response. In fact, cutaneous C fibres displayed a 50% reduction in firing at all force intensities in the absence of TRPA1, whereas the firing of Aδ mechano-nociceptors was only reduced in response to intense force. Slowly adapting Aβ-fibres also exhibited reduced firing across all force intensities. The IA currents recorded here might correspond to that of C-fibres *in vivo,* which are quite strongly reduced in number, as well as in current amplitude, in TRPA1 $^{-/-}$ mice. Moreover, the reduction in the current amplitude observed in TRPA1$^{-/-}$ RA neurons might correspond to the reduced firing of Aβ-fibres observed. Finally, the SA neurons might correspond to Aδ-mechano-nociceptors, even if a significant reduction in the current amplitude of these neurons was not observed *in vitro* in knock-out mice.

In summary, the data presented in this Thesis characterizes the mechanically gated currents in trigeminal neurons evoked using a direct mechanical stimulus, the mechano-clamp. I identified distinct populations of mechanosensitive neurons activated by different mechanical stimuli, suggesting that different stimuli might activate different mechanosensitive channels. However, it was not possible to correlate the expression of specific mechanosensory channels with specific subpopulations of MS neurons. Given that the mechanical sensation perceived from the body is not always identical, my results lend support to data showing that the

cellular and molecular mechanisms underlying touch sensations is likely to be complex, and induced by the activation of different types of molecules and channels that specifically detect different kind of touch stimulus. Moreover, these data reveal a previously unknown role for TRPA1 as an important component of the mechanosensory machinery in adult trigeminal neurons. The role of the TRPA1 channel in mechanotransduction shown here, contributes to further understand the complexity of mechanosensation. Further studies in this field are likely to bring about groundbreaking progress in the development of specific treatment strategies for diseases affecting mechanotransduction.

6. Conclusions

1. In trigeminal sensory neurons is possible to distinguish mechanosensitive neurons responding to different types of mechanical stimulation, *i.e.* hyposmotic solution, static indentation or both stimuli. This suggests that different mechanical stimuli may activate different physiological responses.

2. These mechanosensitive neurons have been found both in newborn and adult mice, with the latter showing a higher proportion of mechano-nociceptive neurons.

3. Static indentation activates three different types of mechanically gated currents in TG neurons, classified according to the inactivating kinetics: the Rapidly, Intermediate and Slowly Adapting currents (RA, IA and SA).

4. Nociceptive and non-nociceptive neurons displayed the three mechanically gated currents, the RA, IA and SA currents.

5. The three types of mechanically activated currents are non-selective currents carried by cations.

6. Gadolinium inhibits the mechanically activated currents indicating that stretch activated channels are mediating the mechanical response.

7. It is not possible to attribute the expression of a specific ion channel either to the RA, SA and IA activated currents or to nociceptive or non-nociceptive mechanosensitive neurons. The final response of a neuron to a mechanical stimulation may depend on the activation of different molecular entities, each of one contributing to the mechanical response in a different way.

8. TRPA1 is not essential to confer mechanosensitivity to trigeminal neurons in newborn and adult mice and it does not play a role in mechanotransduction in newborn animals.

9. TRPA1 modulates the inactivation kinetics of RA and IA in the total population and in the nociceptive group in adult mice. The absence of TRPA1 increases the proportion of neurons displaying RA currents, associated mainly to low threshold neurons, and decrease the proportion of IA currents,

related to small noxious neurons. Moreover, deletion of TRPA1 decreases the amplitude of the currents. This suggests that TRPA may contribute to enhanced mechanical responses in adult mice.

Conclusiones

1. Existen diferentes poblaciones de neuronas trigeminales mecanosensibles, que responden a solución hipoosmótica, deformación de la membrana mediante el desplazamiento de una prueba de vidrio o ambos estímulos. Esto sugiere que diferentes estímulos mecánicos puedan activar diferentes respuestas fisiológicas.

2. Estas tres poblaciones de neuronas mecanosensibles se han identificado tanto en ratones neonatales como adultos, teniendo estos últimos una mayor proporción de neuronas nocivas mecánicas.

3. La deformación de la membrana activa tres tipos diferentes de corrientes iónicas clasificadas según su cinética de inactivación denominándose corrientes de adaptación rápida (RA del inglés rapidly adapting), intermedia (IA, intermediate adapting) o lenta (SA, slowly adapting).

4. Las neuronas nociceptivas y no nociceptivas presentan los tres tipos de corrientes iónicas activadas por estímulo mecánico, las corrientes RA, IA y SA.

5. Los tres tipos de corrientes mecánicas no son selectivas para cationes.

6. El catión gadolinio (Gd^{+3}) inhibe las corrientes mecánicas, lo cual indica que la respuesta mecánica está mediada por canales iónicos activados por estiramiento.

7. No es posible correlacionar la expresión de ninguno de los canales iónicos propuestos como mecanotransductores ni con la expresión de las corrientes RA, IA y SA ni con las neuronas nociceptivas o no nociceptivas. La respuesta final de una neurona a un estímulo mecánico podría depender de la activación de diferentes tipos de moléculas, cada una contribuyendo a la respuesta mecánica de forma distinta.

8. El canal TRPA1 no es esencial para conferir la mecanosensibilidad a las neuronas trigeminales tanto de ratones neonatales como de adultos. Además, no participa en la mecanotransducción en los animales neonatales.

9. El canal TRPA1 modula la cinética de inactivación de las corrientes RA e IA en la población total y en las neuronas nociceptivas en ratones adultos. La ausencia del canal TRPA1 aumenta la proporción de neuronas que presentan corrientes RA, asociadas principalmente a neuronas de bajo umbral, y disminuye la proporción de las neuronas que presentan corrientes IA, asociadas a neuronas nociceptivas o de alto umbral. Además, la supresión del canal TRPA1 disminuye la amplitud de las corrientes mecánicas. Esto sugiere que TRPA1 podría contribuir a aumentar la sensibilidad mecánica en ratones adultos.

UNIVERSITAS
Miguel
Hernández

7. Bibliography

Abrahamsen,B., Zhao,J., Asante,C.O., Cendan,C.M., Marsh,S., Martinez-Barbera,J.P., Nassar,M.A., Dickenson,A.H., and Wood,J.N. (2008). The cell and molecular basis of mechanical, cold, and inflammatory pain. Science *321*, 702-705.

Abraira,V.E. and Ginty,D.D. (2013). The sensory neurons of touch. Neuron *79*, 618-639.

Akopian,A.N., Sivilotti,L., and Wood,J.N. (1996). A tetrodotoxin-resistant voltage-gated sodium channel expressed by sensory neurons. Nature *379*, 257-262.

Alessandri-Haber,N., Dina,O.A., Yeh,J.J., Parada,C.A., Reichling,D.B., and Levine,J.D. (2004). Transient receptor potential vanilloid 4 is essential in chemotherapy-induced neuropathic pain in the rat. J. Neurosci. *24*, 4444-4452.

Alessandri-Haber,N., Yeh,J.J., Boyd,A.E., Parada,C.A., Chen,X., Reichling,D.B., and Levine,J.D. (2003). Hypotonicity induces TRPV4-mediated nociception in rat. Neuron *39*, 497-511.

Alloui,A., Zimmermann,K., Mamet,J., Duprat,F., Noel,J., Chemin,J., Guy,N., Blondeau,N., Voilley,N., Rubat-Coudert,C., Borsotto,M., Romey,G., Heurteaux,C., Reeh,P., Eschalier,A., and Lazdunski,M. (2006). TREK-1, a K+ channel involved in polymodal pain perception. EMBO J. *25*, 2368-2376.

Alvarado-Mallart,M.R., Batini,C., Buisseret-Delmas,C., and Corvisier,J. (1975). Trigeminal representations of the masticatory and extraocular proprioceptors as revealed by horseradish peroxidase retrograde transport. Exp. Brain Res. *23*, 167-179.

Amaya,F., Decosterd,I., Samad,T.A., Plumpton,C., Tate,S., Mannion,R.J., Costigan,M., and Woolf,C.J. (2000). Diversity of expression of the sensory neuron-specific TTX-resistant voltage-gated sodium ion channels SNS and SNS2. Mol. Cell Neurosci. *15*, 331-342.

Anishkin,A. and Kung,C. (2005). Microbial mechanosensation. Curr. Opin. Neurobiol. *15*, 397-405.

Arnadottir,J. and Chalfie,M. (2010). Eukaryotic mechanosensitive channels. Annu. Rev. Biophys. *39*, 111-137.

Bae,C., Sachs,F., and Gottlieb,P.A. (2011). The mechanosensitive ion channel Piezo1 is inhibited by the peptide GsMTx4. Biochemistry *50*, 6295-6300.

Baker,M.D. and Wood,J.N. (2001). Involvement of Na+ channels in pain pathways. Trends Pharmacol. Sci. *22*, 27-31.

Bandell,M., Story,G.M., Hwang,S.W., Viswanath,V., Eid,S.R., Petrus,M.J., Earley,T.J., and Patapoutian,A. (2004). Noxious cold ion channel TRPA1 is activated by pungent compounds and bradykinin. Neuron *41*, 849-857.

Bang,H., Kim,Y., and Kim,D. (2000). TREK-2, a new member of the mechanosensitive tandem-pore K+ channel family. J. Biol. Chem. *275*, 17412-17419.

Bautista,D.M., Jordt,S.E., Nikai,T., Tsuruda,P.R., Read,A.J., Poblete,J., Yamoah,E.N., Basbaum,A.I., and Julius,D. (2006). TRPA1 mediates the inflammatory actions of environmental irritants and proalgesic agents. Cell *124*, 1269-1282.

Bautista,D.M., Movahed,P., Hinman,A., Axelsson,H.E., Sterner,O., Hogestatt,E.D., Julius,D., Jordt,S.E., and Zygmunt,P.M. (2005). Pungent products from garlic activate the sensory ion channel TRPA1. Proc. Natl. Acad. Sci. U. S. A *102*, 12248-12252.

Beech,D.J., Muraki,K., and Flemming,R. (2004). Non-selective cationic channels of smooth muscle and the mammalian homologues of Drosophila TRP. J. Physiol *559*, 685-706.

Bessou,P. and Perl,E.R. (1969). Response of cutaneous sensory units with unmyelinated fibres to noxious stimuli. J. Neurophysiol. *32*, 1025-1043.

Bhattacharya,M.R., Bautista,D.M., Wu,K., Haeberle,H., Lumpkin,E.A., and Julius,D. (2008). Radial stretch reveals distinct populations of mechanosensitive mammalian somatosensory neurons. Proc. Natl. Acad. Sci. U. S. A *105*, 20015-20020.

Birder,L.A., Kanai,A.J., de Groat,W.C., Kiss,S., Nealen,M.L., Burke,N.E., Dineley,K.E., Watkins,S., Reynolds,I.J., and Caterina,M.J. (2001). Vanilloid receptor expression suggests a sensory role for urinary bladder epithelial cells. Proc. Natl. Acad. Sci. U. S. A *98*, 13396-13401.

Birder,L.A., Nakamura,Y., Kiss,S., Nealen,M.L., Barrick,S., Kanai,A.J., Wang,E., Ruiz,G., de Groat,W.C., Apodaca,G., Watkins,S., and Caterina,M.J. (2002). Altered urinary bladder function in mice lacking the vanilloid receptor TRPV1. Nat. Neurosci. *5*, 856-860.

Birnbaumer,L., Yildirim,E., and Abramowitz,J. (2003). A comparison of the genes coding for canonical TRP channels and their M, V and P relatives. Cell Calcium *33*, 419-432.

Birukov,K.G., Shirinsky,V.P., Stepanova,O.V., Tkachuk,V.A., Hahn,A.W., Resink,T.J., and Smirnov,V.N. (1995). Stretch affects phenotype and proliferation of vascular smooth muscle cells. Mol. Cell Biochem. *144*, 131-139.

Black,J.A., Liu,S., Tanaka,M., Cummins,T.R., and Waxman,S.G. (2004). Changes in the expression of tetrodotoxin-sensitive sodium channels within dorsal root ganglia neurons in inflammatory pain. Pain *108*, 237-247.

Bode,F., Sachs,F., and Franz,M.R. (2001). Tarantula peptide inhibits atrial fibrillation. Nature *409*, 35-36.

Brierley,S.M., Castro,J., Harrington,A.M., Hughes,P.A., Page,A.J., Rychkov,G.Y., and Blackshaw,L.A. (2011). TRPA1 contributes to specific mechanically activated currents and sensory neuron mechanical hypersensitivity. J. Physiol *589*, 3575-3593.

Brierley,S.M., Hughes,P.A., Page,A.J., Kwan,K.Y., Martin,C.M., O'Donnell,T.A., Cooper,N.J., Harrington,A.M., Adam,B., Liebregts,T., Holtmann,G., Corey,D.P., Rychkov,G.Y., and Blackshaw,L.A. (2009). The ion channel TRPA1 is required for normal mechanosensation and is modulated by algesic stimuli. Gastroenterology *137*, 2084-2095.

Brierley,S.M., Page,A.J., Hughes,P.A., Adam,B., Liebregts,T., Cooper,N.J., Holtmann,G., Liedtke,W., and Blackshaw,L.A. (2008). Selective role for TRPV4 ion channels in visceral sensory pathways. Gastroenterology *134*, 2059-2069.

Brock JA, McLachlan EM, & Belmonte C (1998). Tetrodotoxin-resistant impulses in single nociceptor nerve terminals in guinea-pig cornea. J Physiol *512*, 211-217.

Brock JA, Pianova S, & Belmonte C (2001). Differences between nerve terminal impulses of polymodal nociceptors and cold sensory receptors of the guinea-pig cornea. J Physiol *533*, 493-501.

Brown,A.G. (1981). The spinocervical tract. Prog. Neurobiol. *17*, 59-96.

Brown,A.G. and Iggo,A. (1967). A quantitative study of cutaneous receptors and afferent fibres in the cat and rabbit. J. Physiol *193*, 707-733.

Bryan-Sisneros,A.A., Fraser,S.P., and Djamgoz,M.B. (2003). Electrophysiological, mechanosensitive responses of Xenopus laevis oocytes to direct, isotonic increase in intracellular volume. J. Neurosci. Methods *125*, 103-111.

Burgess,P.R., Petit,D., and Warren,R.M. (1968). Receptor types in cat hairy skin supplied by myelinated fibres. J. Neurophysiol. *31*, 833-848.

Cabanes,C., Lopez de,A.M., Viana,F., and Belmonte,C. (2002). Postnatal changes in membrane properties of mice trigeminal ganglion neurons. J. Neurophysiol. *87*, 2398-2407.

Caffrey,J.M., Eng,D.L., Black,J.A., Waxman,S.G., and Kocsis,J.D. (1992). Three types of sodium channels in adult rat dorsal root ganglion neurons. Brain Res. *592*, 283-297.

Cain,D.M., Khasabov,S.G., and Simone,D.A. (2001). Response properties of mechanoreceptors and nociceptors in mouse glabrous skin: an in vivo study. J. Neurophysiol. *85*, 1561-1574.

Carr RW, Pianova S, & Brock JA (2002). The effects of polarizing current on nerve terminal impulses recorded from polymodal and cold receptors in the guinea-pig cornea. J Gen Physiol *120*, 395-405.

Carr RW, Pianova S, Fernandez J, Fallon JB, Belmonte C, & Brock JA (2003). Effects of heating and cooling on nerve terminal impulses recorded from cold-sensitive receptors in the guinea-pig cornea. J Gen Physiol *121*, 427-439.

Caterina,M.J. and Julius,D. (2001). The vanilloid receptor: a molecular gateway to the pain pathway. Annu. Rev. Neurosci. *24*, 487-517.

Caterina,M.J., Leffler,A., Malmberg,A.B., Martin,W.J., Trafton,J., Petersen-Zeitz,K.R., Koltzenburg,M., Basbaum,A.I., and Julius,D. (2000). Impaired nociception and pain sensation in mice lacking the capsaicin receptor. Science *288*, 306-313.

Caterina,M.J., Schumacher,M.A., Tominaga,M., Rosen,T.A., Levine,J.D., and Julius,D. (1997). The capsaicin receptor: a heat-activated ion channel in the pain pathway. Nature *389*, 816-824.

Cavanaugh,D.J., Lee,H., Lo,L., Shields,S.D., Zylka,M.J., Basbaum,A.I., and Anderson,D.J. (2009). Distinct subsets of unmyelinated primary sensory fibres mediate behavioral responses to noxious thermal and mechanical stimuli. Proc. Natl. Acad. Sci. U. S. A *106*, 9075-9080.

Chalfie,M. and Au,M. (1989). Genetic control of differentiation of the Caenorhabditis elegans touch receptor neurons. Science *243*, 1027-1033.

Chambers,M.R., Andres,K.H., von,D.M., and Iggo,A. (1972). The structure and function of the slowly adapting type II mechanoreceptor in hairy skin. Q. J. Exp. Physiol Cogn Med. Sci. *57*, 417-445.

Cho,H., Shin,J., Shin,C.Y., Lee,S.Y., and Oh,U. (2002). Mechanosensitive ion channels in cultured sensory neurons of neonatal rats. J. Neurosci. *22*, 1238-1247.

Christensen,A.P. and Corey,D.P. (2007). TRP channels in mechanosensation: direct or indirect activation? Nat. Rev. Neurosci. *8*, 510-521.

Clapham,D.E. (2003). TRP channels as cellular sensors. Nature *426*, 517-524.

Cody,F.W., Lee,R.W., and Taylor,A. (1972). A functional analysis of the components of the mesencephalic nucleus of the fifth nerve in the cat. J. Physiol *226*, 249-261.

Coggeshall,R.E., Pover,C.M., and Fitzgerald,M. (1994). Dorsal root ganglion cell death and surviving cell numbers in relation to the development of sensory innervation in the rat hindlimb. Brain Res. Dev. Brain Res. *82*, 193-212.

Colbert,H.A., Smith,T.L., and Bargmann,C.I. (1997). OSM-9, a novel protein with structural similarity to channels, is required for olfaction, mechanosensation, and olfactory adaptation in Caenorhabditis elegans. J. Neurosci. *17*, 8259-8269.

Corey,D.P., Garcia-Anoveros,J., Holt,J.R., Kwan,K.Y., Lin,S.Y., Vollrath,M.A., Amalfitano,A., Cheung,E.L., Derfler,B.H., Duggan,A., Geleoc,G.S., Gray,P.A., Hoffman,M.P., Rehm,H.L., Tamasauskas,D., and Zhang,D.S. (2004). TRPA1 is a candidate for the mechanosensitive transduction channel of vertebrate hair cells. Nature *432*, 723-730.

Corey,D.P. and Hudspeth,A.J. (1979). Response latency of vertebrate hair cells. Biophys. J. *26*, 499-506.

Cosens,D.J. and Manning,A. (1969). Abnormal electroretinogram from a Drosophila mutant. Nature *224*, 285-287.

Coste,B., Crest,M., and Delmas,P. (2007). Pharmacological dissection and distribution of NaN/Nav1.9, T-type Ca2+ currents, and mechanically activated cation currents in different populations of DRG neurons. J. Gen. Physiol *129*, 57-77.

Coste,B., Mathur,J., Schmidt,M., Earley,T.J., Ranade,S., Petrus,M.J., Dubin,A.E., and Patapoutian,A. (2010). Piezo1 and Piezo2 are essential components of distinct mechanically activated cation channels. Science *330*, 55-60.

Coste,B., Xiao,B., Santos,J.S., Syeda,R., Grandl,J., Spencer,K.S., Kim,S.E., Schmidt,M., Mathur,J., Dubin,A.E., Montal,M., and Patapoutian,A. (2012). Piezo proteins are pore-forming subunits of mechanically activated channels. Nature *483*, 176-181.

Cox,J.J., Reimann,F., Nicholas,A.K., Thornton,G., Roberts,E., Springell,K., Karbani,G., Jafri,H., Mannan,J., Raashid,Y., Al-Gazali,L., Hamamy,H., Valente,E.M., Gorman,S., Williams,R., McHale,D.P., Wood,J.N., Gribble,F.M., and Woods,C.G. (2006). An SCN9A channelopathy causes congenital inability to experience pain. Nature *444*, 894-898.

Dedman,A., Sharif-Naeini,R., Folgering,J.H., Duprat,F., Patel,A., and Honore,E. (2009). The mechano-gated K(2P) channel TREK-1. Eur. Biophys. J. *38*, 293-303.

Dell'Antonio,G., Quattrini,A., Dal Cin,E., Fulgenzi,A., Ferrero,M.E. (2002). Antinociceptive effect of a new P(2Z)/P2X7 antagonist, oxidized ATP, in arthritic rats. Neurosci Lett. 327, 87-90

Delmas,P., Hao,J., and Rodat-Despoix,L. (2011). Molecular mechanisms of mechanotransduction in mammalian sensory neurons. Nat. Rev. Neurosci. *12*, 139-153.

Di,C.A., Drew,L.J., Wood,J.N., and Cesare,P. (2006). Modulation of sensory neuron mechanotransduction by PKC- and nerve growth factor-dependent pathways. Proc. Natl. Acad. Sci. U. S. A *103*, 4699-4704.

Dietrich,A., Kalwa,H., Storch,U., Schnitzler,M., Salanova,B., Pinkenburg,O., Dubrovska,G., Essin,K., Gollasch,M., Birnbaumer,L., and Gudermann,T. (2007). Pressure-induced and store-

operated cation influx in vascular smooth muscle cells is independent of TRPC1. Pflugers Arch. *455*, 465-477.

Dietrich,A., Mederos,Y.S., Gollasch,M., Gross,V., Storch,U., Dubrovska,G., Obst,M., Yildirim,E., Salanova,B., Kalwa,H., Essin,K., Pinkenburg,O., Luft,F.C., Gudermann,T., and Birnbaumer,L. (2005). Increased vascular smooth muscle contractility in TRPC6-/- mice. Mol. Cell Biol. *25*, 6980-6989.

Djouhri,L., Bleazard,L., and Lawson,S.N. (1998). Association of somatic action potential shape with sensory receptive properties in guinea-pig dorsal root ganglion neurones. J. Physiol *513 (Pt 3)*, 857-872.

Djouhri,L., Fang,X., Okuse,K., Wood,J.N., Berry,C.M., and Lawson,S.N. (2003). The TTX-resistant sodium channel Nav1.8 (SNS/PN3): expression and correlation with membrane properties in rat nociceptive primary afferent neurons. J. Physiol *550*, 739-752.

Djouhri,L. and Lawson,S.N. (2004). Abeta-fibre nociceptive primary afferent neurons: a review of incidence and properties in relation to other afferent A-fibre neurons in mammals. Brain Res. Brain Res. Rev. *46*, 131-145.

Dong,X., Han,S., Zylka,M.J., Simon,M.I., and Anderson,D.J. (2001). A diverse family of GPCRs expressed in specific subsets of nociceptive sensory neurons. Cell *106*, 619-632.

Douglas,W.W. and Ritchie,J.M. (1957). Nonmedullated fibres in the saphenous nerve which signal touch. J. Physiol *139*, 385-399.

Drew,L.J., Rohrer,D.K., Price,M.P., Blaver,K.E., Cockayne,D.A., Cesare,P., and Wood,J.N. (2004). Acid-sensing ion channels ASIC2 and ASIC3 do not contribute to mechanically activated currents in mammalian sensory neurones. J. Physiol *556*, 691-710.

Drew,L.J. and Wood,J.N. (2007). FM1-43 is a permeant blocker of mechanosensitive ion channels in sensory neurons and inhibits behavioural responses to mechanical stimuli. Mol. Pain *3*, 1.

Drew,L.J., Wood,J.N., and Cesare,P. (2002). Distinct mechanosensitive properties of capsaicin-sensitive and -insensitive sensory neurons. J. Neurosci. *22*, RC228.

Duncan,L.M., Deeds,J., Hunter,J., Shao,J., Holmgren,L.M., Woolf,E.A., Tepper,R.I., and Shyjan,A.W. (1998). Down-regulation of the novel gene melastatin correlates with potential for melanoma metastasis. Cancer Res. *58*, 1515-1520.

Eijkelkamp,N., Quick,K., and Wood,J.N. (2013). Transient receptor potential channels and mechanosensation. Annu. Rev. Neurosci. *36*, 519-546.

Ernstrom,G.G. and Chalfie,M. (2002). Genetics of sensory mechanotransduction. Annu.Rev.Genet *36*, 411-453

Fang,X., McMullan,S., Lawson,S.N., and Djouhri,L. (2005). Electrophysiological differences between nociceptive and non-nociceptive dorsal root ganglion neurones in the rat in vivo. J. Physiol *565*, 927-943.

Flemming,P.K., Dedman,A.M., Xu,S.Z., Li,J., Zeng,F., Naylor,J., Benham,C.D., Bateson,A.N., Muraki,K., and Beech,D.J. (2006). Sensing of lysophospholipids by TRPC5 calcium channel. J. Biol. Chem. *281*, 4977-4982.

Foster,R.G. (2005). Neurobiology: bright blue times. Nature *433*, 698-699.

Fradette,J., Godbout,M.J., Michel,M., and Germain,L. (1995). Localization of Merkel cells at hairless and hairy human skin sites using keratin 18. Biochem. Cell Biol. *73*, 635-639.

Gaik,G.C. and Farbman,A.I. (1973). The chicken trigeminal ganglion. I. An anatomical analysis of the neuron types in the adult. J. Morphol. *141*, 43-55.

Garrison,S.R., Dietrich,A., and Stucky,C.L. (2012). TRPC1 contributes to light-touch sensation and mechanical responses in low-threshold cutaneous sensory neurons. J. Neurophysiol. *107*, 913-922.

Gaudet,R. (2008). TRP channels entering the structural era. J. Physiol *586*, 3565-3575.

Gees,M., Owsianik,G., Nilius,B., and Voets,T. (2012). TRP channels. Compr. Physiol *2*, 563-608.

Geffeney,S.L. and Goodman,M.B. (2012). How we feel: ion channel partnerships that detect mechanical inputs and give rise to touch and pain perception. Neuron *74*, 609-619.

Gillespie,P.G. and Walker,R.G. (2001). Molecular basis of mechanosensory transduction. Nature *413*, 194-202.

Glazebrook,P.A., Schilling,W.P., and Kunze,D.L. (2005). TRPC channels as signal transducers. Pflugers Arch. *451*, 125-130.

Gold,M.S., Dastmalchi,S., and Levine,J.D. (1996). Co-expression of nociceptor properties in dorsal root ganglion neurons from the adult rat in vitro. Neuroscience *71*, 265-275.

Gomis,A., Soriano,S., Belmonte,C., and Viana,F. (2008). Hypoosmotic- and pressure-induced membrane stretch activate TRPC5 channels. J. Physiol *586*, 5633-5649.

Goodman,M.B. (2006). Mechanosensation. WormBook. 1-14.

Gotoh,H. and Takahashi,A. (1999). Mechanical stimuli induce intracellular calcium response in a subpopulation of cultured rat sensory neurons. Neuroscience *92*, 1323-1329.

Gray,J.A. and Sato,M. (1953). Properties of the receptor potential in Pacinian corpuscles. J. Physiol *122*, 610-636.

Grimm,C., Kraft,R., Sauerbruch,S., Schultz,G., and Harteneck,C. (2003). Molecular and functional characterization of the melastatin-related cation channel TRPM3. J. Biol. Chem. *278*, 21493-21501.

Haeberle,H., Bryan,L.A., Vadakkan,T.J., Dickinson,M.E., and Lumpkin,E.A. (2008). Swelling-activated Ca2+ channels trigger Ca2+ signals in Merkel cells. PLoS. One. *3*, e1750.

Haga,J.H., Li,Y.S., and Chien,S. (2007). Molecular basis of the effects of mechanical stretch on vascular smooth muscle cells. J. Biomech. *40*, 947-960.

Halata,Z., Grim,M., and Bauman,K.I. (2003). Friedrich Sigmund Merkel and his "Merkel cell", morphology, development, and physiology: review and new results. Anat. Rec. A Discov. Mol. Cell Evol. Biol. *271*, 225-239.

Hamill,O.P. and McBride,D.W., Jr. (1996). The pharmacology of mechanogated membrane ion channels. Pharmacol. Rev. *48*, 231-252.

Hao,J. and Delmas,P. (2010). Multiple desensitization mechanisms of mechanotransducer channels shape firing of mechanosensory neurons. J. Neurosci. *30*, 13384-13395.

Hao,J. and Delmas,P. (2011). Recording of mechanosensitive currents using piezoelectrically driven mechanostimulator. Nat. Protoc. *6*, 979-990.

Hardie,R.C. and Minke,B. (1992). The trp gene is essential for a light-activated Ca2+ channel in Drosophila photoreceptors. Neuron *8*, 643-651.

Hillyard,S.D., Willumsen,N.J., and Marrero,M.B. (2010). Stretch-activated cation channel from larval bullfrog skin. J. Exp. Biol. *213*, 1782-1787.

Hjerling-Leffler,J., Alqatari,M., Ernfors,P., and Koltzenburg,M. (2007). Emergence of functional sensory subtypes as defined by transient receptor potential channel expression. J. Neurosci. *27*, 2435-2443.

Ho,C. and O'Leary,M.E. (2011). Single-cell analysis of sodium channel expression in dorsal root ganglion neurons. Mol. Cell Neurosci. *46*, 159-166.

Honore,E. (2007). The neuronal background K2P channels: focus on TREK1. Nat. Rev. Neurosci. *8*, 251-261.

Houk,J. and Henneman,E. (1967). Responses of Golgi tendon organs to active contractions of the soleus muscle of the cat. J. Neurophysiol. *30*, 466-481.

Hu,J., Chiang,L.Y., Koch,M., and Lewin,G.R. (2010). Evidence for a protein tether involved in somatic touch. EMBO J. *29*, 855-867.

Hu,J. and Lewin,G.R. (2006). Mechanosensitive currents in the neurites of cultured mouse sensory neurones. J. Physiol *577*, 815-828.

Huang,M., Gu,G., Ferguson,E.L., and Chalfie,M. (1995). A stomatin-like protein necessary for mechanosensation in C. elegans. Nature *378*, 292-295.

Ichikawa,H. and Sugimoto,T. (2002). The co-expression of ASIC3 with calcitonin gene-related peptide and parvalbumin in the rat trigeminal ganglion. Brain Res. *943*, 287-291.

Iggo,A. (1960). Cutaneous mechanoreceptors with afferent C fibres. J. Physiol *152*, 337-353.

Iggo,A. and Muir,A.R. (1969). The structure and function of a slowly adapting touch corpuscle in hairy skin. J. Physiol *200*, 763-796.

Jerge,C.R. (1963). Organization and function of the trigeminal mensencephalic nucleus. J. Neurophysiol. *26*, 379-392.

Jiang,Y., Lee,A., Chen,J., Cadene,M., Chait,B.T., and MacKinnon,R. (2002). Crystal structure and mechanism of a calcium-gated potassium channel. Nature *417*, 515-522.

Joe,P., Wallen,L.D., Chapin,C.J., Lee,C.H., Allen,L., Han,V.K., Dobbs,L.G., Hawgood,S., and Kitterman,J.A. (1997). Effects of mechanical factors on growth and maturation of the lung in fetal sheep. Am. J. Physiol *272*, L95-105.

Johnson,K.O. (2001). The roles and functions of cutaneous mechanoreceptors. Curr. Opin. Neurobiol. *11*, 455-461.

Jordt,S.E., Bautista,D.M., Chuang,H.H., McKemy,D.D., Zygmunt,P.M., Hogestatt,E.D., Meng,I.D., and Julius,D. (2004). Mustard oils and cannabinoids excite sensory nerve fibres through the TRP channel ANKTM1. Nature *427*, 260-265.

Julius,D. and Basbaum,A.I. (2001). Molecular mechanisms of nociception. Nature *413*, 203-210.

Kahn-Kirby,A.H. and Bargmann,C.I. (2006). TRP channels in C. elegans. Annu. Rev. Physiol *68*, 719-736.

Kahn-Kirby,A.H., Dantzker,J.L., Apicella,A.J., Schafer,W.R., Browse,J., Bargmann,C.I., and Watts,J.L. (2004). Specific polyunsaturated fatty acids drive TRPV-dependent sensory signalling in vivo. Cell *119*, 889-900.

Kang,D. and Kim,D. (2006). TREK-2 (K2P10.1) and TRESK (K2P18.1) are major background K+ channels in dorsal root ganglion neurons. Am. J. Physiol Cell Physiol *291*, C138-C146.

Karashima,Y., Damann,N., Prenen,J., Talavera,K., Segal,A., Voets,T., and Nilius,B. (2007). Bimodal action of menthol on the transient receptor potential channel TRPA1. J. Neurosci. *27*, 9874-9884.

Kernan,M., Cowan,D., and Zuker,C. (1994). Genetic dissection of mechanosensory transduction: mechanoreception-defective mutations of Drosophila. Neuron *12*, 1195-1206.

Kim,J., Chung,Y.D., Park,D.Y., Choi,S., Shin,D.W., Soh,H., Lee,H.W., Son,W., Yim,J., Park,C.S., Kernan,M.J., and Kim,C. (2003). A TRPV family ion channel required for hearing in Drosophila. Nature *424*, 81-84.

Kindt,K.S., Viswanath,V., Macpherson,L., Quast,K., Hu,H., Patapoutian,A., and Schafer,W.R. (2007). Caenorhabditis elegans TRPA-1 functions in mechanosensation. Nat. Neurosci. *10*, 568-577.

Knibestol,M. (1973). Stimulus-response functions of rapidly adapting mechanoreceptors in human glabrous skin area. J. Physiol *232*, 427-452.

Kobayashi,K., Fukuoka,T., Obata,K., Yamanaka,H., Dai,Y., Tokunaga,A., and Noguchi,K. (2005). Distinct expression of TRPM8, TRPA1, and TRPV1 mRNAs in rat primary afferent neurons with adelta/c-fibres and colocalization with trk receptors. J. Comp Neurol. *493*, 596-606.

Koerber,H.R., Druzinsky,R.E., and Mendell,L.M. (1988). Properties of somata of spinal dorsal root ganglion cells differ according to peripheral receptor innervated. J. Neurophysiol. *60*, 1584-1596.

Kostyuk,P.G., Veselovsky,N.S., and Tsyndrenko,A.Y. (1981). Ionic currents in the somatic membrane of rat dorsal root ganglion neurons-I. Sodium currents. Neuroscience *6*, 2423-2430.

Kress,M., Koltzenburg,M., Reeh,P.W., and Handwerker,H.O. (1992). Responsiveness and functional attributes of electrically localized terminals of cutaneous C-fibres in vivo and in vitro. J. Neurophysiol. *68*, 581-595.

Kung,C. (2005). A possible unifying principle for mechanosensation. Nature *436*, 647-654.

Kwan,K.Y., Allchorne,A.J., Vollrath,M.A., Christensen,A.P., Zhang,D.S., Woolf,C.J., and Corey,D.P. (2006). TRPA1 contributes to cold, mechanical, and chemical nociception but is not essential for hair-cell transduction. Neuron *50*, 277-289.

Kwan,K.Y., Glazer,J.M., Corey,D.P., Rice,F.L., and Stucky,C.L. (2009). TRPA1 modulates mechanotransduction in cutaneous sensory neurons. J. Neurosci. *29*, 4808-4819.

Lam,T. and Pearson,K.G. (2002). The role of proprioceptive feedback in the regulation and adaptation of locomotor activity. Adv. Exp. Med. Biol. *508*, 343-355.

Lawson,S.N. (1979). The postnatal development of large light and small dark neurons in mouse dorsal root ganglia: a statistical analysis of cell numbers and size. J. Neurocytol. *8*, 275-294.

Lawson,S.N. (2002). Phenotype and function of somatic primary afferent nociceptive neurones with C-, Adelta- or Aalpha/beta-fibres. Exp. Physiol *87*, 239-244.

Lawson,S.N., Crepps,B.A., and Perl,E.R. (1997). Relationship of substance P to afferent characteristics of dorsal root ganglion neurones in guinea-pig. J. Physiol *505 (Pt 1)*, 177-191.

Le,T. and Saier,M.H., Jr. (1996). Phylogenetic characterization of the epithelial Na+ channel (ENaC) family. Mol. Membr. Biol. *13*, 149-157.

Lechner,S.G., Frenzel,H., Wang,R., and Lewin,G.R. (2009). Developmental waves of mechanosensitivity acquisition in sensory neuron subtypes during embryonic development. EMBO J. *28*, 1479-1491.

Lechner,S.G. and Lewin,G.R. (2009). Peripheral sensitisation of nociceptors via G-protein-dependent potentiation of mechanotransduction currents. J. Physiol *587*, 3493-3503.

Leiser,S.C. and Moxon,K.A. (2006). Relationship between physiological response type (RA and SA) and vibrissal receptive field of neurons within the rat trigeminal ganglion. J. Neurophysiol. *95*, 3129-3145.

Lewin,G.R. and Moshourab,R. (2004). Mechanosensation and pain. J. Neurobiol. *61*, 30-44.

Li,L., Rutlin,M., Abraira,V.E., Cassidy,C., Kus,L., Gong,S., Jankowski,M.P., Luo,W., Heintz,N., Koerber,H.R., Woodbury,C.J., and Ginty,D.D. (2011). The functional organization of cutaneous low-threshold mechanosensory neurons. Cell *147*, 1615-1627.

Li,W., Feng,Z., Sternberg,P.W., and Xu,X.Z. (2006). A C. elegans stretch receptor neuron revealed by a mechanosensitive TRP channel homologue. Nature *440*, 684-687.

Li,Y.S., Haga,J.H., and Chien,S. (2005). Molecular basis of the effects of shear stress on vascular endothelial cells. J. Biomech. *38*, 1949-1971.

Liao, M., Cao,E., Julius, D., Cheng, Y. (2013). Structure of the TRPV1 ion channel determined by electron cryo-microscopy. Nature *504*,107–112.

Liedtke,W., Choe,Y., Marti-Renom,M.A., Bell,A.M., Denis,C.S., Sali,A., Hudspeth,A.J., Friedman,J.M., and Heller,S. (2000). Vanilloid receptor-related osmotically activated channel (VR-OAC), a candidate vertebrate osmoreceptor. Cell *103*, 525-535.

Liedtke,W. and Friedman,J.M. (2003). Abnormal osmotic regulation in trpv4-/- mice. Proc. Natl. Acad. Sci. U. S. A *100*, 13698-13703.

Lingueglia,E. (2007). Acid-sensing ion channels in sensory perception. J. Biol. Chem. *282*, 17325-17329.

Lu,Y., Ma,X., Sabharwal,R., Snitsarev,V., Morgan,D., Rahmouni,K., Drummond,H.A., Whiteis,C.A., Costa,V., Price,M., Benson,C., Welsh,M.J., Chapleau,M.W., and Abboud,F.M. (2009). The ion channel ASIC2 is required for baroreceptor and autonomic control of the circulation. Neuron *64*, 885-897.

Lumpkin,E.A. and Caterina,M.J. (2007). Mechanisms of sensory transduction in the skin. Nature *445*, 858-865.

Lumpkin,E.A., Marshall,K.L., and Nelson,A.M. (2010). The cell biology of touch. J. Cell Biol. *191*, 237-248.

Macpherson,L.J., Dubin,A.E., Evans,M.J., Marr,F., Schultz,P.G., Cravatt,B.F., and Patapoutian,A. (2007). Noxious compounds activate TRPA1 ion channels through covalent modification of cysteines. Nature *445*, 541-545.

Maingret,F., Fosset,M., Lesage,F., Lazdunski,M., and Honore,E. (1999). TRAAK is a mammalian neuronal mechano-gated K+ channel. J. Biol. Chem. *274*, 1381-1387.

Malin,S.A., Davis,B.M., and Molliver,D.C. (2007). Production of dissociated sensory neuron cultures and considerations for their use in studying neuronal function and plasticity. Nat. Protoc. *2*, 152-160.

Maksimovic,A., Nakatani,M., Baba,Y., Nelson,A.M., Marshall, K.L., Wellnitz,A., Firozi,P., Woo,S.H, Ranade,S., Patapoutian,A. & Lumpkin,E.A. (2014). Epidermal Merkel cells are mechanosensory cells that tune mammalian touch receptors. Nature,*1038*, 13250.

Maroto,R., Raso,A., Wood,T.G., Kurosky,A., Martinac,B., and Hamill,O.P. (2005). TRPC1 forms the stretch-activated cation channel in vertebrate cells. Nat. Cell Biol. *7*, 179-185.

Martinac,B. (2004). Mechanosensitive ion channels: molecules of mechanotransduction. J. Cell Sci. *117*, 2449-2460.

Martinez-Salgado,C., Benckendorff,A.G., Chiang,L.Y., Wang,R., Milenkovic,N., Wetzel,C., Hu,J., Stucky,C.L., Parra,M.G., Mohandas,N., and Lewin,G.R. (2007). Stomatin and sensory neuron mechanotransduction. J. Neurophysiol. *98*, 3802-3808.

Matthews,P.B. (1964). Muscle Spindles and their motor control. Physiol Rev. *44*, 219-288.

McCarter,G.C. and Levine,J.D. (2006). Ionic basis of a mechanotransduction current in adult rat dorsal root ganglion neurons. Mol. Pain *2*, 28.

McCarter,G.C., Reichling,D.B., and Levine,J.D. (1999). Mechanical transduction by rat dorsal root ganglion neurons in vitro. Neurosci. Lett. *273*, 179-182.

McCleskey,E.W. and Gold,M.S. (1999). Ion channels of nociception. Annu. Rev. Physiol *61*, 835-856.

McGlone,F., Vallbo,A.B., Olausson,H., Loken,L., and Wessberg,J. (2007). Discriminative touch and emotional touch. Can. J. Exp. Psychol. *61*, 173-183.

McNamara,C.R., Mandel-Brehm,J., Bautista,D.M., Siemens,J., Deranian,K.L., Zhao,M., Hayward,N.J., Chong,J.A., Julius,D., Moran,M.M., and Fanger,C.M. (2007). TRPA1 mediates formalin-induced pain. Proc. Natl. Acad. Sci. U. S. A *104*, 13525-13530.

Medhurst,A.D., Rennie,G., Chapman,C.G., Meadows,H., Duckworth,M.D., Kelsell,R.E., Gloger,I.I., and Pangalos,M.N. (2001). Distribution analysis of human two pore domain potassium channels in tissues of the central nervous system and periphery. Brain Res. Mol. Brain Res. *86*, 101-114.

Mikuni-Takagaki,Y. (1999). Mechanical responses and signal transduction pathways in stretched osteocytes. J. Bone Miner. Metab *17*, 57-60.

Minke,B., Wu,C., and Pak,W.L. (1975). Induction of photoreceptor voltage noise in the dark in Drosophila mutant. Nature *258*, 84-87.

Molliver,D.C., Wright,D.E., Leitner,M.L., Parsadanian,A.S., Doster,K., Wen,D., Yan,Q., and Snider,W.D. (1997). IB4-binding DRG neurons switch from NGF to GDNF dependence in early postnatal life. Neuron *19*, 849-861.

Montell,C. and Rubin,G.M. (1989). Molecular characterization of the Drosophila trp locus: a putative integral membrane protein required for phototransduction. Neuron *2*, 1313-1323.

Moore,E.D., Becker,P.L., Fogarty,K.E., Williams,D.A., and Fay,F.S. (1990). Ca2+ imaging in single living cells: theoretical and practical issues. Cell Calcium *11*, 157-179.

Moore,J.C. (1984). The Golgi tendon organ: a review and update. Am. J. Occup. Ther. *38*, 227-236.

Morris,C.E. (1990). Mechanosensitive ion channels. J. Membr. Biol. *113*, 93-107.

Muraki,K., Iwata,Y., Katanosaka,Y., Ito,T., Ohya,S., Shigekawa,M., and Imaizumi,Y. (2003). TRPV2 is a component of osmotically sensitive cation channels in murine aortic myocytes. Circ. Res. *93*, 829-838.

Nagata,K., Duggan,A., Kumar,G., and Garcia-Anoveros,J. (2005). Nociceptor and hair cell transducer properties of TRPA1, a channel for pain and hearing. J. Neurosci. *25*, 4052-4061.

Nagy,J.I. and Hunt,S.P. (1982). Fluoride-resistant acid phosphatase-containing neurones in dorsal root ganglia are separate from those containing substance P or somatostatin. Neuroscience *7*, 89-97.

Nassar,M.A., Stirling,L.C., Forlani,G., Baker,M.D., Matthews,E.A., Dickenson,A.H., and Wood,J.N. (2004). Nociceptor-specific gene deletion reveals a major role for Nav1.7 (PN1) in acute and inflammatory pain. Proc. Natl. Acad. Sci. U. S. A *101*, 12706-12711.

O'Hagan,R., Chalfie,M., and Goodman,M.B. (2005). The MEC-4 DEG/ENaC channel of Caenorhabditis elegans touch receptor neurons transduces mechanical signals. Nat. Neurosci. *8*, 43-50.

Page,A.J., Brierley,S.M., Martin,C.M., Martinez-Salgado,C., Wemmie,J.A., Brennan,T.J., Symonds,E., Omari,T., Lewin,G.R., Welsh,M.J., and Blackshaw,L.A. (2004). The ion channel ASIC1 contributes to visceral but not cutaneous mechanoreceptor function. Gastroenterology *127*, 1739-1747.

Pannese,E. (1981). The satellite cells of the sensory ganglia. Adv. Anat. Embryol. Cell Biol. *65*, 1-111.

Parra,A., Madrid,R., Echevarria,D., Del OS, Morenilla-Palao,C., Acosta,M.C., Gallar,J., Dhaka, A., Viana,F., & Belmonte,C. (2010). Ocular surface wetness is regulated by TRPM8-dependent cold thermoreceptors of thecornea. Nat Med *16*, 1396-1399.

Park,S.P., Kim,B.M., Koo,J.Y., Cho,H., Lee,C.H., Kim,M., Na,H.S., and Oh,U. (2008). A tarantula spider toxin, GsMTx4, reduces mechanical and neuropathic pain. Pain *137*, 208-217.

Paszek,M.J., Zahir,N., Johnson,K.R., Lakins,J.N., Rozenberg,G.I., Gefen,A., Reinhart-King,C.A., Margulies,S.S., Dembo,M., Boettiger,D., Hammer,D.A., and Weaver,V.M. (2005). Tensional homeostasis and the malignant phenotype. Cancer Cell *8*, 241-254.

Patel,A.J., Honore,E., Lesage,F., Fink,M., Romey,G., and Lazdunski,M. (1999). Inhalational anesthetics activate two-pore-domain background K+ channels. Nat. Neurosci. *2*, 422-426.

Patel,A.J., Lazdunski,M., and Honore,E. (2001). Lipid and mechano-gated 2P domain K(+) channels. Curr. Opin. Cell Biol. *13*, 422-428.

Perl,E.R. (1996). Cutaneous polymodal receptors: characteristics and plasticity. Prog. Brain Res. *113*, 21-37.

Perl,E.R. (1968). Myelinated afferent fibres innervating the primate skin and their response to noxious stimuli. J. Physiol *197*, 593-615.

Perozo,E., Kloda,A., Cortes,D.M., and Martinac,B. (2002). Physical principles underlying the transduction of bilayer deformation forces during mechanosensitive channel gating. Nat. Struct. Biol. *9*, 696-703.

Pickles,J.O., Comis,S.D., and Osborne,M.P. (1984). Cross-links between stereocilia in the guinea pig organ of Corti, and their possible relation to sensory transduction. Hear. Res. *15*, 103-112.

Price,M.P., Lewin,G.R., McIlwrath,S.L., Cheng,C., Xie,J., Heppenstall,P.A., Stucky,C.L., Mannsfeldt,A.G., Brennan,T.J., Drummond,H.A., Qiao,J., Benson,C.J., Tarr,D.E., Hrstka,R.F., Yang,B., Williamson,R.A., and Welsh,M.J. (2000). The mammalian sodium channel BNC1 is required for normal touch sensation. Nature *407*, 1007-1011.

Price,M.P., McIlwrath,S.L., Xie,J., Cheng,C., Qiao,J., Tarr,D.E., Sluka,K.A., Brennan,T.J., Lewin,G.R., and Welsh,M.J. (2001). The DRASIC cation channel contributes to the detection of cutaneous touch and acid stimuli in mice. Neuron *32*, 1071-1083.

Quick,K., Zhao,J., Eijkelkamp,N., Linley,J.E., Rugiero,F., Cox,J.J., Raouf,R., Gringhuis,M., Sexton,J.E., Abramowitz,J., Taylor,R., Forge,A., Ashmore,J., Kirkwood,N., Kros,C.J., Richardson,G.P., Freichel,M., Flockerzi,V., Birnbaumer,L., and Wood,J.N. (2012). TRPC3 and TRPC6 are essential for normal mechanotransduction in subsets of sensory neurons and cochlear hair cells. Open. Biol. *2*, 120068.

Raoux,M., Colomban,C., Delmas,P., and Crest,M. (2007). The amine-containing cutaneous irritant heptylamine inhibits the volume-regulated anion channel and mobilizes intracellular calcium in normal human epidermal keratinocytes. Mol. Pharmacol. *71*, 1685-1694.

Reeh,P.W. (1986). Sensory receptors in mammalian skin in an in vitro preparation. Neurosci. Lett. *66*, 141-146.

Roudaut,Y., Lonigro,A., Coste,B., Hao,J., Delmas,P., and Crest,M. (2012). Touch sense: functional organization and molecular determinants of mechanosensitive receptors. Channels (Austin.) *6*, 234-245.

Rugiero,F., Drew,L.J., and Wood,J.N. (2010). Kinetic properties of mechanically activated currents in spinal sensory neurons. J. Physiol *588*, 301-314.

Rugiero,F. and Wood,J.N. (2009). The mechanosensitive cell line ND-C does not express functional thermoTRP channels. Neuropharmacology *56*, 1138-1146.

Sachs,F. (2010). Stretch-activated ion channels: what are they? Physiology. (Bethesda.) *25*, 50-56.

Sangameswaran,L., Delgado,S.G., Fish,L.M., Koch,B.D., Jakeman,L.B., Stewart,G.R., Sze,P., Hunter,J.C., Eglen,R.M., and Herman,R.C. (1996). Structure and function of a novel voltage-gated, tetrodotoxin-resistant sodium channel specific to sensory neurons. J. Biol. Chem. *271*, 5953-5956.

Sharif-Naeini,R., Folgering,J.H., Bichet,D., Duprat,F., Lauritzen,I., Arhatte,M., Jodar,M., Dedman,A., Chatelain,F.C., Schulte,U., Retailleau,K., Loufrani,L., Patel,A., Sachs,F., Delmas,P., Peters,D.J., and Honore,E. (2009). Polycystin-1 and -2 dosage regulates pressure sensing. Cell *139*, 587-596.

Sheetz, M. and Singer, S.G. (1974). Biological membranes as bilayer couples.A molecular mechanism of drug-erythrocyte interactions.Proc.Nat. Acad. Sci *71*, 4457-4461.

Shields, S.D., Ahn, H.S., Yang, Y., Han, C., Seal, R.P., Wood, J.N., Waxman, S.G., Dib-Hajj, S.D. (2012) Nav1.8 expression is not restricted to nociceptors in mouse peripheral nervous system. Pain *153*, 2017-2030.

Shin,J.B., Adams,D., Paukert,M., Siba,M., Sidi,S., Levin,M., Gillespie,P.G., and Grunder,S. (2005). Xenopus TRPN1 (NOMPC) localizes to microtubule-based cilia in epithelial cells, including inner-ear hair cells. Proc. Natl. Acad. Sci. U. S. A *102*, 12572-12577.

Sidi,S., Friedrich,R.W., and Nicolson,T. (2003). NompC TRP channel required for vertebrate sensory hair cell mechanotransduction. Science *301*, 96-99.

Silverman,J.D. and Kruger,L. (1990). Selective neuronal glycoconjugate expression in sensory and autonomic ganglia: relation of lectin reactivity to peptide and enzyme markers. J. Neurocytol. *19*, 789-801.

Sniadecki,N.J. (2010). A tiny touch: activation of cell signalling pathways with magnetic nanoparticles. Endocrinology *151*, 451-457.

Snider,W.D. and McMahon,S.B. (1998). Tackling pain at the source: new ideas about nociceptors. Neuron *20*, 629-632.

Sotomayor,M., Corey,D.P., and Schulten,K. (2005). In search of the hair-cell gating spring elastic properties of ankyrin and cadherin repeats. Structure. *13*, 669-682.

Spassova,M.A., Hewavitharana,T., Xu,W., Soboloff,J., and Gill,D.L. (2006). A common mechanism underlies stretch activation and receptor activation of TRPC6 channels. Proc. Natl. Acad. Sci. U. S. A *103*, 16586-16591.

Staaf,S., Maxvall,I., Lind,U., Husmark,J., Mattsson,J.P., Ernfors,P., and Pierrou,S. (2009). Down regulation of TRPC1 by shRNA reduces mechanosensitivity in mouse dorsal root ganglion neurons in vitro. Neurosci. Lett. *457*, 3-7.

Staikopoulos, V., Sessle, B.J., Furness, J.B., Jennings, E.A. (2007). Localization of P2X2 and P2X3 receptors in rat trigeminal ganglion neurons. Neuroscience. *144*, 208-216.

Story,G.M., Peier,A.M., Reeve,A.J., Eid,S.R., Mosbacher,J., Hricik,T.R., Earley,T.J., Hergarden,A.C., Andersson,D.A., Hwang,S.W., McIntyre,P., Jegla,T., Bevan,S., and Patapoutian,A. (2003). ANKTM1, a TRP-like channel expressed in nociceptive neurons, is activated by cold temperatures. Cell *112*, 819-829.

Stucky,C.L. and Lewin,G.R. (1999). Isolectin B(4)-positive and -negative nociceptors are functionally distinct. J. Neurosci. *19*, 6497-6505.

Suchyna,T.M., Johnson,J.H., Hamer,K., Leykam,J.F., Gage,D.A., Clemo,H.F., Baumgarten,C.M., and Sachs,F. (2000). Identification of a peptide toxin from Grammostola spatulata spider venom that blocks cation-selective stretch-activated channels. J. Gen. Physiol *115*, 583-598.

Sukharev,S.I., Blount,P., Martinac,B., Blattner,F.R., and Kung,C. (1994). A large-conductance mechanosensitive channel in E. coli encoded by mscL alone. Nature *368*, 265-268.

Talavera,K., Gees,M., Karashima,Y., Meseguer,V.M., Vanoirbeek,J.A., Damann,N., Everaerts,W., Benoit,M., Janssens,A., Vennekens,R., Viana,F., Nemery,B., Nilius,B., and Voets,T. (2009). Nicotine activates the chemosensory cation channel TRPA1. Nat. Neurosci. *12*, 1293-1299.

Talbot,W.H., rian-Smith,I., Kornhuber,H.H., and Mountcastle,V.B. (1968). The sense of flutter-vibration: comparison of the human capacity with response patterns of mechanoreceptive afferents from the monkey hand. J. Neurophysiol. *31*, 301-334.

Tobin,D., Madsen,D., Kahn-Kirby,A., Peckol,E., Moulder,G., Barstead,R., Maricq,A., and Bargmann,C. (2002). Combinatorial expression of TRPV channel proteins defines their sensory functions and subcellular localization in C. elegans neurons. Neuron *35*, 307-318.

Tracey,W.D., Jr., Wilson,R.I., Laurent,G., and Benzer,S. (2003). painless, a Drosophila gene essential for nociception. Cell *113*, 261-273.

Traub,R.J. and Mendell,L.M. (1988). The spinal projection of individual identified A-delta- and C-fibres. J. Neurophysiol. *59*, 41-55.

Trevisani,M., Siemens,J., Materazzi,S., Bautista,D.M., Nassini,R., Campi,B., Imamachi,N., Andre,E., Patacchini,R., Cottrell,G.S., Gatti,R., Basbaum,A.I., Bunnett,N.W., Julius,D., and Geppetti,P. (2007). 4-Hydroxynonenal, an endogenous aldehyde, causes pain and neurogenic inflammation through activation of the irritant receptor TRPA1. Proc. Natl. Acad. Sci. U. S. A *104*, 13519-13524.

Vallbo,A., Olausson,H., Wessberg,J., and Norrsell,U. (1993). A system of unmyelinated afferents for innocuous mechanoreception in the human skin. Brain Res. *628*, 301-304.

Vallbo,A.B. and Johansson,R.S. (1984). Properties of cutaneous mechanoreceptors in the human hand related to touch sensation. Hum. Neurobiol. *3*, 3-14.

Vallbo,A.B., Olausson,H., and Wessberg,J. (1999). Unmyelinated afferents constitute a second system coding tactile stimuli of the human hairy skin. J. Neurophysiol. *81*, 2753-2763.

Vandewauw,I., Owsianik,G., and Voets,T. (2013). Systematic and quantitative mRNA expression analysis of TRP channel genes at the single trigeminal and dorsal root ganglion level in mouse. BMC. Neurosci. *14*, 21.

Venkatachalam,K. and Montell,C. (2007). TRP channels. Annu. Rev. Biochem. *76*, 387-417.

Viana,F. (2011). Chemosensory properties of the trigeminal system. ACS Chem. Neurosci. *2*, 38-50.

Viana,F., de la,P.E., Pecson,B., Schmidt,R.F., and Belmonte,C. (2001). Swelling-activated calcium signalling in cultured mouse primary sensory neurons. Eur. J. Neurosci. *13*, 722-734.

Vilceanu,D. and Stucky,C.L. (2010). TRPA1 mediates mechanical currents in the plasma membrane of mouse sensory neurons. PLoS. One. *5*, e12177.

Voets,T., Talavera,K., Owsianik,G., and Nilius,B. (2005). Sensing with TRP channels. Nat. Chem. Biol. *1*, 85-92.

Vriens,J., Watanabe,H., Janssens,A., Droogmans,G., Voets,T., and Nilius,B. (2004). Cell swelling, heat, and chemical agonists use distinct pathways for the activation of the cation channel TRPV4. Proc. Natl. Acad. Sci. U. S. A *101*, 396-401.

Walker,R.G., Willingham,A.T., and Zuker,C.S. (2000). A Drosophila mechanosensory transduction channel. Science *287*, 2229-2234.

Waters,C.M., Sporn,P.H., Liu,M., and Fredberg,J.J. (2002). Cellular biomechanics in the lung. Am. J. Physiol Lung Cell Mol. Physiol *283*, L503-L509.

Waxman,S.G., Cummins,T.R., Dib-Hajj,S., Fjell,J., and Black,J.A. (1999). Sodium channels, excitability of primary sensory neurons, and the molecular basis of pain. Muscle Nerve *22*, 1177-1187.

Wetzel,C., Hu,J., Riethmacher,D., Benckendorff,A., Harder,L., Eilers,A., Moshourab,R., Kozlenkov,A., Labuz,D., Caspani,O., Erdmann,B., Machelska,H., Heppenstall,P.A., and Lewin,G.R. (2007a). A stomatin-domain protein essential for touch sensation in the mouse. Nature *445*, 206-209.

Williams,D.A., Fogarty,K.E., Tsien,R.Y., and Fay,F.S. (1985). Calcium gradients in single smooth muscle cells revealed by the digital imaging microscope using Fura-2. Nature *318*, 558-561.

Woo,S.H., Ranade,S., Weyer,A.D., Dubin,A.E., Baba,Y., Qiu,Z., Petrus,M., Miyamoto,T., Reddy,K., Lumpkin,E.A., Stucky, C.L., Patapoutanian, A. Piezo 2 is required for Merkel-cell mechanotransduction.Nature.

Woodbury,C.J. and Koerber,H.R. (2003). Widespread projections from myelinated nociceptors throughout the substantia gelatinosa provide novel insights into neonatal hypersensitivity. J. Neurosci. *23*, 601-610.

Wu,Z.Z. and Pan,H.L. (2004). Tetrodotoxin-sensitive and -resistant Na+ channel currents in subsets of small sensory neurons of rats. Brain Res. *1029*, 251-258.

Xiao,R. and Xu,X.Z. (2010). Mechanosensitive channels: in touch with Piezo. Curr. Biol. *20*, R936-R938.

Xiao,R. and Xu,X.Z. (2009). Function and regulation of TRP family channels in C. elegans. Pflugers Arch. *458*, 851-860.

Yang,X.C. and Sachs,F. (1989). Block of stretch-activated ion channels in Xenopus oocytes by gadolinium and calcium ions. Science *243*, 1068-1071.

Zylka,M.J., Rice,F.L., and Anderson,D.J. (2005). Topographically distinct epidermal nociceptive circuits revealed by axonal tracers targeted to Mrgprd. Neuron *45*, 17-25.

UNIVERSITAS
Miguel
Hernández